SEISMIC RESPONSE EVALUATION OF A CONCRETE GRAVITY DAM CONSIDERING DAM-RESERVOIR-FOUNDATION INTERACTION

by

Muhammed Çağatay Kent

A thesis submitted to the Graduate Faculty of
Auburn University
in partial fulfillment of the
requirements for the Degree of
Master of Science in Civil Engineering

Auburn, Alabama
May 4, 2019

Keywords: dam-reservoir-foundation interaction, concrete gravity dam, linear dynamic analysis, nonlinear time-history analysis

Approved by

James S. Davidson, Chair, Gottlieb Endowed Professor of Civil Engineering
Jack Montgomery, Co-chair, Assistant Professor of Civil Engineering
Justin D. Marshall, Associate Professor of Civil Engineering

ABSTRACT

The observation of the behavior of concrete gravity dams that are exposed to seismic loads is the main factor for the safety evaluation of the dams. In this regard, dam-foundation-reservoir interaction can be seen as one of the most significant concerns for the determination of dam safety. Moreover, hydrodynamic pressures may present because of dam-reservoir-foundation interaction and dynamic loads. As a result of this situation, hydrodynamic forces should be included in the safety evaluation to obtain more accurate seismic responses of dams. The dynamic response of gravity dams can be sufficiently illustrated using two-dimensional finite element analysis in the plane strain condition. This research provides both linear and nonlinear dynamic analyses of a roller-compacted concrete gravity dam considering the soil-structure-fluid interaction by using ANSYS 17.1 software. To evaluate the impact of hydrodynamic pressures on the dynamic response more accurately, different water modeling approaches (Westergaard and Euler) and an empty reservoir condition are used. Furthermore, the effects of foundation flexibility, Poisson's ratio, and the presence of alluvium on the seismic response are observed. Nonlinear analyses of the dam are performed using the Drucker Prager model. Based on the US Army Corps of Engineers (USACE) criteria, the seismic responses of the dam in terms of acceleration, displacement, and principal stresses are assessed. Additionally, the influence of the various parameters on the modal response of the dam is evaluated regarding natural frequency, the effective damping ratio, and Rayleigh coefficients.

The research reveals that obtained results related to 1st principal stresses from linear transient analyses are significantly higher than the results of nonlinear time-history analyses. On the other hand, linear time history analyses considerably reduce the 3rd principal stresses

compared to nonlinear dynamic analyses. However, linear analyses are useful methods to predict the displacements and accelerations on the crest of the dam because the results are substantially similar to the outcomes of nonlinear analyses. Based on the attained seismic responses of the Narli Dam from nonlinear dynamic analyses, maximum and minimum principal stresses never exceed the tensile and compressive strength of concrete. It can be concluded from the analyses that the heel of the dam is the high-stress region in terms of tension while the toe of the dam is more susceptible to compressive stresses. Hydrodynamic pressures significantly influence both the modal and dynamic responses of the dam. When the reservoir is considered in the finite element modeling and compared with the empty reservoir condition, tensile and compressive stresses grow up to 70%. On the other hand, the difference in the outcomes of Euler and Westergaard methods is approximately 10%. The foundation flexibility has a massive influence on the dynamic features of the dam and alters both the modal and seismic response of the dam. Highly flexible foundations suffer from excessive principal stresses. As the rigidity of the rock increases, the tensile and compressive stresses on the dam body decrease up to 50% and 70%, respectively. Furthermore, the Poisson's ratio of the foundation is the more effective factor that influences the seismic response almost 10% more than the Poisson's ratio of the concrete which alters the seismic response about 5%. If the thickness of the alluvium increases in the dam site, the dynamic response can change up to 10%.

ACKNOWLEDGEMENTS

I would like to express my sincere gratitude to my advisors, Dr. James Davidson and Dr. Jack Montgomery for their continuous guidance and encouragement throughout this project. The thesis would not have been possible without their endless patience and support. I am also grateful to my committee member, Dr. Justin Marshall, for his knowledge and advice concerning my graduate studies.

I would like to thank my sponsor, The General Directorate of State Hydraulic Works (DSI) in Turkey which has provided me with an excellent opportunity for my academic studies. I would also like to thank Mr. Seckin Aydin, who is my advisor in the DSI, for his help and suggestions on my thesis.

I would also like to deeply acknowledge Fulya Eda Kumral for her valuable contributions and helpful support on my thesis. I also thank my colleagues Anjan Ramesh Babu, Antonio Saldo, and Ufuk Sen for their friendship and help.

I am whole-heartedly appreciative to my lovely parents, Mrs. Pinar Kent and Mr. Sedat Kent, and my lovely sisters, Cagla Aycan and Dilara Kent, for their unwavering support, encouragement, and love during my life. Without you, my thesis would not have been possible. Lastly, I would like to thank God for providing me the ability, strength, knowledge, and opportunity to undertake this research.

TABLE OF CONTENTS

LIST OF TABLES

LIST OF FIGURES

LIST OF ABBREVIATIONS

RCC	Roller-Compacted Concrete
M	The Richter Magnitude
PGA	Peak Ground Acceleration
FEM	Finite Element Model
USACE	United States Army Corps of Engineers
USBR	United States Bureau of Reclamation
2-D	Two-dimensional
MDE	Maximum Design Earthquake
OBE	Operating Basis Earthquake
MCE	Maximum Credible Earthquake
DCR	Demand Capacity Ratio
ASCE	American Society of Civil Engineers
DOFs	Degree of Freedoms
EQs	Earthquakes
SI	System International

CHAPTER 1

INTRODUCTION

1.1 General

Dams have enabled a great contribution to the improvement of civilization over time and will continue to meet increasing requirements for power, irrigation, and drinkable water supplies. Moreover, dams are responsible for the preservation of lives, properties, and surroundings from disastrous floods. Concrete gravity dams, which are large hydraulic structures, are designed to enable flood control, irrigation, power generation, and other purposes. Using their own weight, they resist the external loads and protect their stability. Gravity dams must have enough strength to withstand both normal and extreme loads. While some gravity dams have a vertical face on the upstream side of the dam, others can have a light slope. On the other hand, the incline for the downstream side of the dams can differ between “0.7: 1’’ and “0.8: 1’’.

Roller-compacted concrete is used to build gravity dams because it results in fewer construction costs (e.g. material savings), and faster construction compared to earth-fill and rock-fill dams. Seismic analyses of RCC dams are often required to avoid the collapse of the structure which leads to excessive damage to properties and the loss of life. Cracking due to high principal stresses on the dam body is the most crucial safety issue when gravity dams are subjected to earthquakes.

One of the significant aims of performing a dynamic analysis is to determine the cost-effective design of a dam. Furthermore, the seismic analysis of concrete gravity dams should consider dam-reservoir-foundation interaction to determine the effects of foundation flexibility and water level. Therefore, dam-foundation-water interaction should be evaluated to obtain the most accurate results during time-history analyses (Chopra and Lokke, 2015). Moreover, hydrodynamic forces happen on the upstream face of the dam body due to the oscillation between the dam and reservoir and should be included in the analysis.

Dynamic analysis methods are associated with the dynamic features of the dam-foundation-water system, and ground motions determined for the construction site. Due to the rapid improvements of computer technology, the finite element model is widely used for not only linear dynamic analysis but also nonlinear analysis. Analysis results should include displacements and accelerations of the dam crest and principal stresses on the upstream and downstream faces of the dam. After completing the analyses, the determination of the over-stressed regions plays a significant role in estimating the possible cracking points on the structure.

The safety evaluation of the seismic response is a complex process and depends on some important factors such as using a proper model, boundary conditions, material properties, and the foundation-dam-water interaction. During the 20^{th} century, several seismic analyses of concrete gravity dams have been performed to understand how the dams behave towards the ground motions. According to previous records, the failure of dams generally occurs because of foundation issues (e.g. rigidity of the rock), bad construction, insufficient spillway, strong earthquakes, etc. (Thandavesware, 2009)

Some important examples of strong ground motions that have affected the dams across the world are described below:

1. **The Crystal Springs Dam** (California) is a 46.9 m high curved gravity dam that resisted the 1906 San Francisco Earthquake (moment magnitude M8.3, estimated) without any obvious damage (FEMA, 2005).
2. **The Koyna Dam** (India) is a 103.6 m high concrete gravity dam which withstood the Richter Magnitude M6.4 earthquake in 1967. While the peak horizontal acceleration was 0.51g, the peak vertical acceleration was determined to be 0.36g. Significant cracks have occurred on both upstream and downstream surfaces of the non-overflow sections. On the other hand, there were no cracks on the overflow sections of the dam. After performing the dynamic analysis of the dam, the results demonstrated that tensile stresses of non-overflow sections passed the tensile strength of the concrete up to three times. However, the tensile stresses of overflow sections were almost equal to the tensile strength of the concrete (FEMA, 2005).
3. **Hoover Dam** (Nevada) is a 221.2 m high gravity-arch dam which experienced the Richter Magnitude M5 and survived without any cracking (FEMA, 2005).
4. **Sengari and Aono** (Japan) are concrete gravity dams which were influenced by the Richter Magnitude M7.2 in 1995. The dams did not experience any damage due to ground motion because the dams are located on the sufficiently rigid foundation and felt minimal impacts of the earthquake (FEMA, 2005).
5. **Shih Kang (**Taiwan) is an example for the failure of a concrete gravity dam based on past records. The dam has a 21.4 m height and was affected by the Richter Magnitude M7.6 and failed under the 0.51g PGA in 1999 (USSD, 2017). The dam was also affected by fault rupture.

1.2 Objectives

The main objectives of the thesis are:

1. To determine the dam-foundation-reservoir interaction effects on the seismic response of the concrete gravity dam.
2. To identify the hydrostatic pressure effect on the earthquake analysis of the concrete gravity dam by using both the empty reservoir and full reservoir conditions.
3. To evaluate the durability of the dam using both linear and nonlinear dynamic analyses when the structure is subjected to several earthquakes.
4. To find out the impact of the foundation flexibility on the linear response of the structure.
5. To determine the influence of the Poisson's ratios on the dynamic response of the concrete gravity dam using linear time-history analysis.
6. To obtain the changes in the behavior of the dam under the presence of different alluvium thicknesses via linear dynamic analysis method.
7. To propose a theory on the proper combination of foundation flexibility, Poisson's ratio, and alluvium thickness.

1.2 Scope of the Research

The research has been reported in six chapters, and a summary of each section is described below.

Chapter 1: This section contains a brief explanation about the general characteristic features of concrete gravity dams, the need and objectives of carrying out the research, and some significant examples of occurred earthquakes that have impacted the dams.

Chapter 2: This chapter comprises a literature review of essential studies and methods which are relevant to concrete gravity dams.

Chapter 3: This chapter includes the modeling of the Narli Dam considering structure-fluid-foundation interaction.

Chapter 4: This chapter deals with modal, linear, and nonlinear dynamic analyses of the roller-compacted concrete gravity dam.

Chapter 5: This section includes the influence of several parameters on the seismic responses of the dam.

Chapter 6: This chapter summarizes the whole research and shows significant conclusions attained from the thesis.

CHAPTER 2

LITERATURE REVIEW

2.1 Review of Past Studies on the Dynamic Behavior of Dams

Some researchers have already worked on the seismic behavior of dams considering dam-reservoir-foundation interaction based on distinct water modeling techniques. Westergaard (1933), for example, performed the first hydrodynamic analysis for the dam-fluid systems and assumed water is incompressible. He came up with the idea that the effect of the reservoir should be created by added mass on the dam body to evaluate the linear response of the structure-fluid system. On the other hand, Chopra proposed that the water incompressibility estimation does not provide the exact impact of hydrodynamic pressure on the dam body (Chopra, 1967; Chopra, 1970). Based on Chopra's studies, the dam and reservoir only interacted with each other at the dam-reservoir interface. Furthermore, the infinite reservoir must be interrupted using proper boundary condition to simplify the finite element modeling. "Sommerfeld boundary condition" is an appropriate boundary to truncate some portion of the reservoir. Chopra and Hall (1982) evaluated the impact of hydrodynamic pressure on the seismic response of the dam using time-domain analysis. In work presented by Fenves and Chopra (1985), the structure-fluid-rock interaction using frequency-domain analysis has been studied, and they found that the bottom absorption of rock increases the effective damping ratio of the system while it reduces the structure response under dynamic loading conditions. Zienkiewicz and Taylor (1991) provided the solution of equations of motion

for the reservoir-structure using FEM. Fathi and Lotfi (2008) carried out the dynamic analysis of concrete gravity dams using different reservoir lengths. They claimed that when the reservoir length increases, the rigidity of the foundation reduces and oscillation between foundation and reservoir is inclined to vanish. Bayraktar (2009,2010) considered near- and far-field ground motion conditions in the seismic analyses of the concrete gravity dams. Based on the results, plastic deformations of the structure exposed to near-fault ground motions increase compared to far-field earthquakes. Akkose (2010) investigated the nonlinear seismic performance of the concrete gravity dams considering dam-reservoir-foundation-sediment interaction and far- and near-fault ground motions. According to the nonlinear results, the crest displacements of the dam grow if near-fault ground motions are considered instead of far-fault ground motions. However, the accelerations of the dam crest do not change when the location of the earthquake is altered. Sevim et al. (2011) studied the influence of reservoir length and height on the seismic behavior of dam-reservoir-foundation interaction system by performing the Lagrange approach. Depending on the dynamic analysis results, if the reservoir length increases, the results associated with displacements and principal stresses of the dam rises. Moreover, principal stresses generally tend to become higher from the base to the crest of the structure. It is clear that there is insufficient research for the dynamic analysis of gravity dams considering dam-foundation-water interaction using distinct water approaches and their comparisons.

2.2 Dam Concrete Properties

Concrete for a gravity dam design must fulfill the design criteria relevant to strength, durability, permeability, and any other essential features (USBR, 1977). The strength and elastic features of roller-compacted concrete dams are based on the mix components and mix rates. Notably, the quality of aggregate and the water-cement ratio are the primary determinants that

impact the strength and elastic features of the concrete. The compressive strength, tensile strength, shear strength, Young's Modulus of elasticity, Poisson's ratio, and unit weight of concrete are important factors in the seismic analysis is performed (USACE, 1995a). It is an well recognized that Poisson's ratio and modulus of elasticity for both concrete and foundation impact the stress distributions in the dam significantly (USBR, 1977). As the concrete strength increases, the modulus of elasticity will also increase.

In terms of the durability of structures, the minimum compressive strength of RCC should generally be at least 14 MPa (USACE, 1995a). However, higher compressive strengths can be necessary to meet the required tensile and shear strength if the site of the dam is under high seismicity. Therefore, the compressive strength must be increased if the tensile stresses calculated by a preliminary analysis on the dam body exceed the estimated tensile strength of the dam. Otherwise, excessive tensile cracking may take place on the structure.

2.3 Finite Element Modeling

Two-dimensional modeling in the finite element method is usually suitable for gravity dams (USACE, 1995b). The dam, reservoir, and rock sections are modeled as a compound structural system when using the standard finite element method (USACE, 2003). The dam body and foundation can often be assumed linear, isotropic, and homogenous, but it is important to verify these assumptions.

During finite element modeling processes, plane stress or plane strain can be used for the selected elements. Both of them have three components: X normal stress, Y normal stress, and XY shear stress. However, while the plane stress elements assume the out of plane stress is zero, the plane strain elements assume the out of plane strain is zero. For the analyses presented in this

paper, the plane strain condition is considered, and the Gauss numerical integration method is performed for the calculation of the element matrices. To solve the equations of motion, the Newmark method that considers Rayleigh damping in the analysis is applied. When computing the analysis of dams, maximum displacements and accelerations, 1st and 3rd principal stresses, and 1st and 3rd mechanical principal strains are attained.

Concrete gravity dams, as shown as a typical cross-section in Figure 2.1, are built as monoliths which are divided by transverse contraction joints. The 2-D model of the tallest monolith or cross-section is generally used for the standard finite element procedures (USACE, 2003). The finite element model is able to model the resistance mechanism of the dam because the process considers the dynamic conditions of the structure-reservoir-rock system and the features of ground motions (USACE, 2003). Finite element modeling considering structure-rock interaction is a useful tool for linear elastic static and dynamic analyses and nonlinear analyses since complicated geometries, and various material properties can be used for the analyses (USACE, 1995b). The boundary conditions that are used for this research differ from the boundary conditions which are illustrated in Figure 2.1.

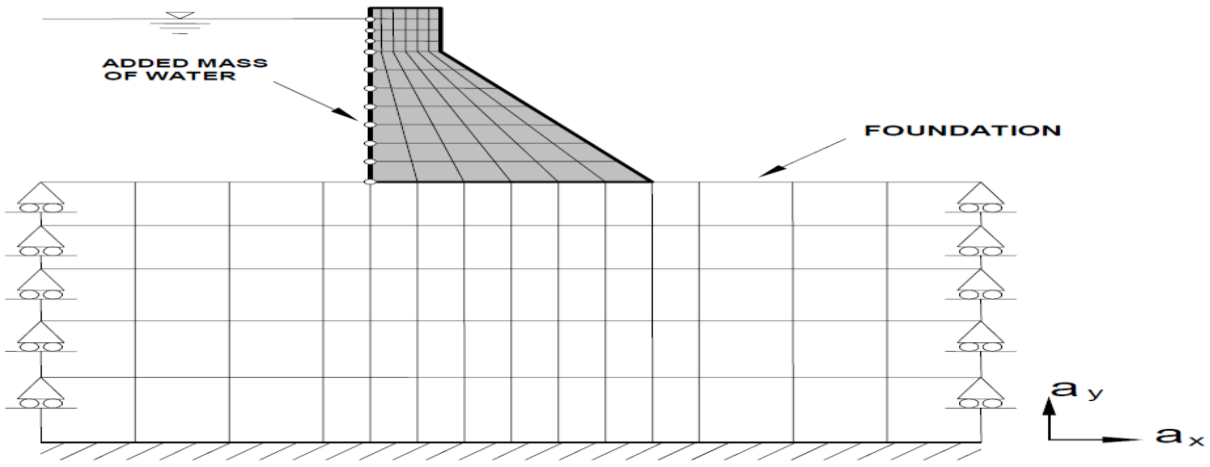

Figure 2.1 Typically Finite Element Model of Gravity Dam (USACE, 2003)

2.4 Reservoir Modeling Approaches

The hydrodynamic pressure from the reservoir influences the dynamic response when the structure is exposed to ground motions because it changes mode shapes and the values of modal frequency and effective damping ratio (USACE, 1995a). Thus, it should be included in the dynamic analysis using proper methods such as Westergaard and Euler approaches.

2.4.1 The Westergaard Method

In 1933, Westergaard created the added mass method which is shown in Figure 2.2. According to the method, the dam is assumed as a rigid body and semi-infinite. The surface waves in the reservoir are disregarded. The distribution of water pressure happens along the upstream surface and thus added masses should be calculated using the distribution of hydrodynamic forces on the dam body. It is clear that the pressure will change depending on the depth of fluid. As a result, the dam-reservoir interaction can be used as an equivalent added mass model of water when the reservoir water is estimated to be incompressible.

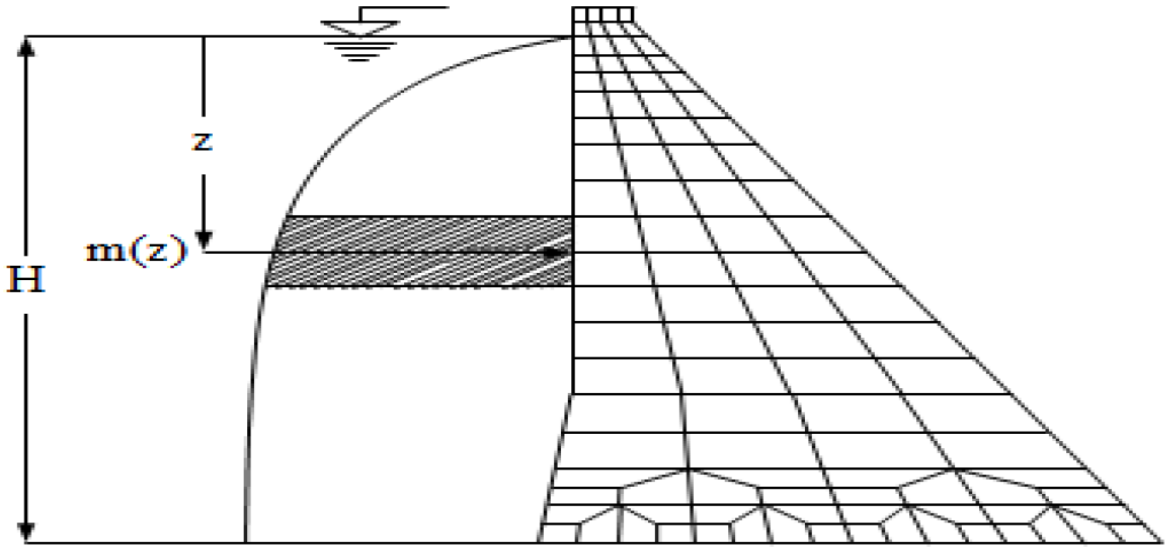

Figure 2.2 Distribution of the Hydrodynamic Pressure on Finite Mesh (Altunisik and Sesli, 2015)

Added mass can be determined using the following formula (Westergaard, 1933):

$$m(z) = \frac{7}{8} \cdot \frac{w}{g} \cdot \sqrt{H \cdot z} \tag{2.1}$$

where m(z), w, g, H, and z are mass distribution based on the depth of water, unit weight of water, acceleration of gravity, maximum depth of reservoir, and water depth from the top surface, respectively.

2.4.2 The Euler Method

The Euler method is frequently preferred for the finite element analysis when fluid-dam interaction is considered. In this method, the structure is measured by displacements while water behavior is expressed with pressures. Particular interface equations must be defined because the structure and fluid move together depending on the water-dam interface.

The behavior of compressible, non-viscous, and non-rotational water exposed to small displacements is explained as the wave equation in the literature (Cook et al., 1989; Zeinkiewicz and Taylor, 1991).

$$P_{,xx} + P_{,yy} + P_{,zz} = \left(\frac{1}{C^2}\right) \cdot \left(P_{,tt}\right) \tag{2.2}$$

in which x, y, and z represent coordinates. C, $P_{,ii}$, and t are wave velocity of water, the second derivative of hydrodynamic pressure based on i variable and time, respectively.

Hydrodynamic pressures occur due to boundary conditions. Some proper boundary conditions in the literature are shown below:

$$P = 0 \text{ (when there is no wave on the free surface)} \tag{2.3}$$

$$P = p \cdot g \cdot u_{sf} \quad \text{(when there are waves on the free surface)} \tag{2.4}$$

$$P = p \cdot \ddot{u}_n \tag{2.5}$$

in which p, g, $\ddot{u}_n$, and u_{sf} are referred to the mass density of water, acceleration because of gravity, acceleration of fluid in the normal direction, and displacement of fluid in the vertical direction, respectively.

Since surface waves can often be ignored when modeling dams (Chopra, 1967), the impact of fluid surface waves is not considered in this research. The equation of motion of fluid for the finite element method can be written as:

$$\left[M^p{}_f\right] \cdot \{P''\} + \left[K^p{}_f\right] \cdot \{P\} = -p \cdot [R]^T \cdot \{\ddot{u}_{fs}\} \tag{2.6}$$

in which $[M^p{}_f]$, {P"}, $[K^p{}_f]$, {P}, $[R]^T$, and $\{\ddot{u}_{fs}\}$represent mass matrix, vector for second derivative of hydrodynamic pressure, stiffness matrix, vector for hydrodynamic pressure, matrix for fluid-structure interface and vector for accelerations due to only dam structure in the water-dam interface, respectively.

On the other hand, the dynamic equation of motion for the structure can be written as:

$$[M_s] \cdot \{\ddot{u}_s\} + [C_s] \cdot \{\upsilon_s\} + [K_s] \cdot \{u_s\} = \{F\} + \{F_{fs}\} \tag{2.7}$$

where $[M_s]$, $\{\ddot{u}_s\}$, $[C_s]$, $\{\upsilon_s\}$, $[K_s]$, $\{u_s\}$, {F}, and$\{F_{fs}\}$ are mass matrix for the structure, the vector for acceleration of structure, damping matrix, the vector for velocity, stiffness matrix of the structure, displacement vector, the vector of external load, and the vector for additional external load, respectively.

Using the virtual work principle, the vector $\{F_{fs}\}$ can be expressed with the following formula:

$$\{F_{fs}\} = [R] \cdot \{P\} \tag{2.8}$$

By combining the Equations [2.6] and [2.7], the dynamic equation of motion for the whole fluid-structure system can be written as:

$$\begin{bmatrix} [M_{sn}] & [0] \\ [M_{fs}] & [M_{pf}] \end{bmatrix} \cdot \begin{pmatrix} \ddot{u}_s \\ P'' \end{pmatrix} + \begin{bmatrix} [C_s] & [0] \\ [0] & [0] \end{bmatrix} \cdot \begin{pmatrix} \upsilon_s \\ P' \end{pmatrix} + \begin{bmatrix} [K_s] & [K_{fs}] \\ [0] & [K_{pf}] \end{bmatrix} \cdot \begin{pmatrix} u_s \\ P \end{pmatrix} = \begin{pmatrix} F \\ 0 \end{pmatrix} \tag{2.9}$$

where $[M_{fs}] = p \cdot [R]^T$ and $[K_{fs}] = -[R]$

2.5 Fluid-Dam-Foundation Interaction

Stress distributions related to the dam body are influenced by foundation deformations (USBR, 1977). Furthermore, stress distributions in the foundation are affected by external loads and deformation of the foundation, which are related to the response of the dam and reservoir. Thus, proper foundation properties are necessary to determine the accurate seismic analysis of the dam (USBR, 1977). The foundation and dam interaction ratios such as the elastic modulus for foundation divided by the modulus elasticity of the concrete (E_f/E_c) can be used for the determination of the impact of foundation flexibility on the dynamic response of the dam (Bakenaz, 2014).

Dynamic characteristics of dams can be influenced by both the hydrodynamic effects on the structure and dam-foundation-water interaction because the dam and water behave differently due to hydrodynamic pressures during an earthquake event. Since the length of the reservoir is wide, it should be interrupted at the sufficient distance from the dam body. The length of the

reservoir should be selected as sufficiently large to obtain nearly accurate results in comparison to results for the infinite length of reservoir water (Brahtz and Heilbron, 1933). The reservoir length should be selected at least two or three times its depth for the accurate evaluation of the hydrodynamic effects on the dam. To determine the reservoir effect more precisely, the Eulerian-Lagrangian method should be used. The gravity dam-reservoir interaction occurs due to hydrodynamic pressures, which influences the structure deformations at the dam-reservoir interface (USACE, 2003). When considering this interaction, the energy loss can impact the pressures at the water boundary. Uncertainty on the boundary conditions of the fluid-dam-foundation interaction still persists in current analyses.

Due to the different material behavior of foundation, reservoir, and dam structure, interaction among them should be considered during the dynamic analysis. To evaluate the effect of hydrostatic pressure distribution in the results, the first analysis should be performed with an empty reservoir condition, and then the second analysis should be performed with the presence of water on the finite element model.

2.6 Static Analysis

A static analysis of the structure defines the impact of steady-state loading conditions on it without using the time-dependent load effects such as inertia and damping. The displacements, stresses, forces, and strains in the structure can be evaluated by carrying out the static analysis. The static response of both the loads and the properties of the structure are to change slowly with time (ANSYS, 1999).

According to the static analysis, the dam is a 2-D solid block. Before using other analysis methods such as modal and linear dynamic analyses, the static analysis should be performed. It is

a fact that the toe of the dam body does not create sufficient stress distribution in the foundation when static analysis is used. This situation leads to underestimated base cracking.

2.7 Modal Analysis

The modal analysis calculates the natural frequencies and mode shapes which are significant factors for the structure design when considering seismic conditions. These parameters are also called the vibration characteristics of a structure. The modal analysis exclusively considers the linear behavior of a structure and thus any nonlinear properties will be neglected during the analysis (ANSYS, 1999). There are several methods in the modal analysis such as Block Lanczos and Unsymmetric methods. While the Block Lanczos method is only valid for symmetric eigenvalue problems the Unsymmetric method is generally used for water-structure interaction problems that are composed of nonsymmetric matrices.

The modal analysis approach depends on the simplifying response estimation of each natural mode of vibration separately and the total modal responses might be calculated with the combination of each vibration mode (Chopra, 1987). The response of the higher modes of vibration, foundation-water interaction effects, and the horizontal and vertical accelerations of the earthquake are neglected in this approach, but can be considered in the finite element method.

2.8 The Procedure of a Dynamic Analysis

The primary objective of performing a dynamic analysis is to determine the damage level of the structure during earthquake motion.

The procedure of the dynamic analysis comprises the following steps (Subramani and Ponnuvel, 2012):

1) Review the geological condition and seismologic features of the site where the dam is constructed.

2) Determination of the ground motion sources.

3) Selection of the maximum credible and operating basis earthquakes for the area.

4) Selection of the response spectra for the selected earthquakes.

5) In the case of the time-history analysis, selection of the most proper acceleration records which is suitable to the response spectra.

6) Determination of the dynamic material properties for the dam, foundation, and fluid.

7) Selection of the dynamic analysis method.

8) Performing the dynamic analysis.

9) Evaluation of displacements, accelerations, and stresses from the results of the dynamic analysis.

There are four characteristics which define a specific dynamic analysis method (USACE, 1995a):

1) Material behavior: can be either linear-elastic or nonlinear behavior.

2) Design Earthquake description: could be either a design response spectrum or time-history ground motion.

3) Dimensional type: may be either two-dimensional or three-dimensional representation.

4) Model format: can be a standardized model, finite element equivalent mass design, and finite element-substructure type.

2.9 Transient Dynamic Analysis

Transient dynamic analysis, which is also defined as the time-history method, is generally used to determine the seismic response of a structure under the time-domain loads. By performing this type of method, the time-dependent displacements, strains, stresses, and forces of the system can be determined considering the combination loads such as static and dynamic loads (ANSYS, 1999). Although the method is similar to the response spectrum method, the form of the earthquake is the acceleration of time histories instead of response spectra, and the results are in the form of displacement and stress histories.

The time-history method is employed to calculate deformations and stresses more precisely by using the nature of the seismic response to ground motions (USACE, 2003). When acceleration records are applied in the time-history method, the linear analysis calculates the seismic response as both magnitudes and time-varying features. Transient dynamic analysis has three types of solutions: full, reduced, and mode superposition methods. The full method solves the matrices without using reduction in the matrices, and thus it is the most powerful method in the possible solutions. However, the full method is considerably expensive in comparison with the other two types of the time-history method (ANSYS, 1999).

Either direct integration or mode superposition methods can be used to solve equations of motion for hydraulic structures (USACE, 2003). The direct integration approach implements a combined form, which is a step by step method, for the equations of motions without using any distinct form. On the other hand, the mode superposition approach first converts the equations into modal forms and then solves the equations as a step-by-step combination in the time domain (USACE, 2003).

The time-history method is one of the dynamic modal methods and enables more meticulous solutions because vibration for each mode is calculated using the Duhamel integral technique and all mode responses are algebraically added to each other using the time step technique until the end of the earthquake motion. Even if the time-history method is more accurate than the response spectrum method, it should be performed based on several ground motions to avoid wrong consequences.

The response spectrum method could be used for the assessment of structures when the dams are exposed to experience low or moderate earthquakes (USACE, 2003). However, the restricted representation of the dam-water-foundation impacts, and the neglecting of the time-domain features of the earthquake and structural response are some limitations for the method that does not present valuable time-dependent knowledge. Thus, the time-history method should be selected to avoid these limitations of the response spectrum method and to attain more accurate representation for the time-domain characteristics of the earthquake and structure (USACE, 2003).

2.9.1 Seismic Design

There are a lot of significant factors that influence the response of the dam significantly such as the types of materials, strength parameters, and loading conditions (USACE, 1995a). The impact of each factor must be considered in the seismic design. This evaluation could be performed using a basic cross-section of the dam and material properties. Each factor should also be modified separately to obtain the impact of each parameter on the seismic response. On the other hand, pore pressures, temperature stresses, and wind and ice loads are not significant parameters on the seismic evaluation of the gravity dam (USACE, 1995a).

The most critical dynamic factor is the inertia load generated by the response of the dam body to ground motion accelerations applied by the earthquake (USACE, 1995a). The structural response for the vertical component of ground motions can be similar in amplitude caused by horizontal earthquake motions, and both directions should be evaluated in the analysis (Chopra, 1987). The next significant factor is the hydrodynamic effect resulted from the high reservoir condition (USACE, 1995a). Frequency-dependent hydrodynamic pressures resulting from fluid-structure interaction can be evaluated as an added force, an added damping and an added mass (Chopra, 1987).

To perform the internal stress analysis of the dam in severe seismicity sites, a dynamic seismic analysis must be applied (USACE, 1995b). The structural response associated with characteristics of the dam and foundation and the character of the ground motion can be determined with a dynamic analysis. A 2-D finite element model is generally checked for both vertical and horizontal directions. Although the earthquake can happen in any direction, the seismic analysis should be applied for the unfavorable direction (USACE, 1995b). The maximum ground motion in the vertical direction has frequently been selected as 1/2 or 2/3 of the seismic load in the horizontal direction. Also, the peak acceleration in the vertical direction can be similar to the peak horizontal acceleration or can exceed this value (FEMA, 2005).

The ground motion stemmed from the seismic behavior may lead to micro or minor cracks on the RCC dam. Seismic vibrations must be decreased using convenient practices of dam engineering principles. At this point, the proper evaluation of seismic behavior of concrete gravity dams is a significant criterion to reduce the seismic vibrations. Additionally, the design earthquake should be performed using the 5% of critical damping for just the concrete dam body. However,

the damping ratio of the concrete dam body must be altered with the foundation damping to represent the whole system (USACE, 1995a).

2.9.1.1 Maximum Design Earthquake

MDE is referred to as the maximum design earthquake for which a structure is evaluated. The structure must illustrate performance without significant failure when subjected to MDE. However, severe damage or economic loss may be acceptable (USACE, 2003). On the other hand, while ground motions related to Operating Basis Earthquake (OBE) can be seen as unusual forces, Maximum Design Earthquake (MDE) is attributed to extreme loads (USACE, 2007). In accordance with MDE, the ground motion can exceed 10% over an expected earthquake for the construction site in a century. The Maximum Credible Earthquake (MCE), which is the maximum earthquake that is expected to happen, can be accepted as similar with MDE for the critical structures (USACE, 2007).

If structures demonstrate enough strength to remain almost elastic when exposed to MDE, linear analyses are acceptable. It is important to note that concrete gravity dams subjected to MDE ground motions may perform within the inelastic range, but they should respond in the linear-elastic-range when exposed to Operating Basis Earthquake (OBE) (USACE, 2007).

The strength design code for the MDE conditions of the hydraulic structures can be expressed with the following formula (USACE, 2007):

$$Q_{DC} = Q_D + Q_L + Q_{MDE} \tag{2.10}$$

in which Q_{DC} is the combined response because of dead, live, and seismic loads to determine safety evaluation of the dam. Q_D, QL, and Q_{MDE} are dead, live, and earthquake loads, respectively. The live load effect is represented by the hydrostatic forces.

2.9.1.2 Equations of Motion

The equations of motion are computed based on the degrees of freedom with effective forces for hydraulic structures (Clough and Penzien, 1993). The matrix form can be expressed as:

$$m \cdot \ddot{u}(t) + c \cdot \upsilon(t) + k \cdot u(t) = p(t) \tag{2.11}$$

in which m, c, and k are mass, damping, and stiffness matrices, respectively. ü(t), υ(t), and u(t) are acceleration, velocity, and displacement vectors, respectively. p(t) represents the load effect of a ground motion. If the foundation-water-structure interaction is included in the finite element model, the matrices and load factor must contain the interaction contribution effects (USACE, 2003).

In the standard finite element method, when massless foundation and incompressible water are selected, the mass matrix m comprises not only the mass of the dam but also the added mass of fluid. Similarly, the stiffness matrix k contains the stiffness from both structure and foundation. Additionally, the load factor is combined with ground motion and inertia effects resulting from the dam mass and added mass of water.

2.9.1.3 Rayleigh Damping

Rayleigh damping is used to model the other sources of damping that are not captured in the analysis. Rayleigh damping is not fundamental, and it is just a computationally simple way to include damping. Hence, it can be used for performing seismic analysis of hydraulic structures.

As a simple explanation, a damping matrix can be formed with the linear combination of mass and stiffness matrices and applying Rayleigh damping coefficients.

$$[C] = \alpha \cdot [M] + \beta \cdot [K] \tag{2.12}$$

where α and β are Rayleigh damping coefficients. [C], [M], and [K] are damping, mass and stiffness matrices, respectively.

Rayleigh damping coefficients can be calculated using frequency values obtained from the modal analysis and with selected proper viscous damping (ANSYS, 1999).

$$\alpha = 2 \cdot \xi \cdot \frac{w_1 \cdot w_2}{w_1 + w_2} \tag{2.13}$$

$$\beta = \frac{2 \cdot \xi}{w_1 + w_2} \tag{2.14}$$

in which ξ and w represent viscous damping and natural frequencies of the system, respectively.

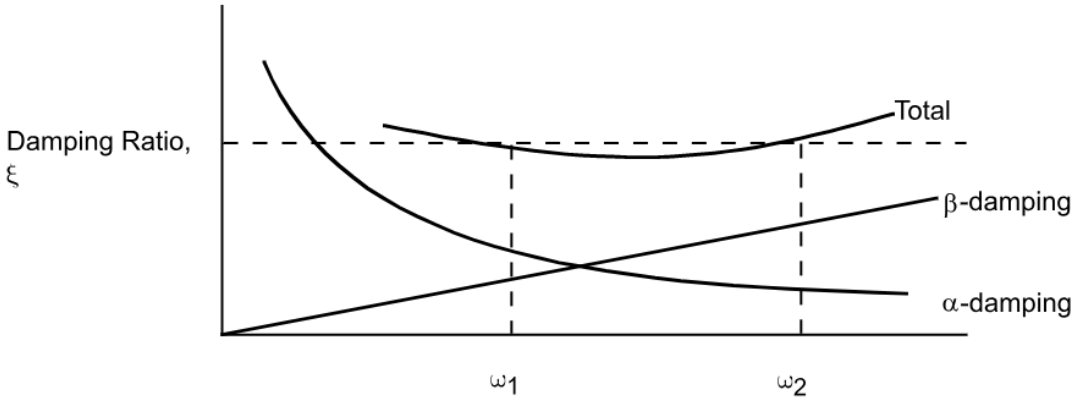

Figure 2.3 Rayleigh Damping (ANSYS, 1999)

2.9.2 Massless Foundation Modeling

The design earthquake should be performed considering the 5% of critical damping for just the concrete dam body. However, the damping ratio must be altered with the foundation damping. The two characteristic features of the foundation are the modulus of elasticity and damping ratio which have a considerable contribution to the seismic response (USACE, 1995a).

Instead of using only the damping ratio of the dam body, the damping ratio of the connected dam-foundation model must be applied in the dynamic analysis.

It is important to note that if the modulus of elasticity for rock is low, the damping ratio of the connected system is significantly higher than the damping ratio of the concrete structure alone. The foundation has two types of damping: (1) material and (2) radiation. Thus, the effective viscous damping ratio of the connected model is required to represent the whole system in the analysis (USACE, 1995a).

The simplified earthquake analysis method, created by A. K. Chopra, depends on the fundamental mode of vibration (Fenves and Chopra, 1987). The fundamental frequency values of the finite element model must be obtained to determine the impact of the damping ratio on the dynamic response of the concrete. The damping parameter for the rock can have a significant contribution to the seismic response, so it should be determined carefully (USACE, 1995a).

The effective damping ratio for the whole system can be determined using the following graphs and formulas in Figure 2.4 and the Equations 2.15 and 2.16 (Fenves and Chopra, 1987).

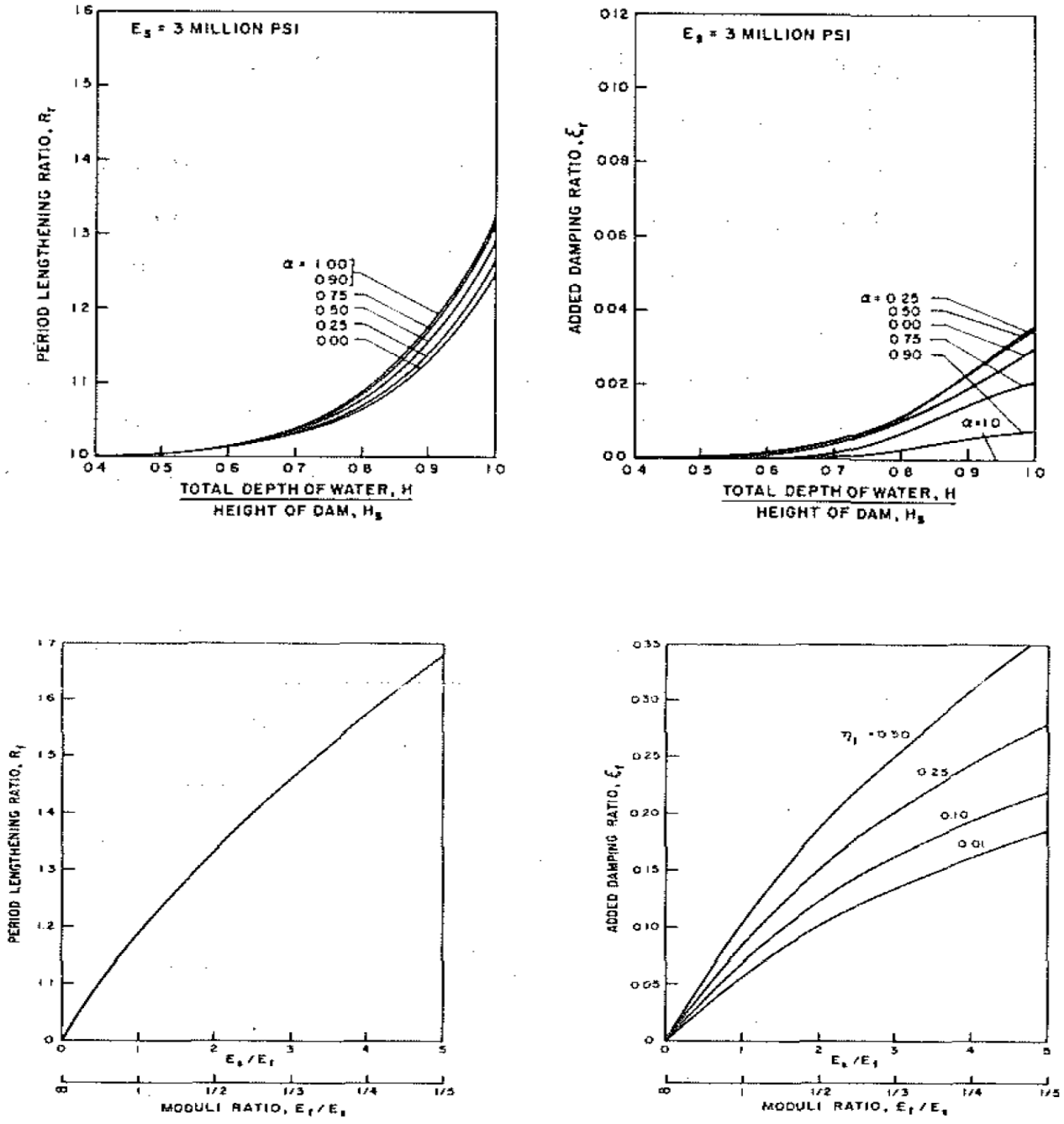

Figure 2.4 Chopra's Graphs for the Massless Foundation Dynamic Analysis Method (Chopra and Fenves, 1987)

The Effective Damping Ratio Formula for Full Reservoir Condition (Chopra and Fenves, 1987):

$$\xi = \left(1/R_r\right)\cdot\left(\xi_1/R_f^{\,3}\right)+\xi_f+\xi_b \qquad (2.15)$$

The Effective Damping Ratio Formula based on Empty Reservoir Condition (USACE, 1995a):

$$\xi_{eff} = \left(1/R_f^{\,3}\right)\cdot\left(\xi_1\right)+\xi_f \qquad (2.16)$$

Where

ξ = the effective viscous damping ratio for the full reservoir condition

ξ_1 = the viscous damping ratio for the gravity dam only

ξ_{eff} = the effective viscous damping ratio based on the empty reservoir condition

R_f = the ratio of the deformation modulus of foundation to Young's modulus of concrete

R_r = the ratio of total depth of water to the height of the dam

ξ_f = added damping ratio because of structure-foundation interaction taken from Figure 2.4

ξ_b = added damping ratio due to hydrodynamic effects taken from Figure 2.4

2.9.3 Linear Elastic Analyses

A dynamic analysis should begin with simplified techniques and pursue a more complex analysis as needed (USACE, 2003). Unit weight, Young's Modulus, and Poisson's ratio of the concrete should be applied in the linear seismic analysis. It is important to note that if the seismic analysis considers the foundation in the model, the modulus of elasticity and Poisson's ratio of the

rock are necessary for the analysis. Structural properties remain constant within each time-step for linear elastic behavior.

The selected earthquake is used as an inertial force implemented statically to the dam body because of the horizontal acceleration of the structure (USACE, 1995b). The other type of loading is called hydrodynamic forces, which are caused by the reservoir towards the structure. Depending on static and dynamic conditions of the structure, the stress analysis is performed to identify the stress distributions on the dam body and structural sufficiency of the rock.

If the linear-elastic time-history analysis is implemented, the allowable tensile stress will be the primary criterion to evaluate the acceptable response (USACE, 1995a). The dynamic response is evaluated as admissible for linear analysis when the tensile stresses are within allowable values. If the ground motion results in critical tensile cracking at the dam body-rock interface, more refined analyses are required to determine cracking such as a nonlinear time-history method (USACE, 1995a). As shown in Figure 2.5, the regions that are more susceptible to tensile cracking should first be evaluated using linear seismic analysis and pursue more refined analyses if needed. Also, the regions that are more prone to tensile cracking, as shown in Figure 2.5, can change due to the geometry of the dams.

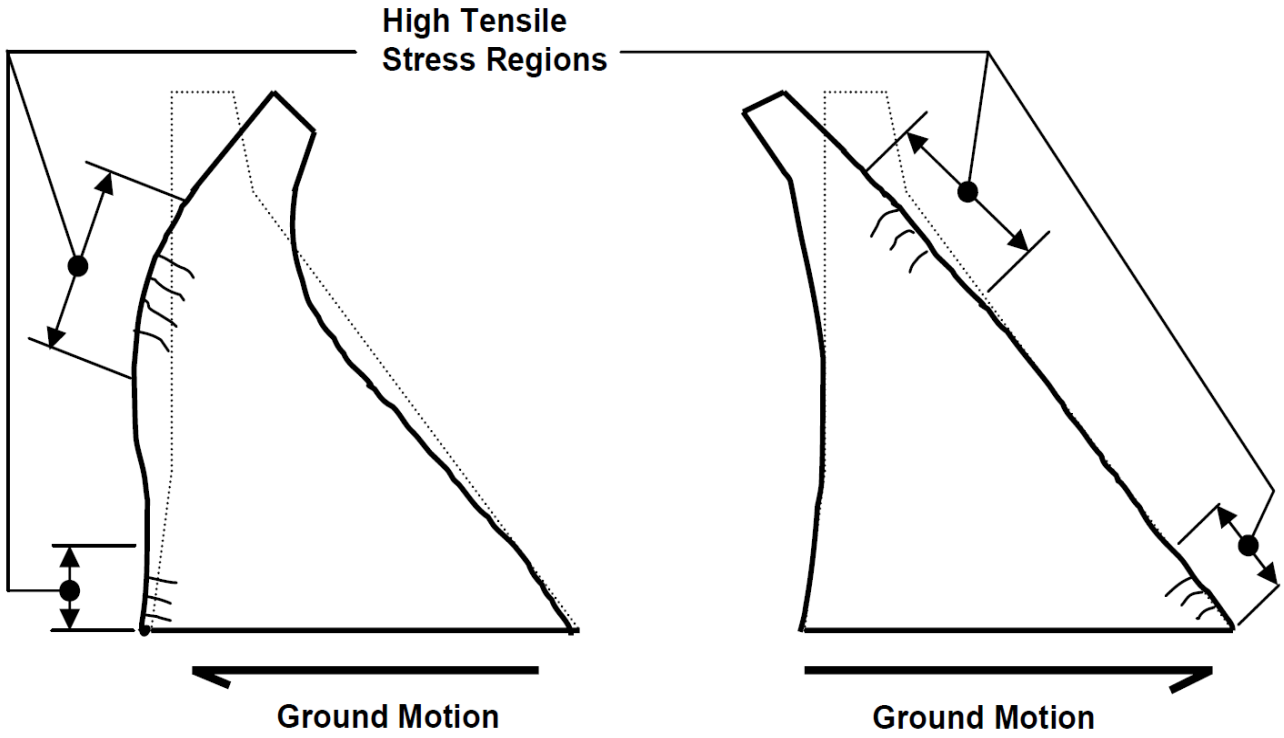

Figure 2.5 High Tensile Stress Regions for Gravity dam exposed to Ground Motions (USACE, 2007)

When ground motions resulting from earthquakes occur in the upstream direction, the heel of the dam and high-level water areas will be more susceptible to tensile cracking. If ground motions happen in the downstream direction, on the other hand, slope discontinuity areas and the toe of the dam will be critical for the potential cracking.

According to the acceptance criteria of compressive stresses, the compressive strength of concrete should be higher than 1.5 times the compressive stresses for new hydraulic structures (USACE, 1995a; USACE, 2000). In general, the tensile strength of concrete should be higher than the tensile stresses. If the tensile stress exceeds more than 150% of the flexural strength, evaluation of cracking must be determined using the nonlinear analysis (USACE, 1995b).

Linear analysis is adequate if the estimated damage level is under the acceptance curve, which is shown in Figure 2.6, for the dam structure. Otherwise, massive damages must be evaluated using a nonlinear time-history analysis, which is a type of more refined analyses (USACE, 2003). The dam response will be in the linear elastic range with no significant damage when the demand-capacity ratio is less than or equal to 1. Furthermore, the nonlinear response of the structure will be acceptable if the demand-capacity ratio does not exceed 2.0 (USACE, 2007).

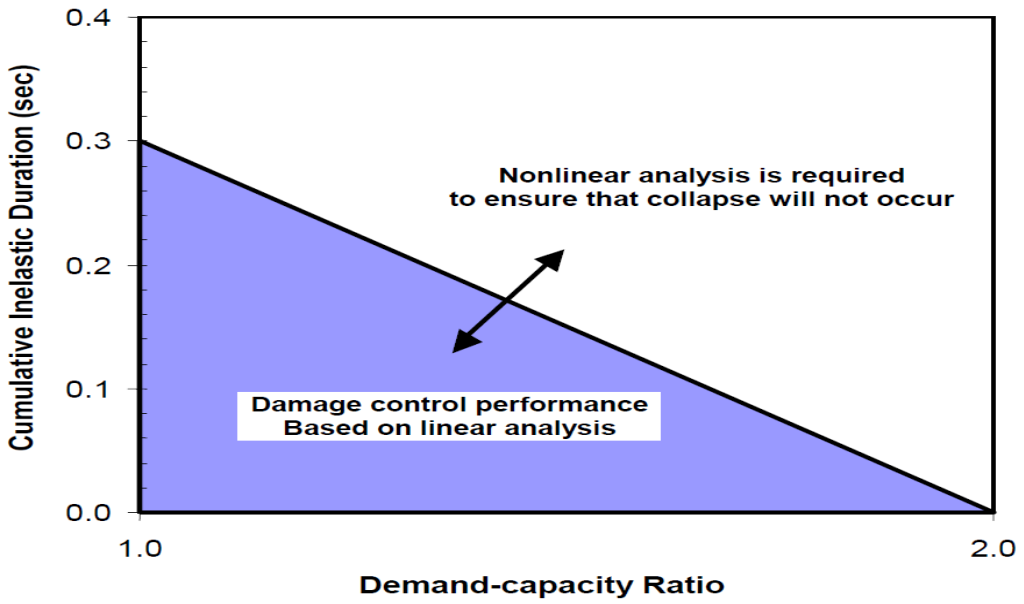

Figure 2.6 Performance Curve for Concrete Gravity Dams (USACE, 2007)

Although tensile cracking in new gravity dams located in severe seismic areas, and in existing dams established in all seismic areas is permitted, it should be restricted to minor cracking that needs little repair (USACE, 1995a).

The dynamic response of the structure is acceptable when the DCR (demand-capacity ratio) for each result is less than or equal to the allowable value (DCR ≤ Allowable value).

2.9.4 Nonlinear Time-History Analysis

Nonlinear time-history analysis is the most effective method to determine the seismic response of structures since the method contains the direct integration procedure for the equations of motion (USACE, 2007). By using this procedure, the displacements and stresses can be identified within short time increments from the initial conditions. Thus, the method uses the procedure associated with the step-by-step integration. Through this method, the equations of motion could be established for the initial condition and after each short time increment (USACE, 2007). One of the most important advantages of the time-history method is that it can be performed for not only linear analysis but also for nonlinear analysis.

During nonlinear transient dynamic analysis, the induced stresses and displacements are obtained from the direct integration procedure for the equations of motion, which is a step-by-step integration method (USACE, 2007). Acceleration time histories for the earthquake demands should be computed as a seismic input for the nonlinear dynamic analyses. Then, the results should be compared with the capacity of the structure and decided for whether the performance is sufficient or not (USACE, 2007). Based on nonlinear dynamic analysis results, the designer should be decided on whether the tensile cracking leads to the failure of the dam.

2.9.4.1 The Drucker Prager Model

The Drucker Prager model is applicable to granular (frictional) materials such as concrete and rock. The yield surface of this approach, which is illustrated in Figure 2.7, is pressure dependent (ANSYS, 1999).

$$\sigma_e = 3 \cdot \beta \cdot \sigma_m + \left[1/2 \cdot \{s\}^T \cdot [M] \cdot \{s\} \right]^{0.5} \quad (2.17)$$

where σ_e, β, and σ_m are the modified equivalent stress, a material constant, and hydrostatic pressure, respectively.

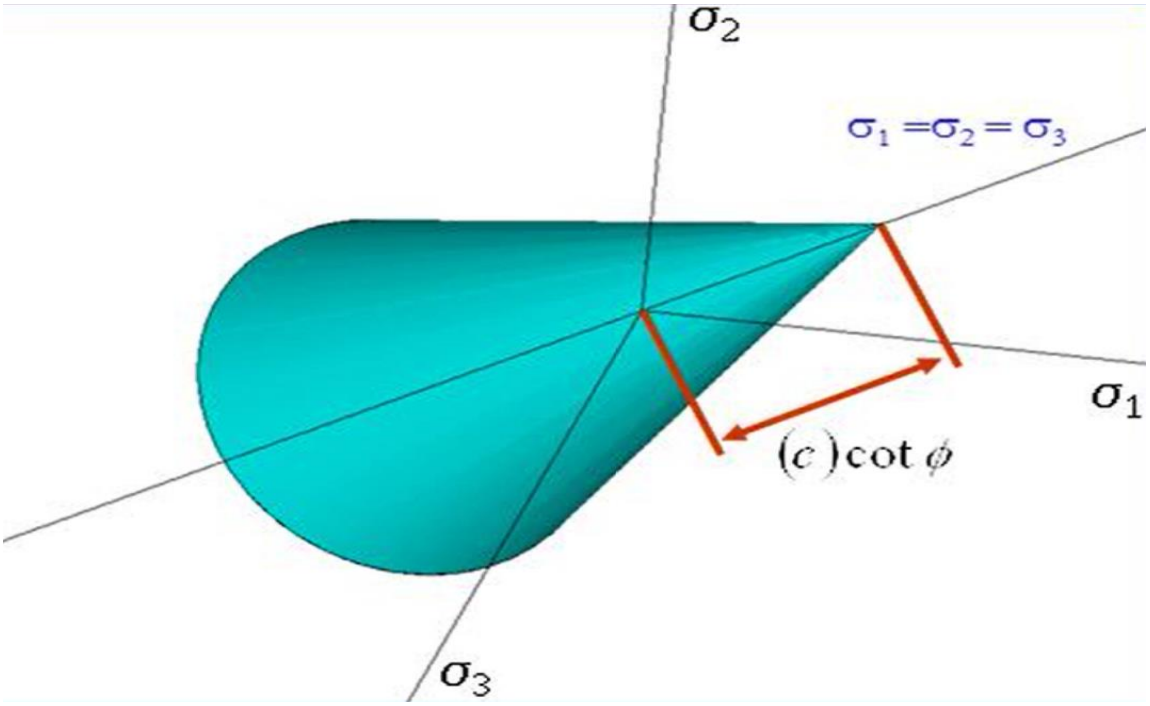

Figure 2.7 Yield Surface for Drucker Prager Plasticity (ANSYS, 1999)

If the increase takes place in hydrostatic pressure σ_m, this situation leads to an increase in the yield strength σ_y when the material is in the compression part.

Since the hardening part of the element is not used in this thesis, the material is elastic-perfectly-plastic. Also, the yield criterion of the Drucker Prager plasticity model can be expressed in the following form (ANSYS, 1999):

$$\sigma_e = 3 \cdot \beta \cdot \sigma_m + \left[1/2 \cdot \{s\}^T \cdot [M] \cdot \{s\} \right]^{0.5} - \sigma_y \qquad (2.18)$$

The material constant β and yield strength σ_y are defined as (ANSYS, 1999):

$$\beta = \frac{2 \cdot \sin\phi}{\sqrt{3} \cdot (3 - \sin\phi)} \tag{2.19}$$

$$\sigma_y = \frac{6 \cdot (c).\cos\phi}{\sqrt{3} \cdot (3 - \sin\phi)} \tag{2.20}$$

in which ϕ represents the angle of internal friction and c is cohesion (shear yield stress).

The yield stress in compression is a higher value compared to the yield stress in tension. When uniaxial tensile σ_t and compressive σ_c yield stresses are known, these values can be transformed into material parameters ϕ and c by using the following formulas.

$$\beta = \frac{\sigma_c \cdot \sigma_t}{\sqrt{3} \cdot (\sigma_c + \sigma_t)} \tag{2.21}$$

$$\sigma_y = \frac{2 \cdot \sigma_c \cdot \sigma_t}{\sqrt{3} \cdot (\sigma_c + \sigma_t)} \tag{2.22}$$

$$\phi = \sin^{-1}\left(\frac{3\sqrt{3} \cdot \beta}{2 + \sqrt{3} \cdot \beta}\right) \tag{2.23}$$

$$c = \frac{\sigma_y \cdot \sqrt{3} \cdot (3 - \sin\phi)}{6 \cdot \cos\phi} \tag{2.24}$$

Dilatancy angle ϕ_f is the additional parameter and is responsible for the amount of volumetric expansion dilation in the analysis.

If $\phi_f = \phi$, associated plasticity.

If $\phi_f < \phi$, less volumetric expansion will happen.

If $\phi_f = 0$, no shear-induced dilation will occur.

2.9.4.2 The Newmark Method

The internal force is not linearly proportional to nodal displacement and stiffness matrices for the nonlinear systems. The load depends on the current displacement (ANSYS, 1999).

The semi-discrete equation of motion for the nonlinear dynamic analyses by the Newmark-Raphson method can be expressed with the following formula (Newmark, 1959; Hughes, 1987):

$$[M]\cdot\{\ddot{u}_{n+1}\}+[C]\cdot\{\upsilon_{n+1}\}+\left\{F^{i}_{n+1}\left(\{u_{n+1}\}\right)\right\}=\left\{F^{a}_{n+1}\right\} \tag{2.25}$$

Where;

$\{\ddot{u}_{n+1}\}$ = acceleration vector $\{\ddot{u}(t_{n+1})\}$ at time t_{n+1}

$\{\upsilon_{n+1}\}$ = velocity vector $\{\dot{u}(t_{n+1})\}$ at time t_{n+1}

$\{u_{n+1}\}$ = displacement vector $\{u(t_{n+1})\}$ at time t_{n+1}

$\{F^{a}_{n+1}\}$ = applied force $\{F^{a}_{n+1}(t_{n+1})\}$ at time t_{n+1}

$\{F^{i}_{n+1}(\{u_{n+1}\})\}$ is only depending on the current displacement $\{u_{n+1}\}$ at time t_{n+1}

By applying the residual vector $\{R_{n+1}(\{u_{n+1}\})\}$ in Equation 2.25, we can obtain:

$$\left\{R_{n+1}\left(\{u_{n+1}\}\right)\right\}=\left\{F^{a}_{n+1}\right\}-\left\{F^{i}_{n+1}\left(\{u_{n+1}\}\right)\right\}-[C]*\{\upsilon_{n+1}\}-[M]*\{\ddot{u}_{n+1}\} \tag{2.26}$$

The linearized form of the time integration procedure will be (ANSYS, 1999):

$$\left\{R_{n+1}\left(\{U^{k}_{n+1}\}\right)\right\}+\partial\left\{R_{n+1}\left(\{U^{k}_{n+1}\}\right)\right\}/\partial\left\{u^{i}_{n+1}\right\}\cdot\{\Delta u^{k}_{n+1}\}=\{0\} \tag{2.27}$$

Where;

$\{U^{k}_{n+1}\}$ is the assumption of $\{u_{n+1}\}$at the k^{th} iteration.

$\{\Delta u^{k}_{n+1}\}$is the increment for displacement of $\{u_{n+1}\}$ at the k^{th} iteration.

Combining Equations 2.26 and 2.27 results in the following formula:

$$\left[a_0 \cdot [M] + a_1 \cdot [C]\right] + [K^{T}_{n+1}(\{u^{k}_{n+1}\})] = \left\{R_{n+1}(\{U^{k}_{n+1}\})\right\} \tag{2.28}$$

Where;

$$a_0 = 1/\alpha \cdot \Delta t^2 \tag{2.29}$$

$$a_1 = \delta/\alpha \cdot \Delta t \tag{2.30}$$

in which α and δ represent Newmark's parameters.

$[K^{T}_{n+1}(\{u^{k}_{n+1}\})]$ is the tangent stiffness matrix at time t_{n+1}

Also, the vectors for the displacement and velocity, which are demonstrated in Equations 2.25 and 2.26, can be calculated by the following formulas:

$$\{\upsilon_{n+1}\} = \{\upsilon_n\} + [(1-\delta)\cdot\{\ddot{u}_n\} + \ddot{u}_{n+1}\}]\cdot\Delta t \tag{2.31}$$

$$\{u_{n+1}\} = \{u_n\} + \{\ddot{u}_n\}\cdot\Delta t + [(1/2-\alpha)\cdot\{\ddot{u}_n\} + \alpha\cdot\{\ddot{u}_{n+1}\}]\cdot\Delta t^2 \tag{2.32}$$

in which;

$\{\ddot{u}_n\}$ is the acceleration vector $\{\ddot{u}(t_n)\}$ at time t_n

$\{\upsilon_n\}$ is the velocity vector $\{\dot{u}(t_n)\}$ at time t_n

$\{u_n\}$ is the displacement vector $\{u(t_n)\}$ at time t_n

2.10 Safety Evaluations of Concrete Gravity Dams

Even if many dams exposed to strong earthquakes survive without severe damages, high dams which are located near major faults can suffer from extensive cracking when seismic loads are applied (Chopra and Chakrabarti, 1973).

Leger and Leclerc claimed that the cracking begins at the dam base in the upstream direction (Leger and Leclerc, 1996). Cracking at the top of the dam occurs in the downstream direction most of the time.

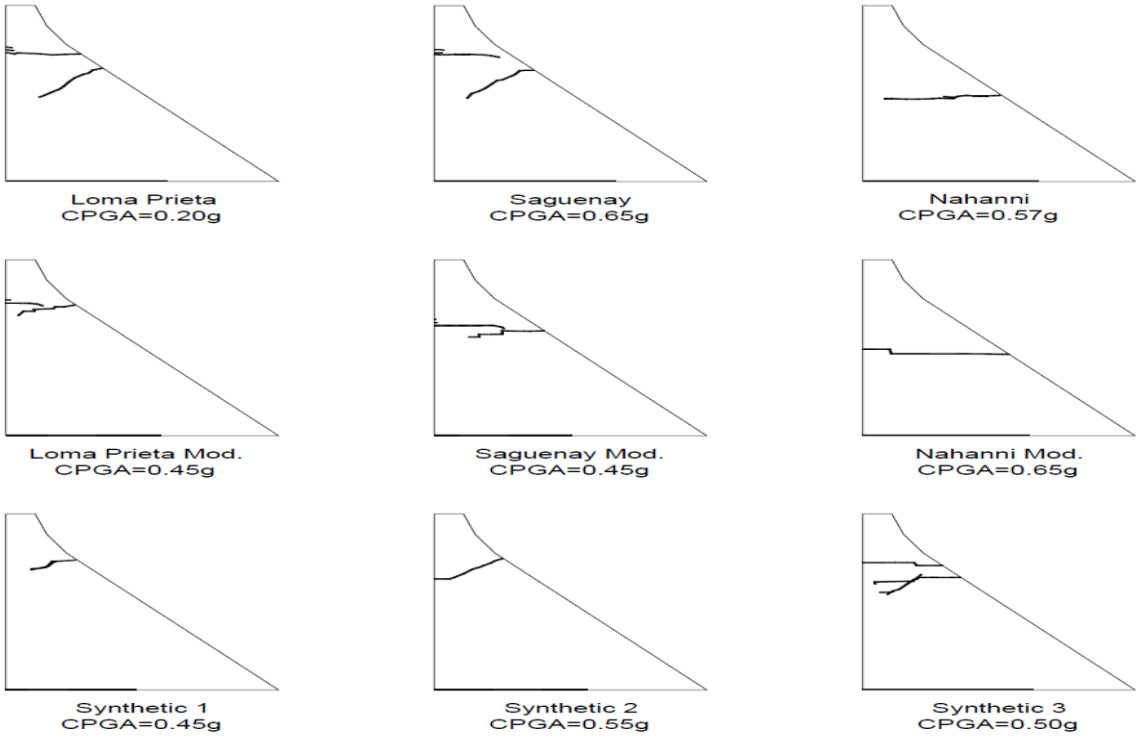

Figure 2.8 Possible Cracking Profiles for Concrete Gravity Dams Exposed to Various Types of Ground Motions (Leger and Leclerc, 1996)

The accurate prediction of the stresses and deformations in the dam body subjected to seismic motion is highly significant for the evaluation of safety for the dams that will be exposed to further ground motions. In this way, the earthquake resistant dams can be designed in the future.

Maximum and minimum principal stresses originated from both seismic and static loads should be illustrated using contour or vector plots (USACE, 2003). Vector plots can be more beneficial in comparison to contour plots because vector plots point out not only the magnitude of stresses, but also their directions. In this way, the direction of tensile cracking may be estimated with vector plots (USACE, 2003). While the maximum stresses represent the largest tensile (positive) stresses on the dam body, the minimum stresses provide the largest compressive (negative) stresses. Additionally, tensile and compressive stresses generally happen at different times during ground motion. Using those vectors, overstressed regions can be determined.

CHAPTER 3

MODELING OF THE ROLLER-COMPACTED CONCRETE GRAVITY DAM

3.1 Introduction

Since the longitudinal length (thickness) of the gravity dam is considerably greater than its other two dimensions, the 2-D plane structure has generally been performed in the finite element modeling. Dam and foundation are commonly considered as linear and elastic, and fluid is commonly assumed to be acoustic, inviscid, and incompressible. It is important to remember that fluid is assumed as compressible for only the Euler method. Also, the dam and foundation are performed using plane strain conditions. To create a model associated with the reservoir water, proper representation of boundary conditions and initial conditions with acoustic elements is required.

This research studies the seismic behavior of the Narli concrete gravity dam using water-reservoir-foundation interaction. In this research, the composite finite element-equivalent mass system model is considered as a model configuration for the dynamic analysis. The modeling of this method uses finite elements for both the dam body and rock.

The foundation should be a rectangular shape with a height at least 1.5 times the height of the structure and with a width at least 3 times the base width of dam-foundation interface (USACE, 1995a). For this model, however, boundary conditions should be used along the base of the

foundation instead of at the dam-foundation interface where the ground motion is applied. Thus, the foundation is estimated massless to implement the earthquake ground motion on the ground surface (dam-foundation interface). In this way, wave propagation never occurs in the massless rock, and the earthquake records are transferred to ground surface without using alteration (USACE, 1995a). Therefore, the massless foundation approach is selected in all modeling presented herein.

To reduce the boundary condition effects, reservoir length in the upstream face of the dam and foundation length in the downstream face of the dam are accepted two times the maximum dam height. Since the length of the reservoir is wide, it should be interrupted at the sufficient distance from the dam body. The reservoir length should be selected at least 2 or 3 times its depth for the accurate evaluation of the hydrodynamic effects on the dam (Zienkiewicz and Taylor, 2000).

3.2 Dam-Foundation-Reservoir Model of the Narli Dam

The Narli Dam will be established on the Dalaman River in 2019, which is located in Mugla, Turkey. The reservoir will be used for energy purposes. The water in the reservoir will be delivered to the hydroelectric plant via energy tunnel, which has 4199 m length.

The cross section of the concrete gravity dam is shown in Figure 3.1. The maximum height of the dam is 99.5 m. The upstream slope is 1:0.60 from the base of the dam to 51 m height, and the slope is vertical from 51 m to the maximum dam height. The downstream slope was designed as 1:0.8. The crest width is 10 m, and the crest length is 299.0 m. The maximum operation water level is 97.5 m, which is 2.0 m below the maximum height.

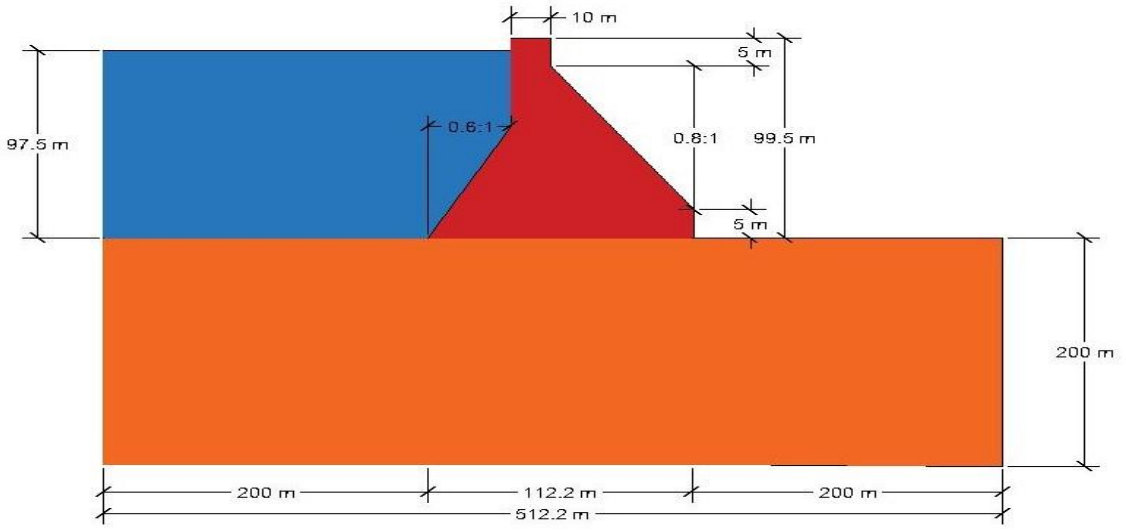

Figure 3.1 Geometry of Non-Overflow Section of Dam-Reservoir-Foundation System

3.3 Material Properties of the Dam-Foundation-Reservoir System

According to the geological and geotechnical assessments on the construction site, the deformation modulus of the foundation has been determined as E_f = 2.854 GPa using laboratory experiments (GF Proje ve Muhendislik, 2018 [GF Project and Engineering, 2018]). The foundation has been estimated as a B ground type from the seismic risk analysis report. The velocity of shear waves for dynamic deformation modulus of the foundation is generally selected between 760 m/s and 1500 m/s for B ground type based on ASCE 7-02 and ASCE 7-05 codes. The assumed approximate value for the Narli Dam is 1130 m/s.

Maximum shear modulus calculation can be performed with the following equation:

$$G_{max} = \rho \cdot (V_s)^2 \tag{3.1}$$

where ρ is total mass density, and V_s is the velocity of shear waves.

Dynamic modulus of elasticity for the foundation can be calculated using the following equation:

$$E_{dynamic} = G_{max} \cdot 2 \cdot (1 + \upsilon) \tag{3.2}$$

where G_{max} is the maximum shear modulus, and υ is Poisson's ratio of the rock.

Assumed Poisson's ratio for the foundation of the Narli Dam is 0.30.

The specified 28-day compressive strength of concrete has been determined as 15 MPa using preliminary analyses for the Narli Dam (GF Proje ve Muhendislik, 2018 [GF Project and Engineering, 2018]). By using the target compressive strength, the modulus of elasticity of concrete can be calculated using the following equation, which is valid for normal weight and normal density concrete:

$$E_{concrete} = 4700 \cdot \sqrt{f_c'} \tag{3.3}$$

Weight should be between 1440 kg/m^3 and 2560 kg/m^3 for normal weight concrete. This value is 2400 kg/m^3 for the Narli Dam.

Based on Raphael's studies (1984), the dynamic tensile strength should be determined by increasing the static tensile strength with the factor of 1.5. Also, in work by Raphael, the static tensile strength should be increased by the factor of 2.0 to find the apparent dynamic tensile strength (Raphael, 1984).

$$f_t = 2.3 \cdot f_c'^{2/3} \tag{3.4}$$

where f_t' and f_c' represent tensile and compressive strength of concrete based on psi units, respectively. The maximum allowable DCR is 1.5 for roller-compacted concrete gravity dams (Cannon, 1995; Raphael, 1984).

The compressive strength of concrete that is used for the Narli Dam is 15 MPa (2175.57 psi). Using Equation 3.4 and increasing by the 150% for the dynamic conditions, the flexural strength of concrete can be calculated as 3.99 MPa.

Using the Cannon (1995) formula, which is mentioned in the USACE (2000) criteria, the tensile strengths in the principal direction for the structure and vertical direction for the joints have been identified as given below. For dynamic conditions, the tensile strengths have increased by 150%.

$$\sigma_{tp} = 0.17 \cdot \sigma_c \tag{3.5}$$

$$\sigma_{tv} = 0.15 \cdot \sigma_c \tag{3.6}$$

$$\sigma_{tp-dynamic} = 1.5 \cdot \sigma_{tp} \tag{3.7}$$

$$\sigma_{tv-dynamic} = 1.5 \cdot \sigma_{tv} \tag{3.8}$$

where σ_{tv} and $\sigma_{tv\text{-}dynamic}$ illustrate tensile strengths in the vertical direction, respectively static and dynamic. σ_{tp} and $\sigma_{tv\text{-}dynamic}$ show tensile strengths in the principal direction, respectively static and dynamic.

Although there are differences between the results for two methods (Cannon, 1995; Raphael, 1984), both are accepted in the literature by USACE criteria. Thus, one of them can be selected for the evaluation of tensile stresses on the dam body.

Table 3.1 Material Properties Used in the Seismic Analysis of the Dam

Parameters	Concrete	Foundation	Reservoir
Static Modulus of Elasticity (GPa)	18.4	2.85	2.02
Dynamic Modulus of Elasticity (GPa)	23	8.6	-
Poisson's Ratio	0.20	0.30	-
Density (kg/m^3)	2400	2600	1000
Compressive Strength (MPa)	15	-	-
Static Tensile Strength in Vertical Direction (MPa)	2.25	-	-
Dynamic Tensile Strength in Vertical Direction (MPa)	3.38	-	-
Static Tensile Strength in Principal Direction (MPa)	2.55	-	-
Dynamic Tensile Strength in Principal Direction (MPa)	3.83	-	-
Sonic Velocity (m/s)	-	-	1440
Boundary Admittance	-	-	1

Required parameters for the dynamic analyses of the Narli Dam are obtained from GF Proje ve Muhendislik [GF Project and Engineering, 2018].

3.4 Element Description of the Dam-Foundation-Reservoir System

Quad and triangular elements are two of the most prevalent 2-D elements. Whereas quad elements are created by four nodes and four combining joints, triangular elements have three nodes and one combining joint. Quad elements for dynamic analyses of the concrete gravity dam are considered in this research.

3.4.1 Plane 42 2-D Structural Solid

Plane 42 element is used for the two-dimensional modeling approach of solid structures (ANSYS, 1999). Plane 42 can be selected either as plane stress or plane strain. The element has 4 nodes that have two degrees of freedom per node (UX-UY). Having plasticity and stress stiffening, and large deflection and strain capacities are some significant features of the element (ANSYS, 1999). The element was used to create dam structure and foundation in the finite element modeling. The solid structural geometry of the element is shown in Figure 3.2.

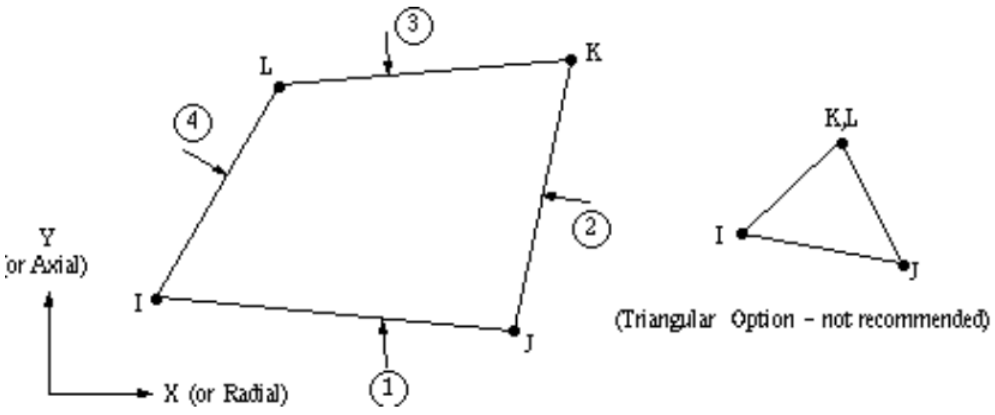

Figure 3.2 The geometry of Plane 42 Element (ANSYS, 1999)

3.4.2 Mass 21 3-D Structural Mass

Mass 21 is defined as a point element, which has only a single node (ANSYS, 1999). The element has up to 6 degrees of freedom. Each coordinate direction can have different mass and/or rotational inertia. The element was used to perform the Westergaard (added mass) method in the seismic analysis. The structural mass geometry for the element is shown in Figure 3.3.

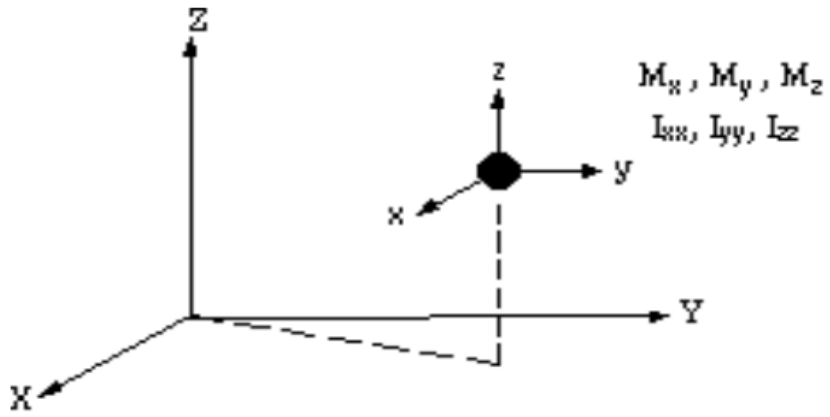

Figure 3.3 The geometry of Mass 21 Element (ANSYS, 1999)

3.4.3 Fluid 29 2-D Acoustic Fluid

Fluid 29 is primarily used for water-structure interaction problems (ANSYS, 1999). The element comprises sound wave propagation and structure dynamics implementations. The main equation for acoustics, also called 2-D wave equation, is based on discretization between structural motion and acoustic pressure at the interface. The element contains four nodes which have three degrees of freedom at each node (UX, UY, Pressure). During modal, harmonic, and transient analyses, the element can be applied with other two-dimensional elements (ANSYS, 1999). The element was used to perform the Euler method in the seismic analysis of the dam. The acoustic fluid geometry of the element is shown in Figure 3.4.

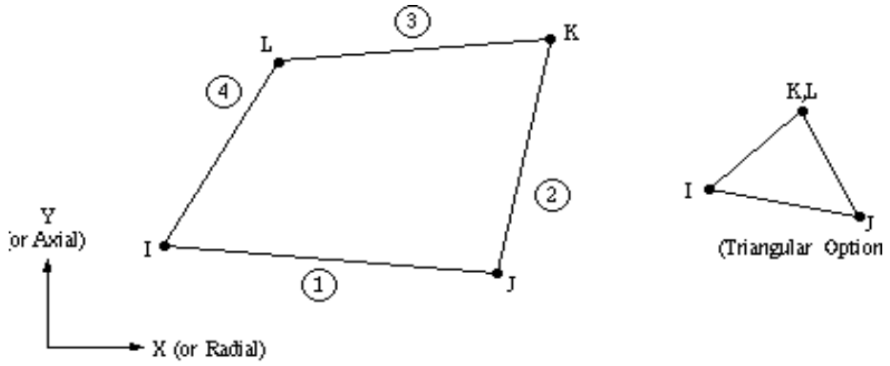

Figure 3.4 The geometry of Fluid 29 Element (ANSYS, 1999)

Assumptions (ANSYS, 1999):

1) The water is compressible (density alters because of pressure variations).

2) The fluid is inviscid (no dissipative impact because of viscosity).

3) The density and pressure are identical for each part of the water.

CHAPTER 4

DYNAMIC ANALYSES OF THE CONCRETE GRAVITY DAM

4.1 Introduction

The primary purpose of this research is to determine and compare the dynamic responses of the concrete gravity dam including dam-reservoir-foundation interaction based on different reservoir modeling approaches. Then, the seismic response of the dam will be evaluated using USACE criteria.

The finite element modeling of the dam considering dam-water-foundation interaction depending on empty reservoir condition, Westergaard, and Euler-Lagrange approaches are performed using ANSYS 17.1 software. Solid elements are used for the dam body and foundation. According to the Westergaard method, the water effect is considered as the added mass on the dam structure. The reservoir is modeled as fluid elements to obtain hydrodynamic effects. For the Westergaard approach, no boundary condition is used because the reservoir effects are added mass on the dam body. On the other hand, there are important differences between Westergaard and Euler methods such as different boundary conditions for the reservoir and different types of elements used in the modeling. For all modeling approaches, Plane 42 elements are selected for the dam and foundation. Mass 21 and Fluid 29 elements are used to represent for the reservoir for Westergaard and Euler methods, respectively.

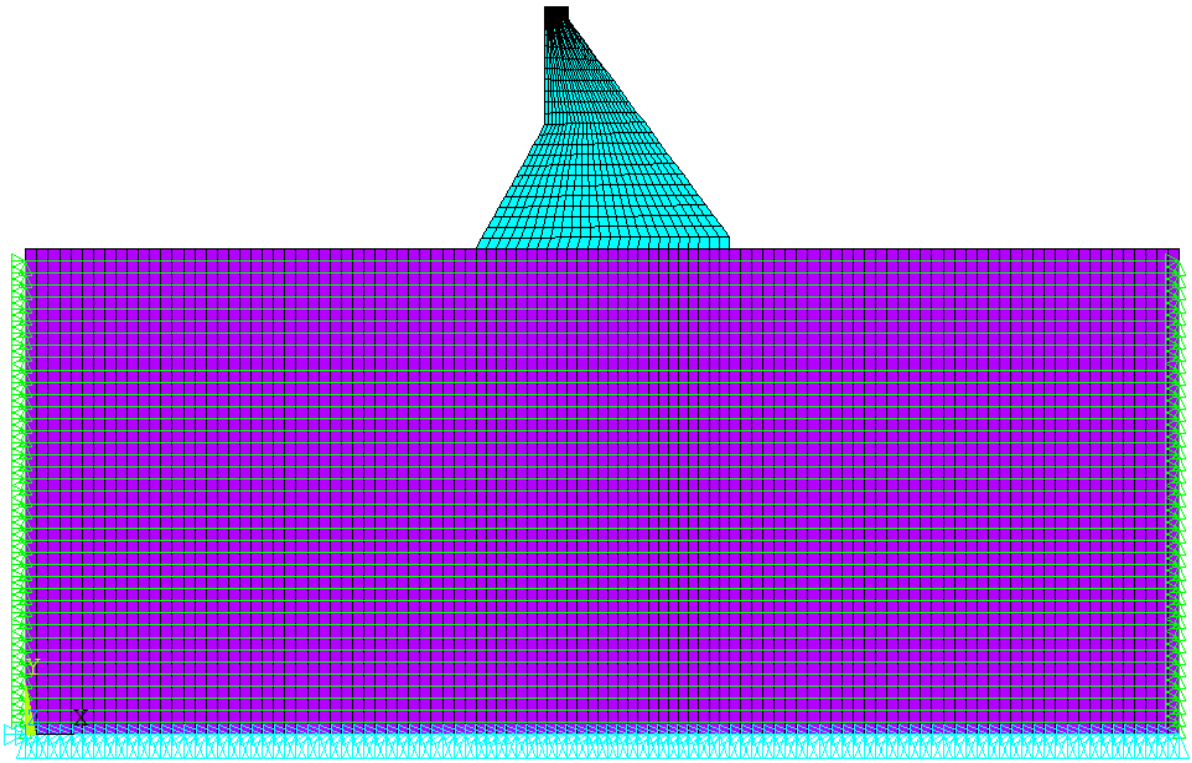

Figure 4.1 Empty Reservoir Modeling

To reveal the exact influence of the reservoir on the dynamic response, the analysis primarily should be performed without the presence of water modeling, and then the reservoir should be added with either Mass 21 or Fluid 29 elements. The model is divided into 4944 nodes and 4775 elements for the empty reservoir modeling as shown in Figure 4.1. Fixed boundary conditions are considered for the base of the foundation at the sufficiently far distance from the dam-foundation interface. Furthermore, coupled DOFs are used for both sides of the rock. In this way, similar movements are obtained for both sides of the rock approximating a simple shear mode of deformation.

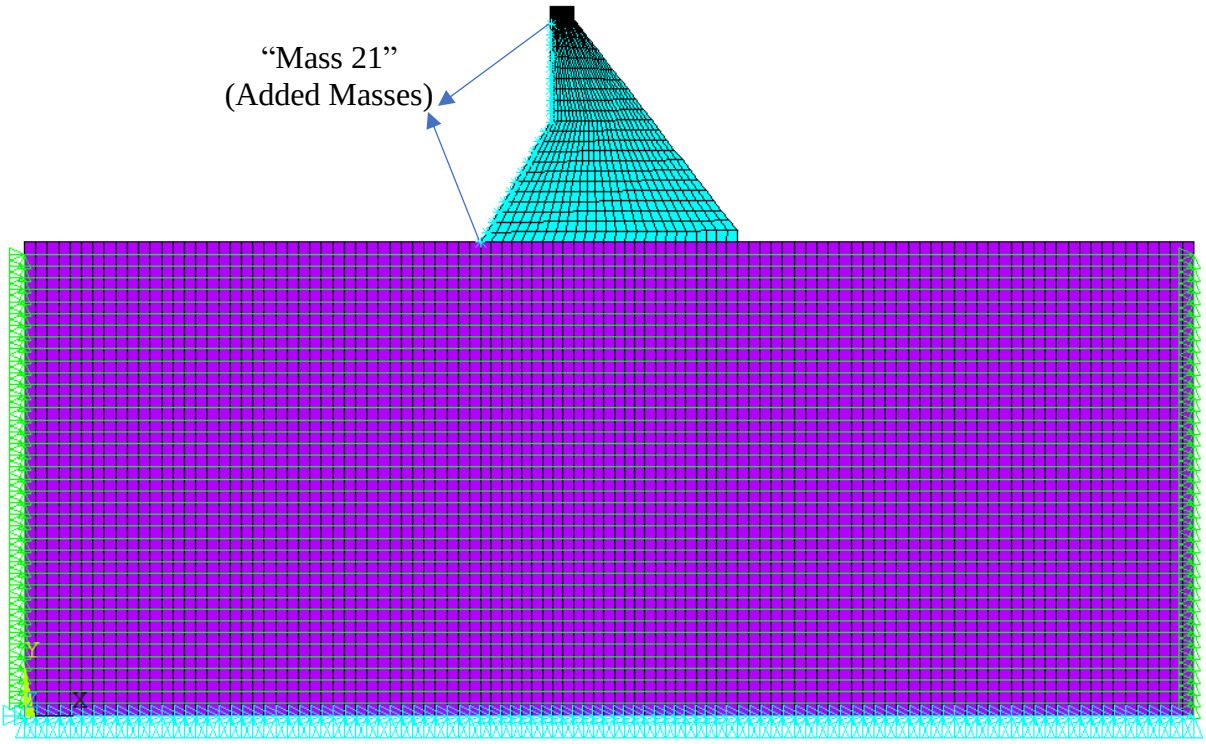

Figure 4.2 Westergaard Method Modeling

The finite element model has 22 structural masses to create reservoir effects on the dam body associated with the Westergaard approach. Each added mass is equally located in an interval of about 4.64 m. The model is divided into 4944 nodes and 4797 elements for the Westergaard method as shown in Figure 4.2 and has the same boundary conditions relevant to empty reservoir modeling. Each added mass is calculated based on Equation 2.1. Mass distribution m(z) on the dam body takes higher values when the distance is farther away from the maximum operating water level. As a result of this situation, the maximum mass distribution takes place at the dam-foundation interface. The aim of using this approach in the research is to investigate the differences with results from the Euler method when modal, linear and nonlinear analyses are performed.

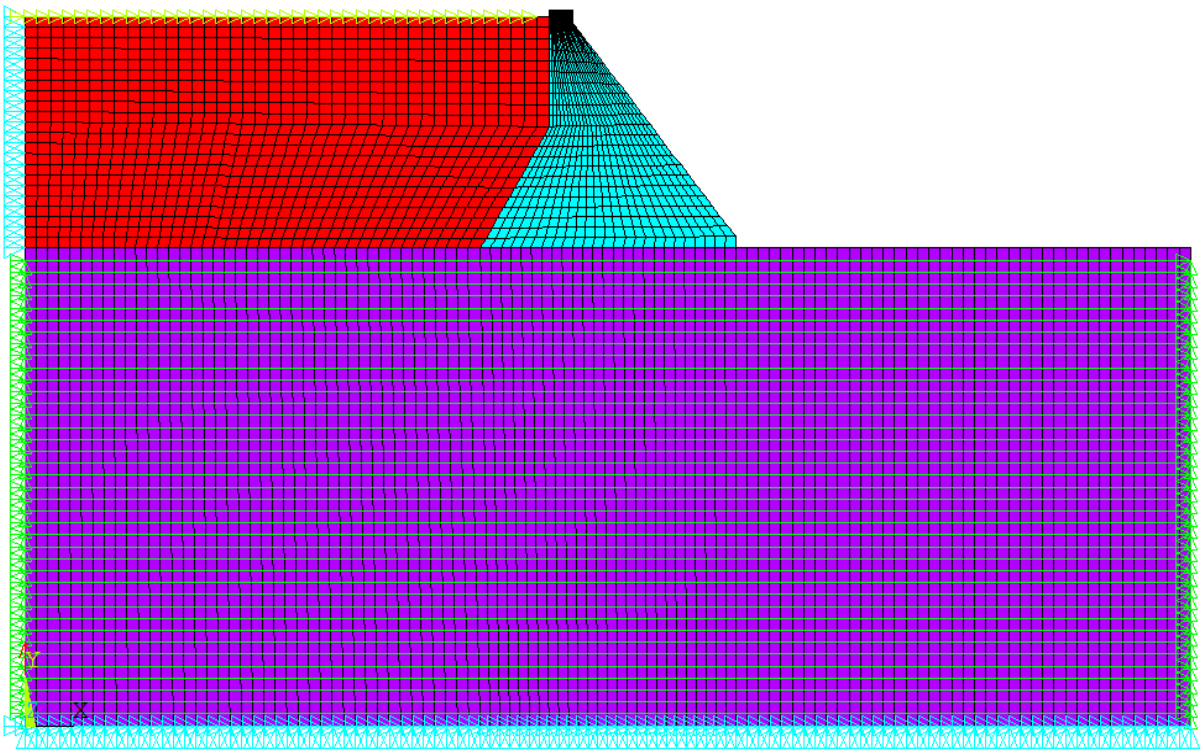

Figure 4.3 Euler Method Modeling

The model has been divided into 5887 nodes and 5717 elements using the proper meshing capabilities of ANSYS software as shown in Figure 4.3. Similar boundary conditions of the foundation selected for both empty reservoir modeling and Westergaard method are applied for Euler method. Additionally, the infinite reservoir interrupts at a sufficiently far away distance from the dam body in the finite element modeling using Sommerfeld boundary conditions to obtain more realistic results. Since the pressure waves on the top surface of the reservoir are negligible, zero water pressure is applied at the maximum water level. It is important to note that although Euler-Lagrange method uses some coupled equations to create modeling of water, similar equations are applied to dam and foundation for Lagrange-Lagrange method that can be performed using Fluid-79 element which is no longer accessible at ANSYS software.

4.2 Modal Analysis

Even if the modal analysis is not a sufficient method to evaluate seismic response, it should be performed to solve out the frequency values and mode shapes of the model. Natural frequencies and modes of vibration enable significant knowledge about the dynamic response of the structure. Natural frequencies obtained from the modal analysis are used for the application of Rayleigh damping during dynamic analyses. The materials for the foundation and dam are accepted as linear-elastic, homogenous, and isotropic when a modal analysis is applied. Massless foundation method is not considered for the modal analysis because there is no application of ground motions on the dam-foundation-reservoir system. Although the frequency for the first mode of the model can be determined using a massless foundation model, higher modes should not be considered as massless foundation models to avoid exaggeration of frequency values. All modal analyses are performed with considering foundation mass instead of using the massless foundation modeling in this thesis.

4.2.1 Modal Analyses Results

The first two mode shapes and frequency values for all approaches are illustrated in this section (Figures 4.4-4.9). Natural frequencies that used the calculation of Rayleigh damping of the system can be selected from first two frequency results for the model if these values are not close to each other. Otherwise, third mode shape and frequency should be considered for the dynamic analyses. Natural frequency values for linear and nonlinear seismic analyses and their periods of vibration, which are shown in Table 4.1, can be calculated using the following equations:

$$w_1 = 2 \cdot \pi \cdot f_1 \tag{4.1}$$

$$w_2 = 2 \cdot \pi \cdot f_2 \tag{4.2}$$

$$T_{1,2} = 1/f_{1,2} \tag{4.3}$$

where w, f, and T represent natural frequency, frequency obtained from the modal analysis and period of vibration of the model, respectively.

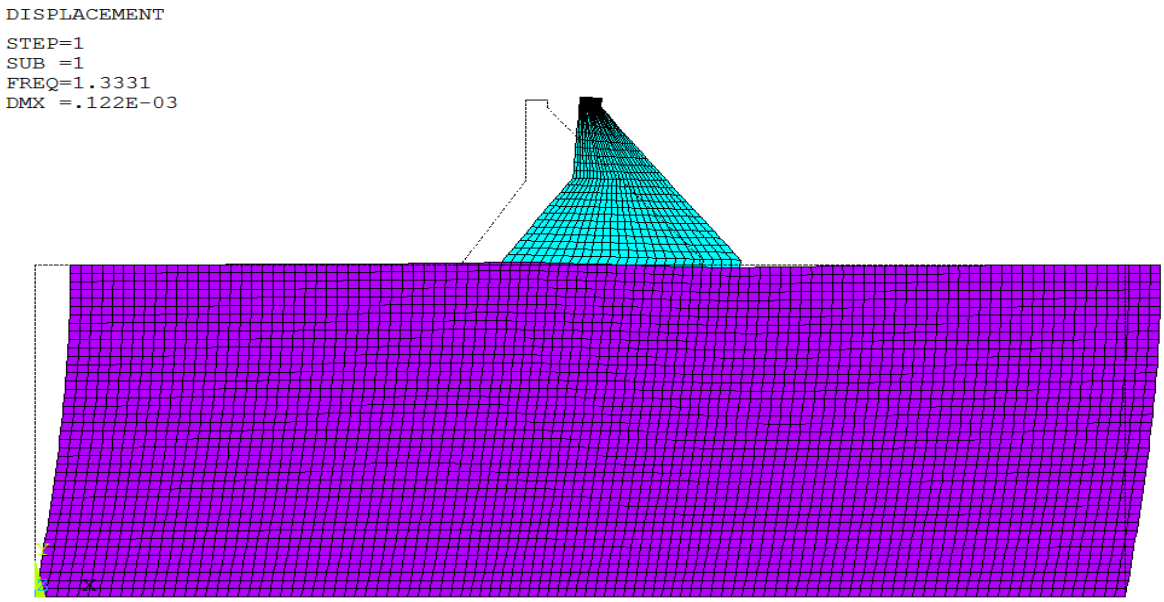

Figure 4.4 Empty Reservoir Condition-Mode Shape 1

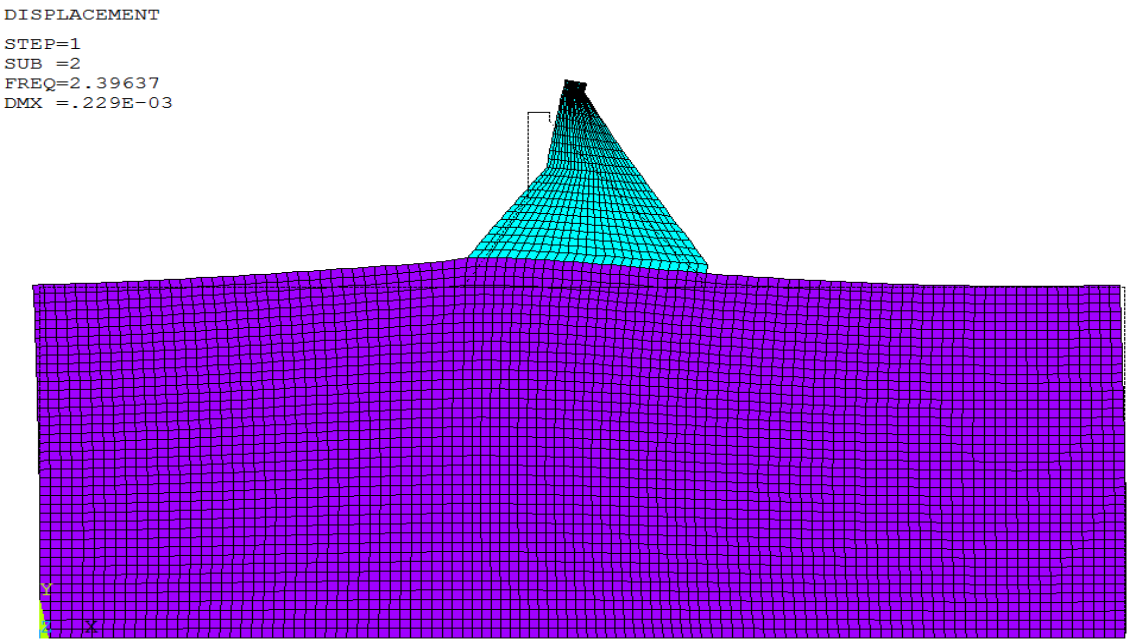

Figure 4.5 Empty Reservoir Condition-Mode Shape 2

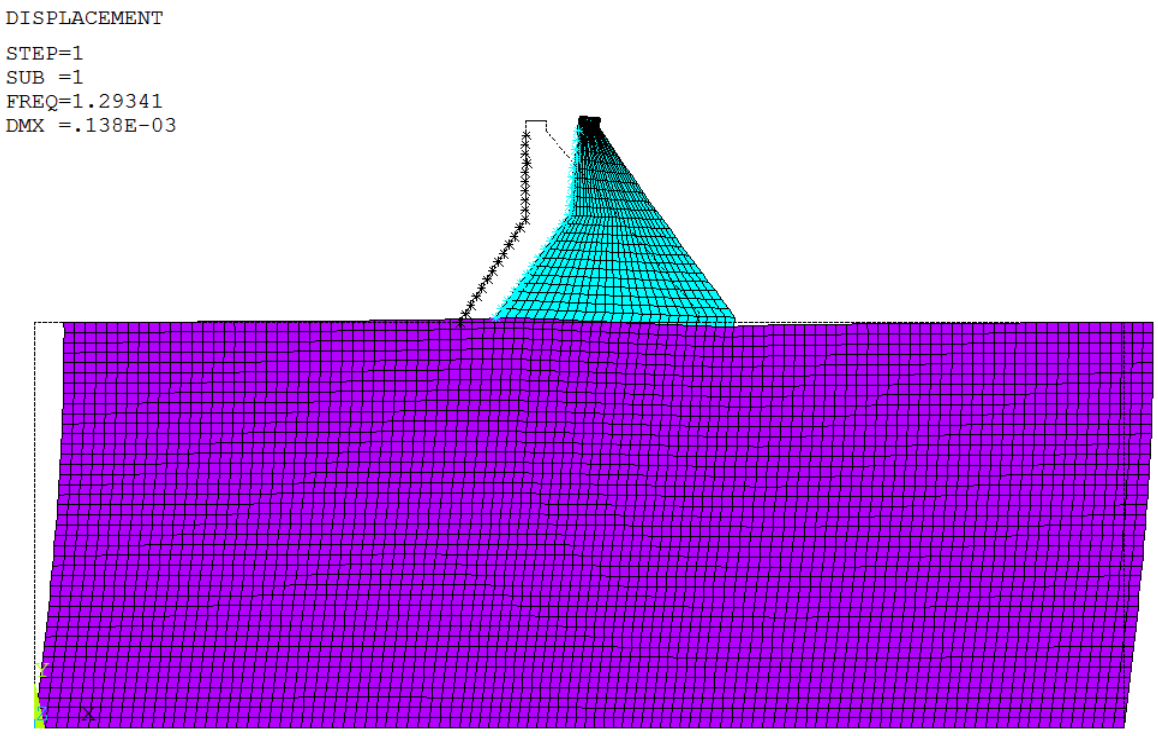

Figure 4.6 Westergaard Method-Mode Shape 1

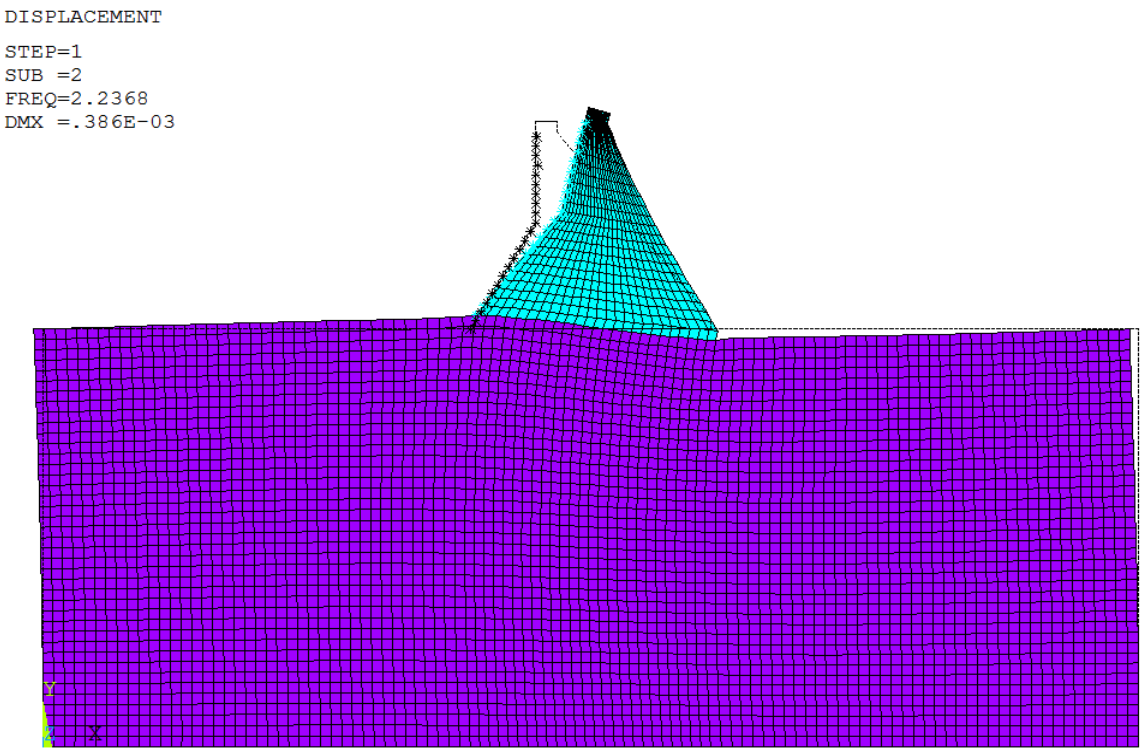

Figure 4.7 Westergaard Method-Mode Shape 2

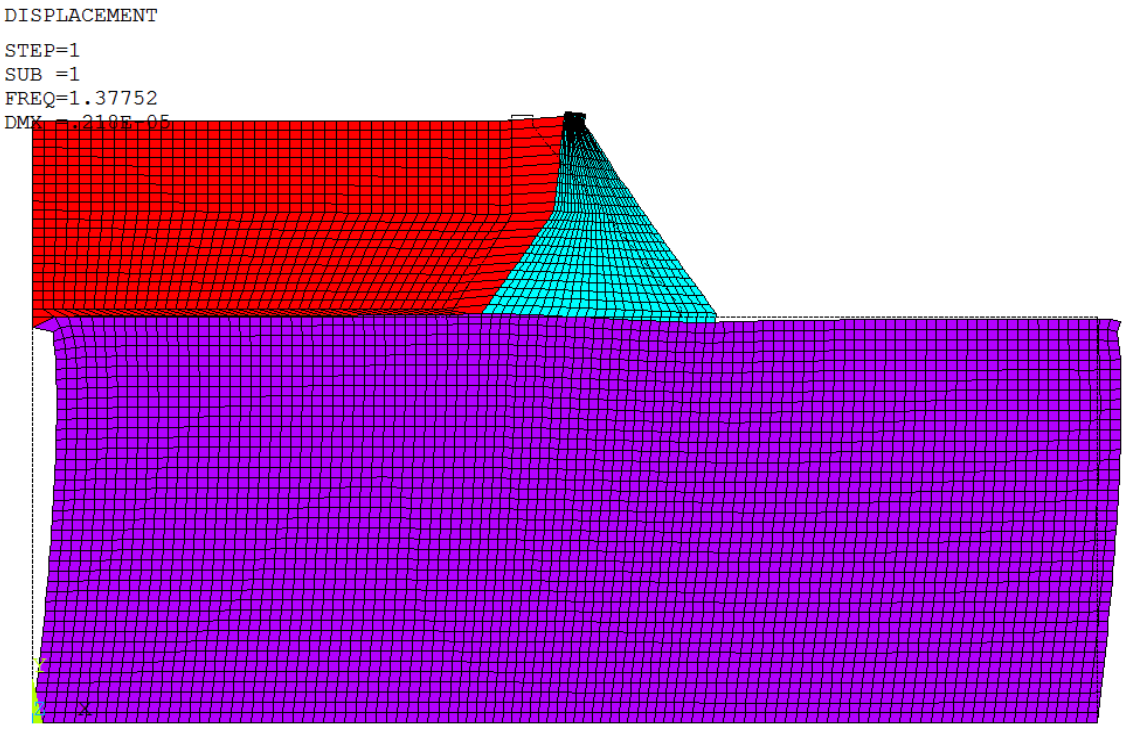

Figure 4.8 Euler Method-Mode Shape 1

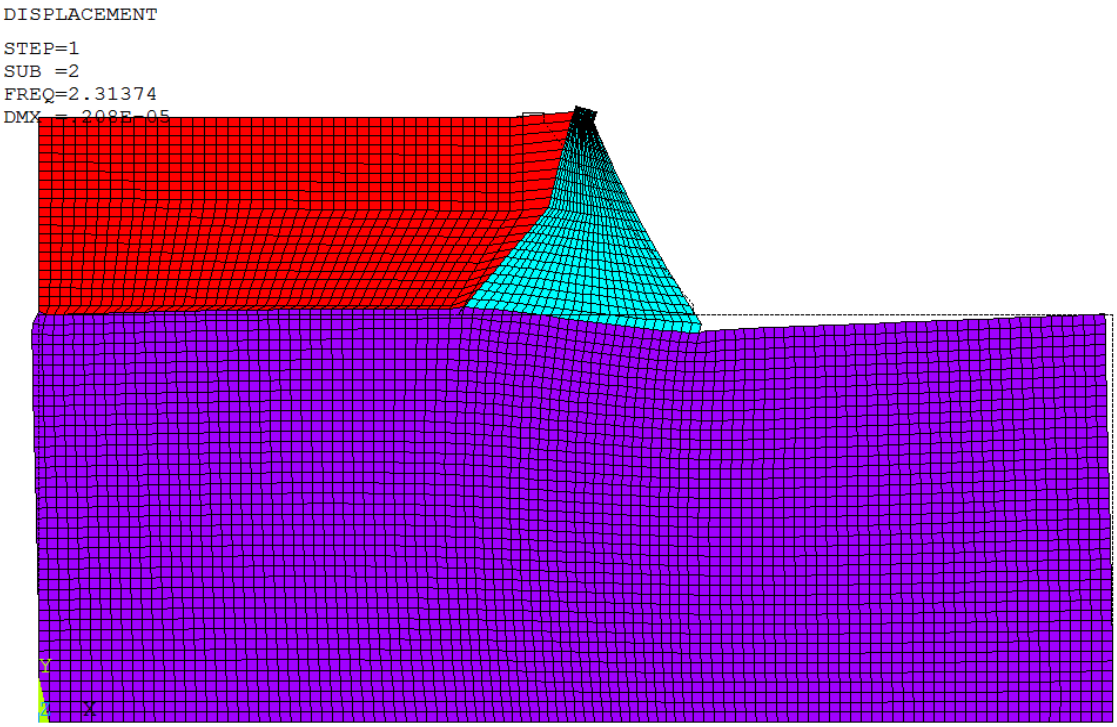

Figure 4.9 Euler Method-Mode Shape 2

Table 4.1 Modal Analysis Results

Methods	Natural Frequency (Hz)		Period (sec)	
	W_1	W_2	T_1	T_2
Empty Reservoir	8.36	15.02	0.752	0.418
Westergaard	8.11	14.07	0.775	0.446
Euler	8.61	14.51	0.729	0.433

4.3 Selected Ground Motions

According to the Seismic Hazard Analysis Report of the Narli dam, the maximum peak ground acceleration for the dam was assumed as 0.51g (GF Proje ve Muhendislik, 2018 [GF Project and Engineering, 2018]). Three acceleration records that occurred on the B ground type of foundations were considered for the dynamic analyses of the dam, and all ground acceleration records were taken from the General Directorate of State Hydraulic Works (DSI). Those acceleration records that were used in the dynamic analyses may not represent actual earthquakes.

Based on USACE criteria, at least two ground motions are required for the seismic analysis. Therefore, three proper MDE's are selected to perform dynamic analyses of the dam. The first ground motion is referred to Coyote Lake with 0.43 PGA (peak ground acceleration), and the entire length of the earthquake recording is 20.28 seconds. The second selected ground motion is attributed to Loma Prieta with 0.40 PGA that continues for 30.17 seconds. The last earthquake is Palm Springs with 0.38 PGA, and it occurs for 20.015 seconds. The horizontal ground accelerations for these three earthquakes are shown below.

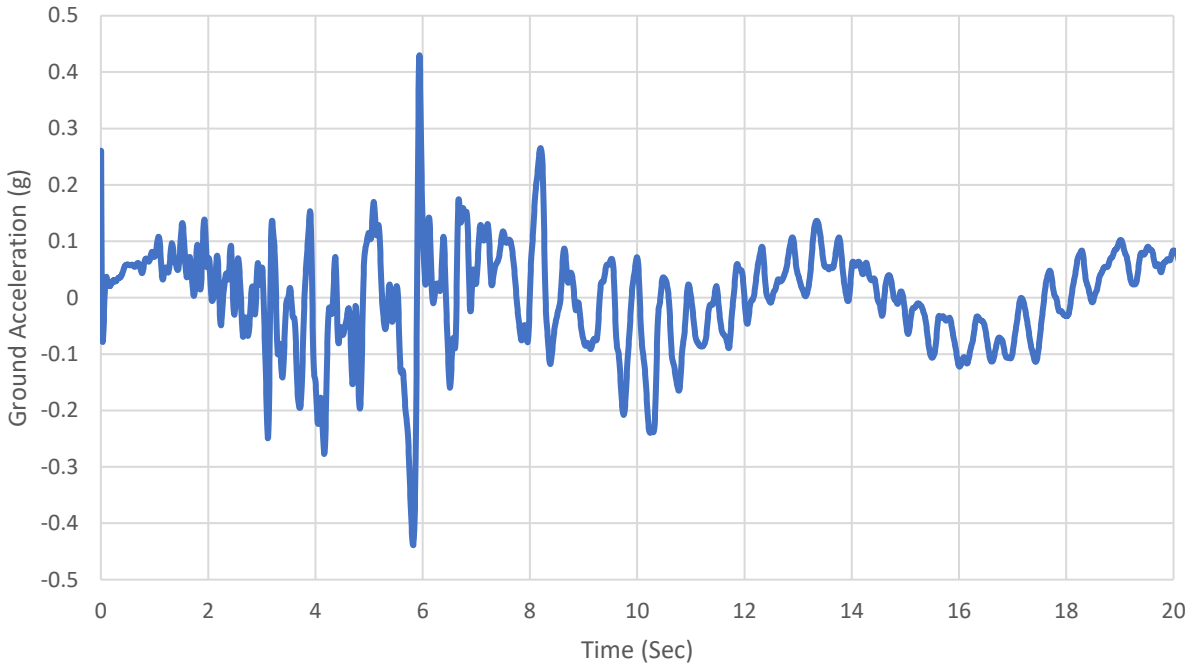

Figure 4.10 Ground Acceleration History for 1979 Coyote Lake Earthquake

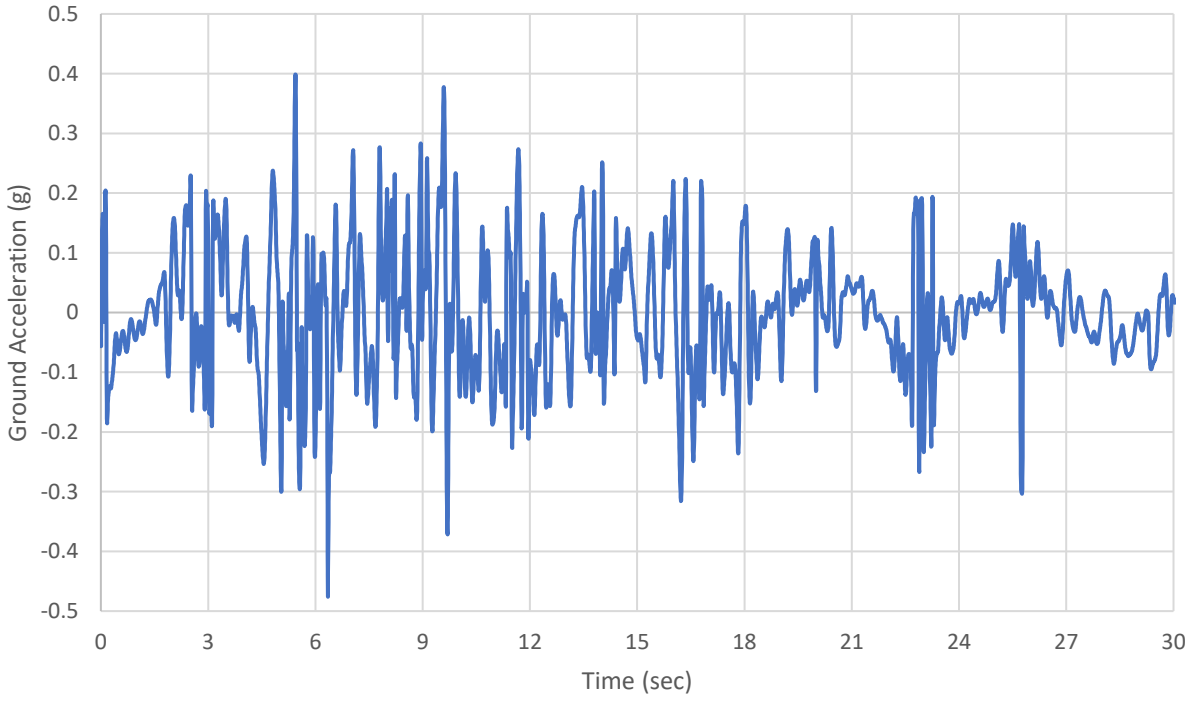

Figure 4.11 Ground Acceleration History for 1989 Loma Prieta Earthquake

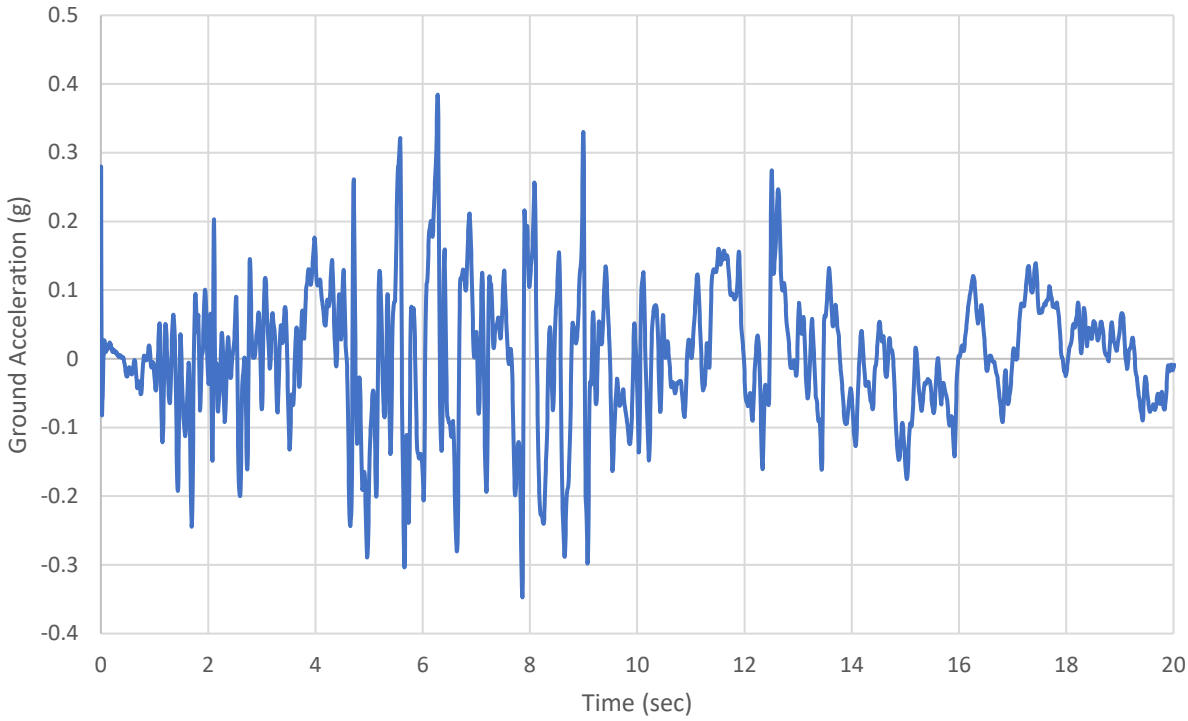

Figure 4.12 Ground Acceleration History for 1986 Palm Springs Earthquake

In regard to USACE criteria, the ground motions take into account for not only horizontal direction but also vertical direction. Hence, the vertical ground accelerations of three earthquakes are considered as half of the ground motions in the horizontal directions (FEMA, 2005) and applied for all dynamic analyses.

4.4 Linear Dynamic Analysis of the Narli Dam

To consider Rayleigh damping in the analysis, the effective viscous damping ratio of the system should be determined based on Equations 2.15 and 2.16 and using Chopra's graphs mentioned in Figure 2.4. Then, Rayleigh coefficients α and β can be calculated, which are shown in Equations 2.13 and 2.14, considering the first two natural frequency values obtained from modal analyses and the effective viscous damping ratio of the system.

The effective viscous damping ratio for the empty reservoir condition will be less than the ratio for the other two approaches (Euler and Westergaard Methods) because the additional damping resulting from the reservoir is ignored for the empty reservoir condition. Used damping ratios and Rayleigh coefficients for the linear dynamic analyses are displayed in Table 4.2.

Table 4.2 Rayleigh Coefficients and the Effective Damping Ratio Results associated with Linear Analyses

Methods	**Rayleigh Coefficients**		**The Effective Viscous Damping Ratios**
	α	**β**	**ξ_{eff} (%)**
Empty Reservoir	1.894	0.0150	17.6
Westergaard	1.853	0.0162	18.0
Euler	1.952	0.0155	18.0

It is important to note that the ground motions for all EQs shown in Figures 4.11, 4.12, and 4.13 are given based on unit g. For the dynamic analysis, this unit must be converted to unit m/s^2 when SI units are applied in the analyses. Also, the materials for the foundation and dam are accepted as linear-elastic, homogenous, and isotropic in the linear dynamic analyses. The presence

of the reservoir can be recognized as either compressible for the Euler method or incompressible for the Westergaard method.

Using a short time interval for the time-history of ground motions such as 0.005 and 0.01 sec. provides more realistic results than long time intervals for the seismic analysis. Therefore, 0.005 sec. was chosen as time intervals for all types of ground motions in this research.

The reason why the empty reservoir condition has been considered is that the impact of the presence of the reservoir on the dynamic response of the roller-compacted concrete gravity dam will be investigated. As a result of this situation, the results for Euler and Westergaard methods will be compared with the consequences of empty reservoir condition to understand the hydrodynamic pressure effect.

The dam response is estimated based on unit weight and elastic material properties of concrete and foundation such as elastic modulus and Poisson's ratio. Since the time-history method enables better representation for the foundation-structure and fluid-structure interaction impacts in comparison to the response spectrum method, it was selected for the application of seismic loads (USACE, 2003).

Time-domain analyses are commonly dependent on step-by-step methods that provide numerical integration procedures to fulfill the equations of motion. Time intervals with a sequence are used to create the response history. The response and loading history during each step are calculated from the initial conditions. The static loads are considered as the initial condition of the dynamic analysis because the 2-D model of the dams should also be performed considering the impacts of static loads (USACE, 2003).

4.4.1 Linear Transient (Time-History) Dynamic Analysis Results

In this section, the results for displacements, accelerations, compressive stresses, and tensile stresses on the dam body will be provided based on all approaches. In the case of the massless foundation model in the finite element analysis, there is no displacement at the bottom of foundation. In addition, the critical nodes for displacement and acceleration are located on the crest of the dam. Thus, displacement-time and acceleration-time histories for the peak of the dam during three maximum design earthquakes will be shown with graphs in this section.

4.4.1.1 Time-History Results for Displacement and Acceleration

The horizontal displacements and accelerations of the crest of the Narli concrete gravity dam in the upstream and downstream directions attained from linear dynamic analyses for three distinct methods under three different earthquakes are shown with time-history graphs (Figs. 4.13-4.30). The maximum horizontal displacements, which are shown in Table 4.3, are obtained as 4.14 cm, 5.67 cm, and 6.16 cm for empty reservoir condition, Westergaard approach, and Euler method, respectively. The maximum horizontal accelerations, which are shown in Table 4.3, are attained from the transient analysis and are 1.19 g, 1.15 g, and 1.23 g for empty reservoir condition, Westergaard approach, and Euler method, respectively.

Depending on the given figures, it is clear that the presence of the reservoir highly contributes to the crest displacement. Up to a 50% increase in the displacement occurs due to the hydrodynamic pressures. On the other hand, the difference in the results of Westergaard and Euler methods is approximately 10%. Based on the results, Euler method provides higher estimations for the crest displacements than Westergaard method.

The results demonstrate that there is no evidence that the presence of water has a significant influence on providing more accelerations for the concrete gravity dam when the added mass method was considered. However, about a 25% increase in the crest accelerations takes place when the reservoir is assumed as compressible rather than assuming incompressible. Thus, the added mass method may be seen as an insufficient approach to figure out the reservoir effect on the crest accelerations.

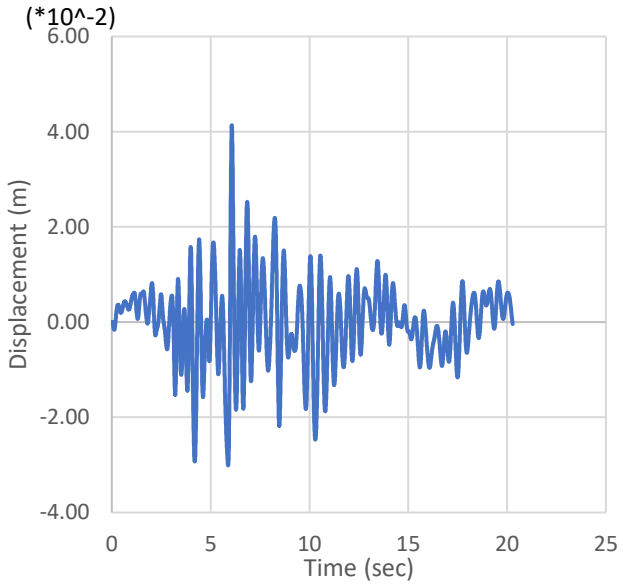

Figure 4.13 Displacement (m) vs Time (sec) History for Coyote Lake Earthquake – Empty Reservoir Condition

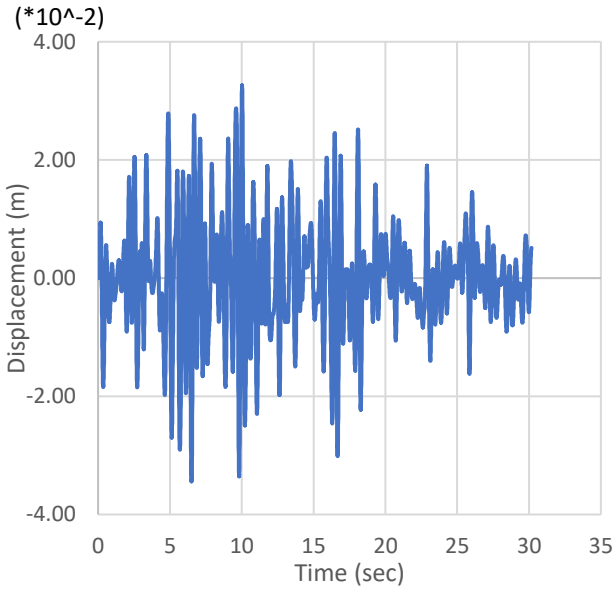

Figure 4.14 Displacement (m) vs Time History (sec) for Loma Prieta Earthquake – Empty Reservoir Condition

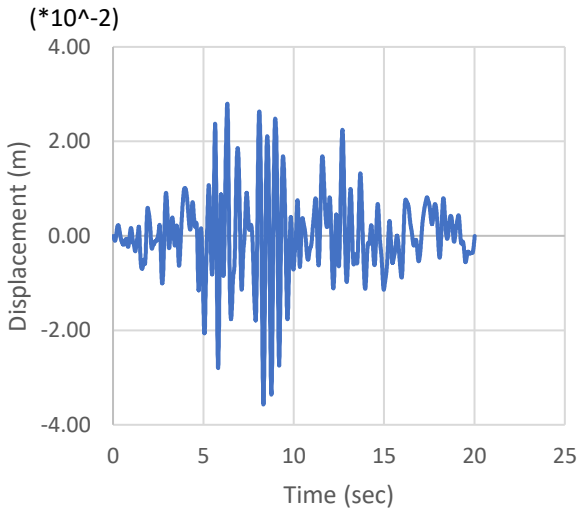

Figure 4.15 Displacement (m) vs Time History (sec) for Palm Springs Earthquake – Empty Reservoir Condition

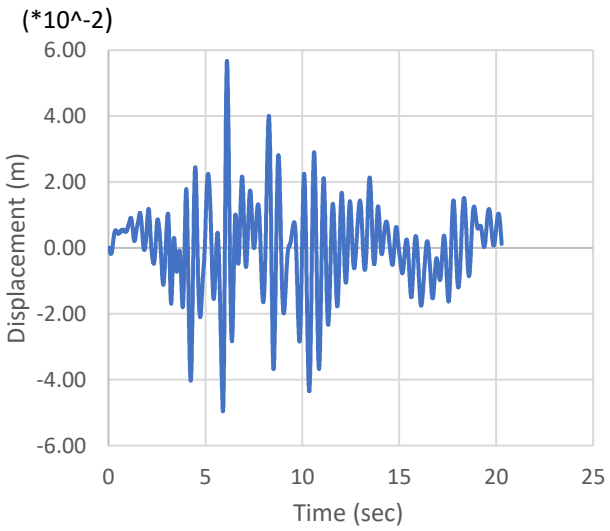

Figure 4.16 Displacement (m) vs Time (sec) History for Coyote Lake Earthquake – Westergaard Method

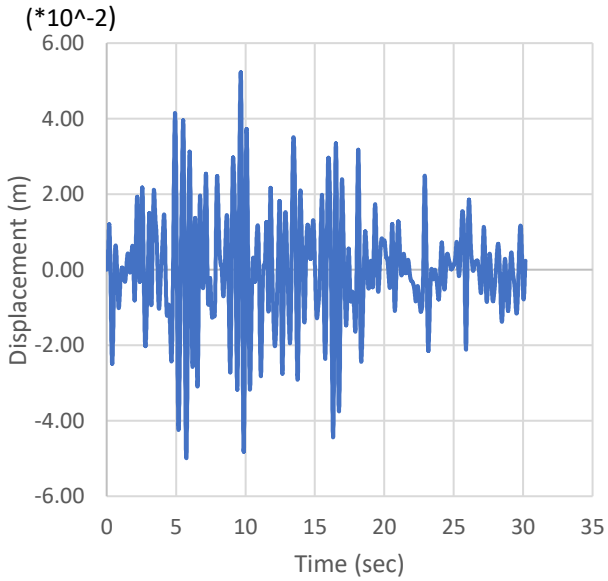

Figure 4.17 Displacement (m) vs Time History (sec) for Loma Prieta Earthquake – Westergaard Method

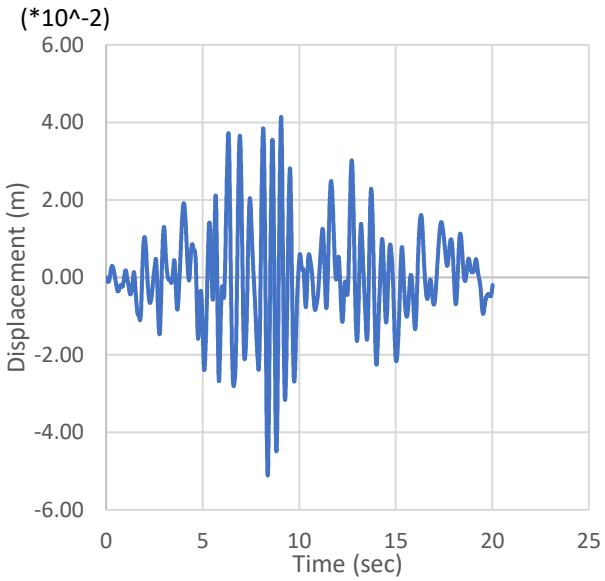

Figure 4.18 Displacement (m) vs Time History (sec) for Palm Springs Earthquake – Westergaard Method

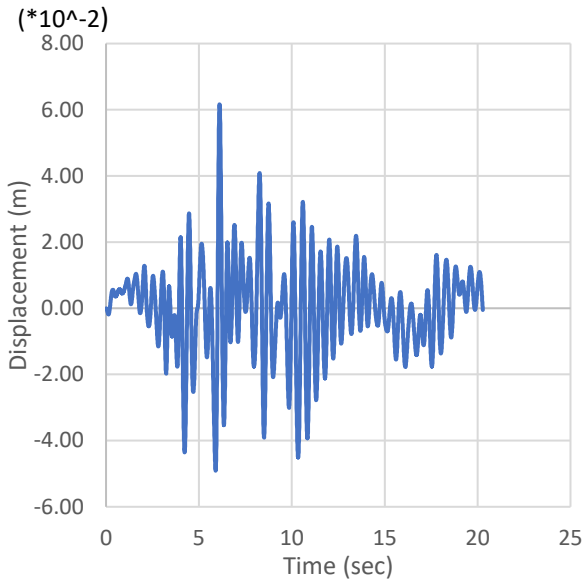

Figure 4.19 Displacement (m) vs Time (sec) History for Coyote Lake Earthquake – Euler Method

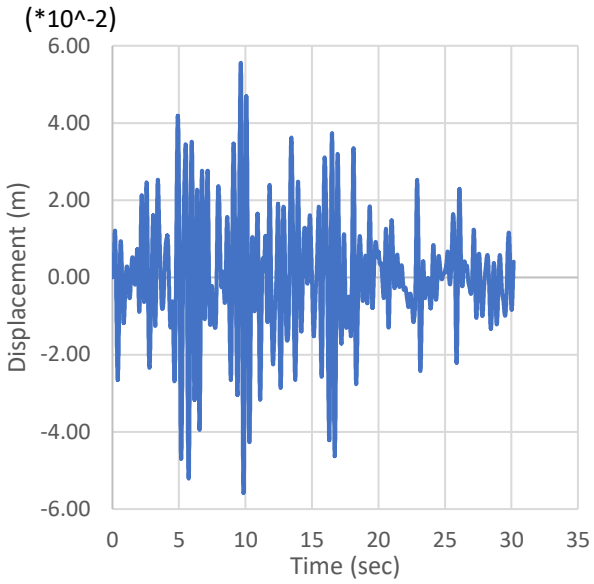

Figure 4.20 Displacement (m) vs Time History (sec) for Loma Prieta Earthquake – Euler Method

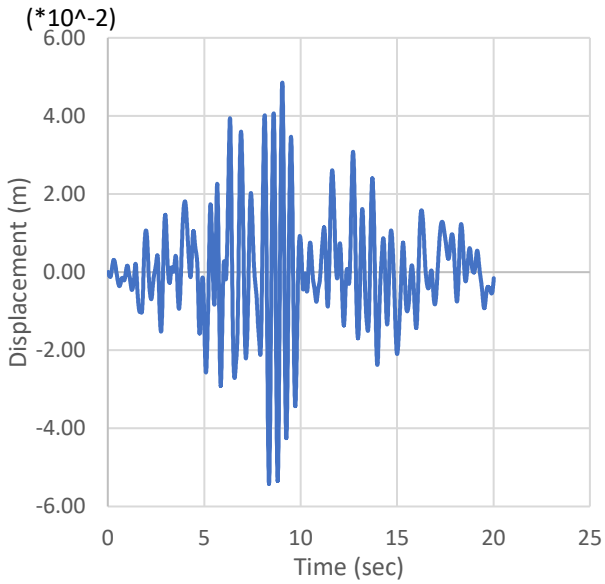

Figure 4.21 Displacement (m) vs Time History (sec) for Palm Springs Earthquake – Euler Method

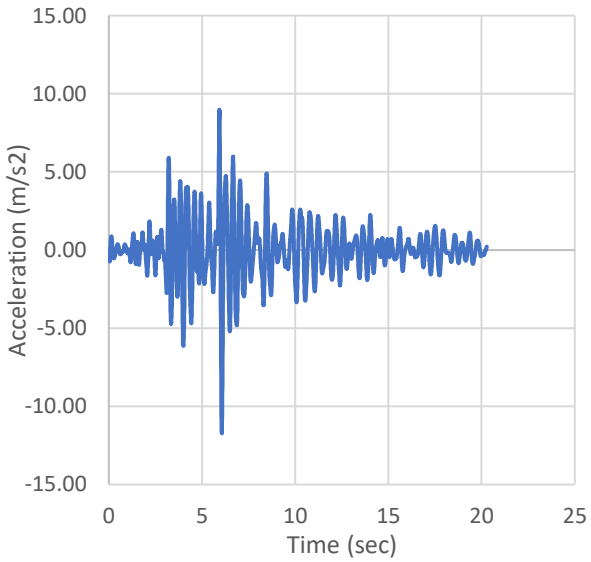

Figure 4.22 Acceleration (m/s^2) vs Time (sec) History for Coyote Lake Earthquake – Empty Reservoir Condition

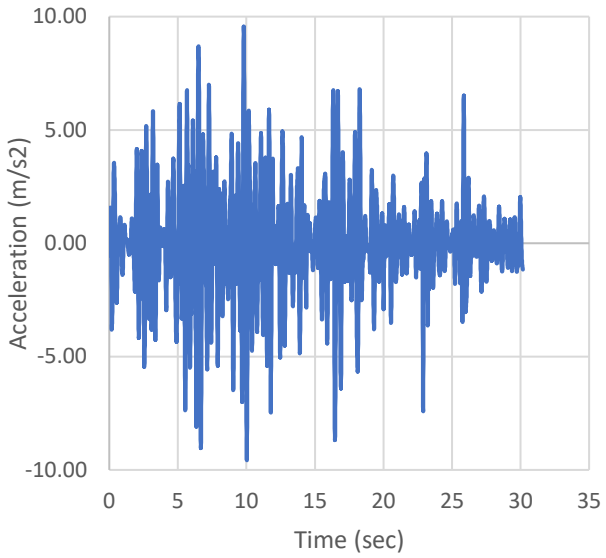

Figure 4.23 Acceleration (m/s^2) vs Time (sec) History for Loma Prieta Earthquake – Empty Reservoir Condition

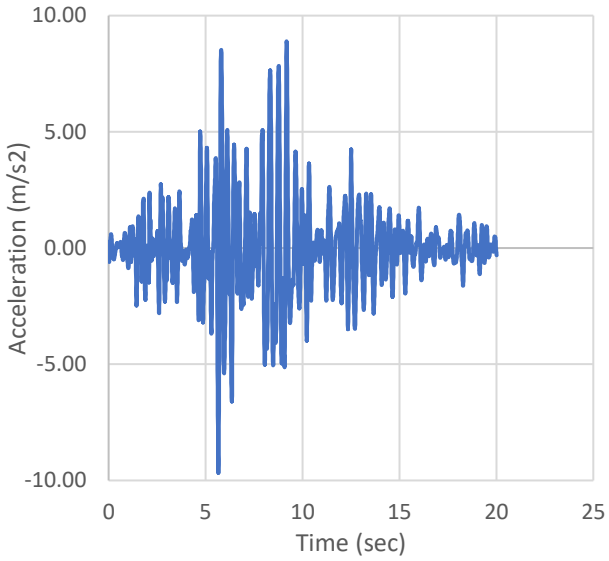

Figure 4.24 Acceleration (m/s^2) vs Time (sec) History for Palm Springs Earthquake – Empty Reservoir Condition

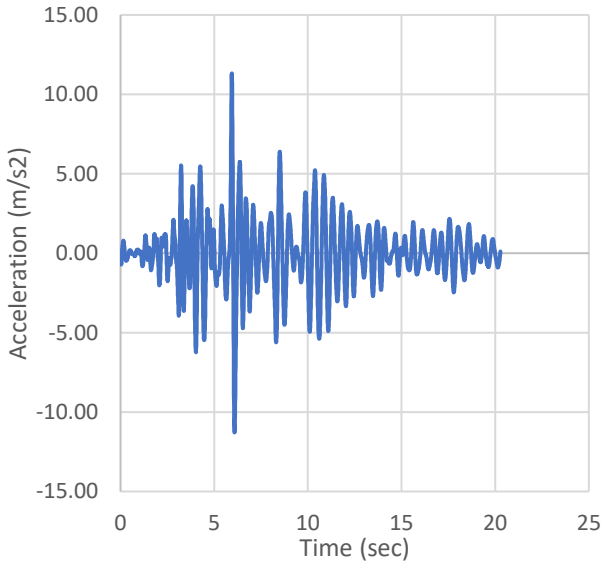

Figure 4.25 Acceleration (m/s^2) vs Time (sec) History for Coyote Lake Earthquake – Westergaard Method

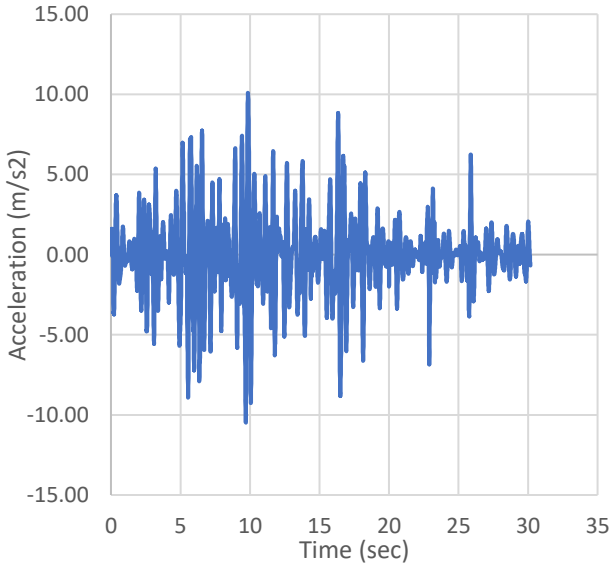

Figure 4.26 Acceleration (m/s^2) vs Time (sec) History for Loma Prieta Earthquake – Westergaard Method

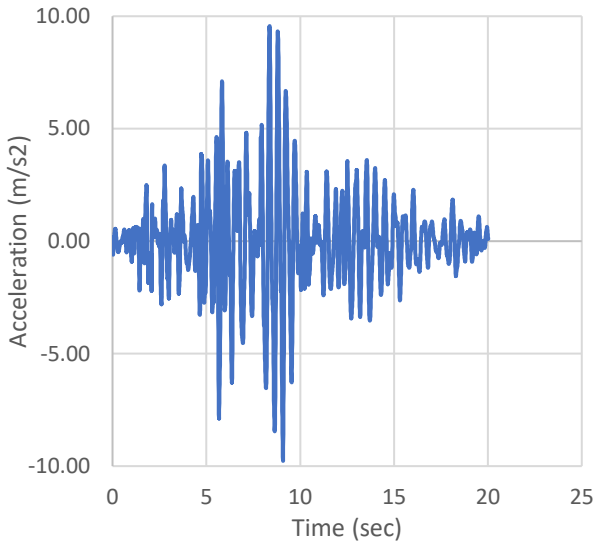

Figure 4.27 Acceleration (m/s^2) vs Time (sec) History for Palm Springs Earthquake – Westergaard Method

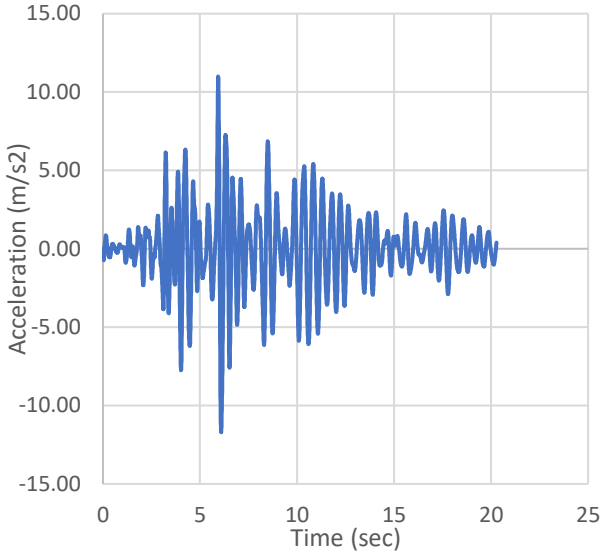

Figure 4.28 Acceleration (m/s^2) vs Time (sec) History for Coyote Lake Earthquake – Euler Method

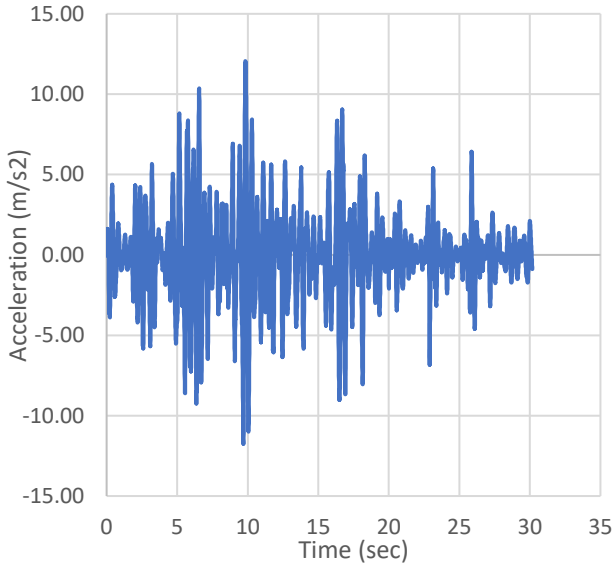

Figure 4.29 Acceleration (m/s^2) vs Time (sec) History for Loma Prieta Earthquake – Euler Method

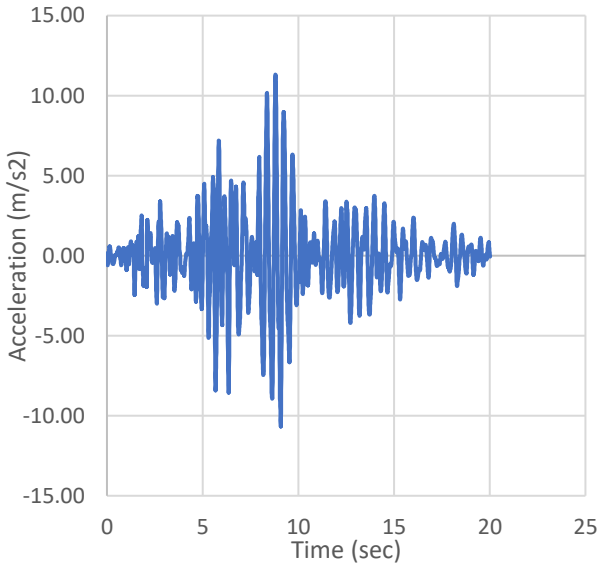

Figure 4.30 Acceleration (m/s^2) vs Time (sec) History for Palm Springs Earthquake – Euler Method

The observed maximum results associated with the displacement and acceleration of the dam crest from the linear analysis in the time-domain are indicated in Table 4.3. Furthermore, the research results are compared with the official results, which were obtained by a responsible company (G.F. Project and Engineering) for the construction of the Narli Dam. The official results were approved by DSI, which is a government company in Turkey. The maximum difference between the research and official results of both the displacement and acceleration of the crest of the dam is about 8%. The difference can be caused by the different selection of the boundary conditions relevant to the foundation. The responsible company selected boundary conditions for both sides of the rock as fixed in the y-direction and free in the x-direction.

Table 4.3 Comparison Time-History Results with Official Results based on Euler Method

Earthquakes	Research Results		Official Results	
	Max. Crest Displacement (cm)	Max. Crest Acceleration (g)	Max. Crest Displacement (cm)	Max. Crest Acceleration (g)
Coyote Lake	6.1	1.19	6.0	1.10
Loma Prieta	5.5	1.23	5.1	1.27
Palm Springs	5.4	1.15	5.9	1.10

***Official Results are obtained from GF Proje ve Muhendislik [GF Project and Engineering, 2018].**

4.4.1.2 Maximum and Minimum Principal Stress Results

Maximum and minimum principal stresses based on three approaches under three different ground motions are presented with the time-history plots (Figures 4.31-4.47). The positive values on the figures show the tensile stresses, whereas the negative numbers demonstrate the compressive stresses. The maximum principal stresses on the dam body are obtained as 5.61 MPa,

7.96 MPa, and 8.46 MPa for empty reservoir condition, Westergaard approach, and Euler method, respectively. All attained maximum tensile stresses from the linear transient analyses exceed the tensile strength of the concrete. The flexural strength of the structure was calculated as 3.99 MPa and 3.83 MPa based on Raphael (1984) and Cannon (1995), respectively. Since the demand capacity ratio is more than 2.0, more refined analyses are required to determine the tensile cracking profile of the Narli Dam such as nonlinear transient dynamic analysis. On the other hand, the minimum principal stresses on the dam body are attained as 4.43 MPa, 6.66 MPa, and 6.48 MPa for empty reservoir condition, Westergaard approach, and Euler method, respectively. In the contrast of tensile stresses, compressive stresses never exceed the compressive strength of the concrete, which was determined as 15 MPa for the Narli Dam.

The time-history figures indicate that the maximum stresses for tension and compression should not be expected to occur at the same time even though the happening time for them are generally close to each other. By observing time-history plots, it can be stated that the maximum tensile principal stresses occur in the upstream face of the gravity dam, whereas the maximum compressive principal stresses happen in the downstream face of the structure. Therefore, the figures show that the heel of the dam is more susceptible to tensile cracking than the dam toe while the toe of the structure is more prone to cracking relevant to compression than the dam heel.

The figures clearly illustrate that the presence of the reservoir increases the principal stresses on the dam body. The tensile stresses generally decrease between 42% and 58% when water is not considered in comparison to the added mass method. When considering the reservoir is compressible, moreover, the maximum principal stresses increase between 50% and 73% relative to the empty condition. The difference between Westergaard and Euler methods depending on tensile stress results is about 10%, and supposing the incompressible water condition

(Westergaard approach) underestimates the results than estimating compressible condition (Euler approach). Similarly, when the reservoir is considered in the linear transient analysis, the minimum principal stresses increase up to 68% and 71% due to hydrodynamic forces for Westergaard and Euler methods, respectively. The other critical point is the midpoint of the structure in the upstream direction. The maximum principal stress is determined as about 3.80 MPa which is less than the flexural strength of concrete, and thus tensile cracking is not expected at this point.

As a result, the maximum compressive stress is not a concern for the seismic evaluation of the Narli dam. Because of high tensile stress results, on the other hand, the nonlinear time-history dynamic analysis should be performed.

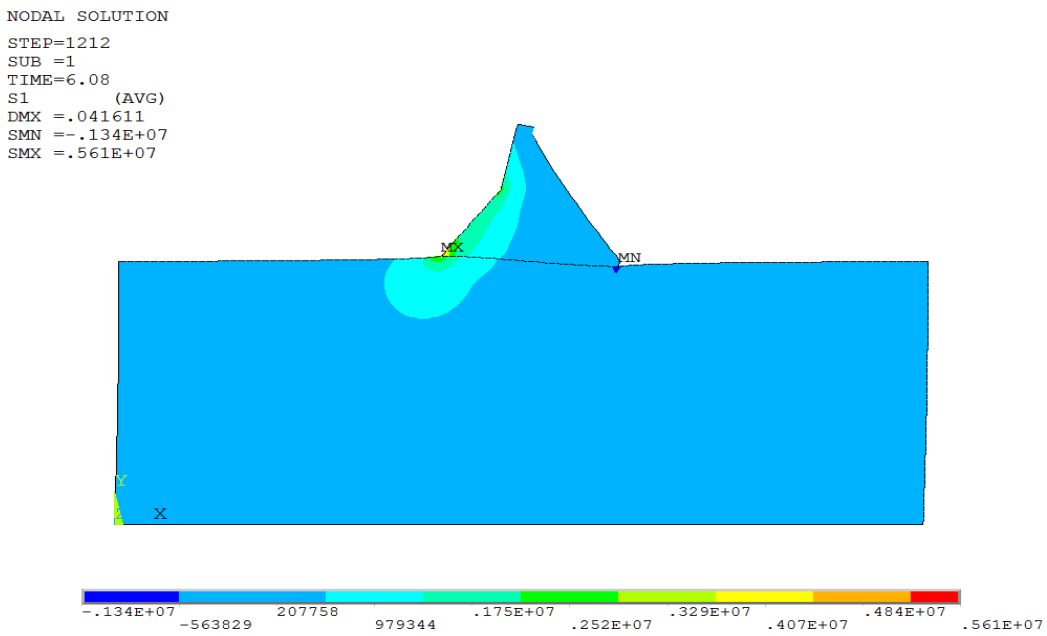

"Principal Stresses (N/m^2)"

Figure 4.31 Maximum Tensile Stress (+) Distributions at 6.08 sec. for Coyote Lake Earthquake – Empty Reservoir Condition

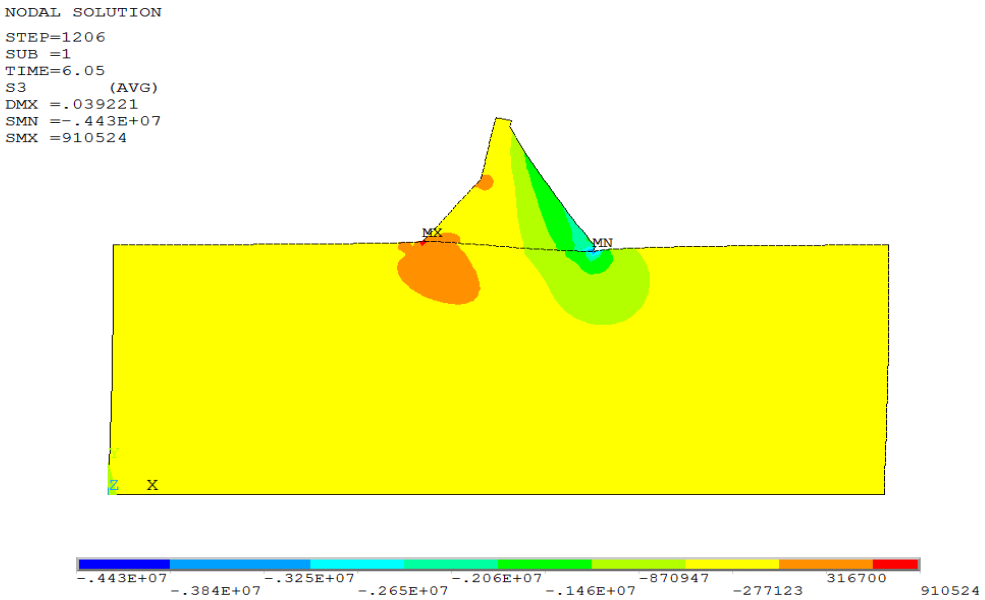

"Principal Stresses (N/m^2)"

Figure 4.32 Maximum Compressive Stress (-) Distributions at 6.05 sec. for Coyote Lake Earthquake – Empty Reservoir Condition

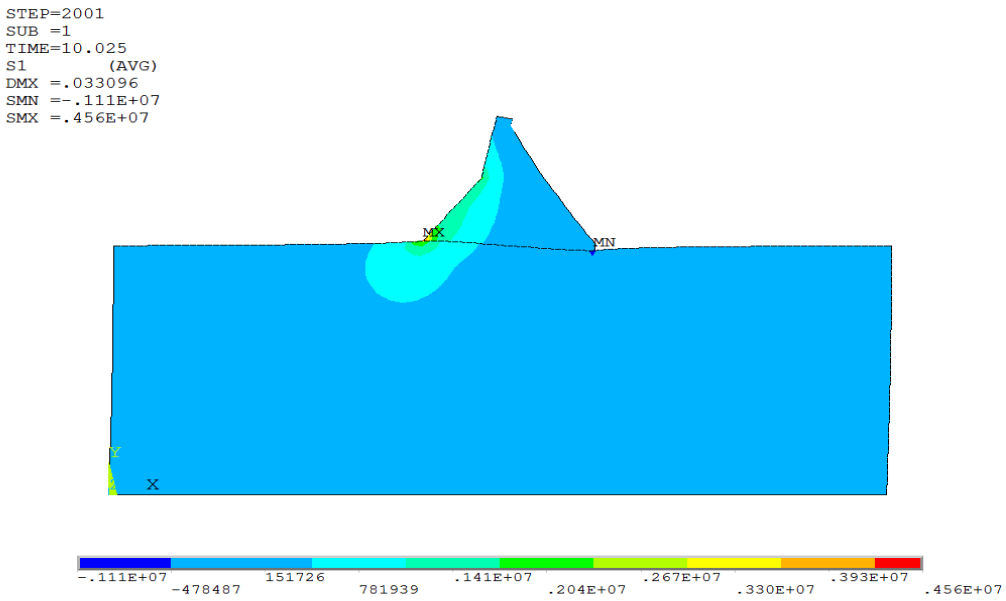

"Principal Stresses (N/m^2)"

Figure 4.33 Maximum Tensile Stress (+) Distributions at 10.025 sec. for Loma Prieta Earthquake – Empty Reservoir Condition

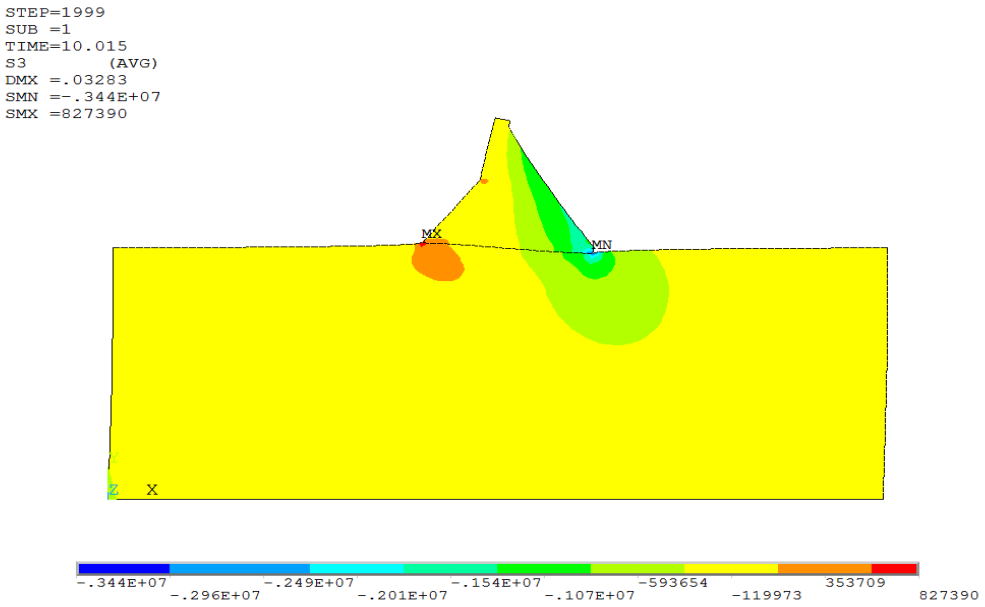

"Principal Stresses (N/m^2)"

Figure 4.34 Maximum Compressive Stress (-) Distributions at 10.015 sec. for Loma Prieta Earthquake – Empty Reservoir Condition

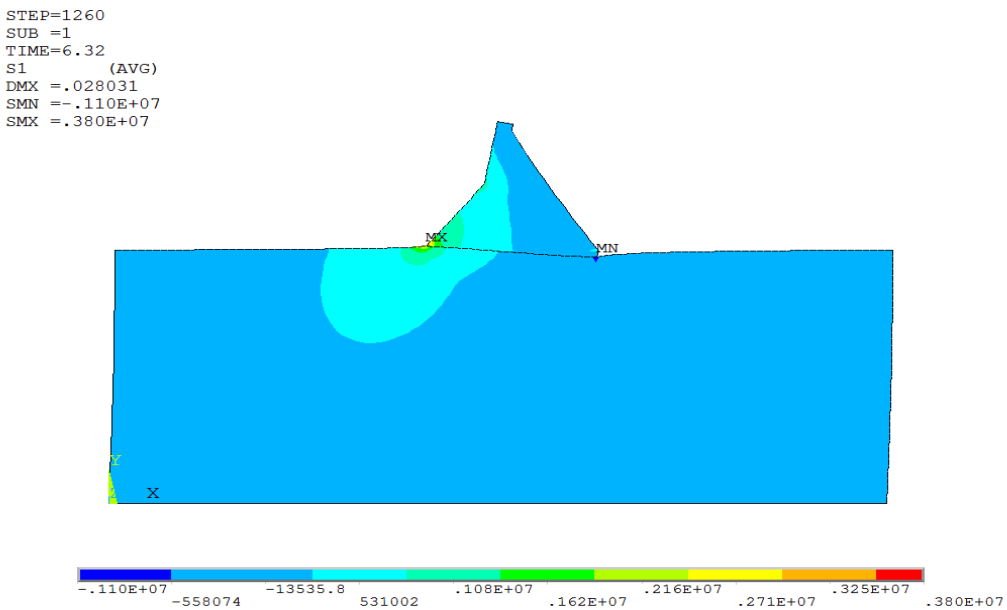

"Principal Stresses (N/m^2)"

Figure 4.35 Maximum Tensile Stress (+) Distributions at 6.32 sec. for Palm Springs Earthquake – Empty Reservoir Condition

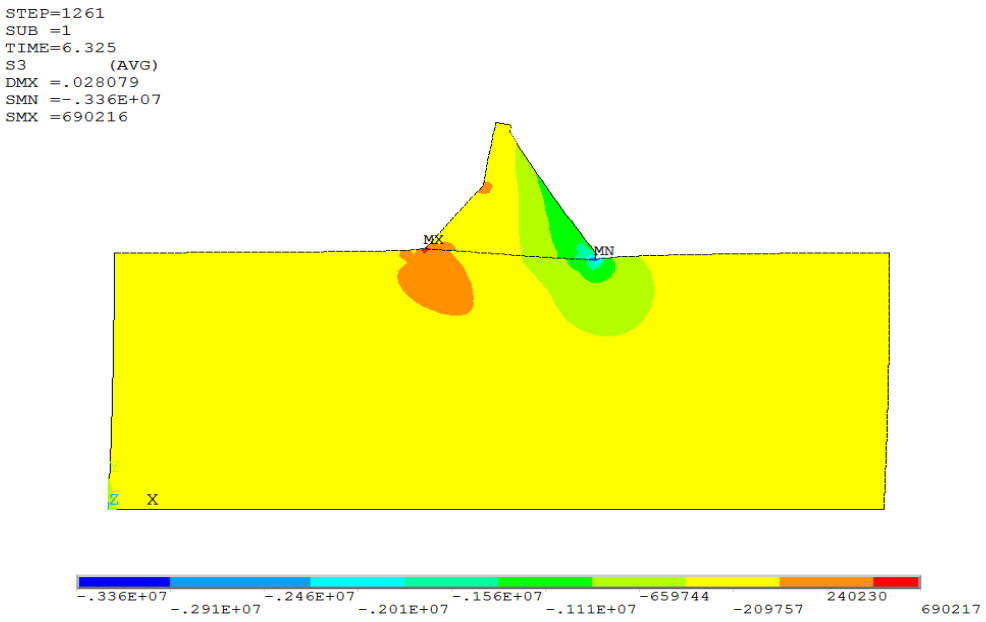

"Principal Stresses (N/m^2)"

Figure 4.36 Maximum Compressive Stress (-) Distributions at 6.325 sec. for Palm Springs Earthquake – Empty Reservoir Condition

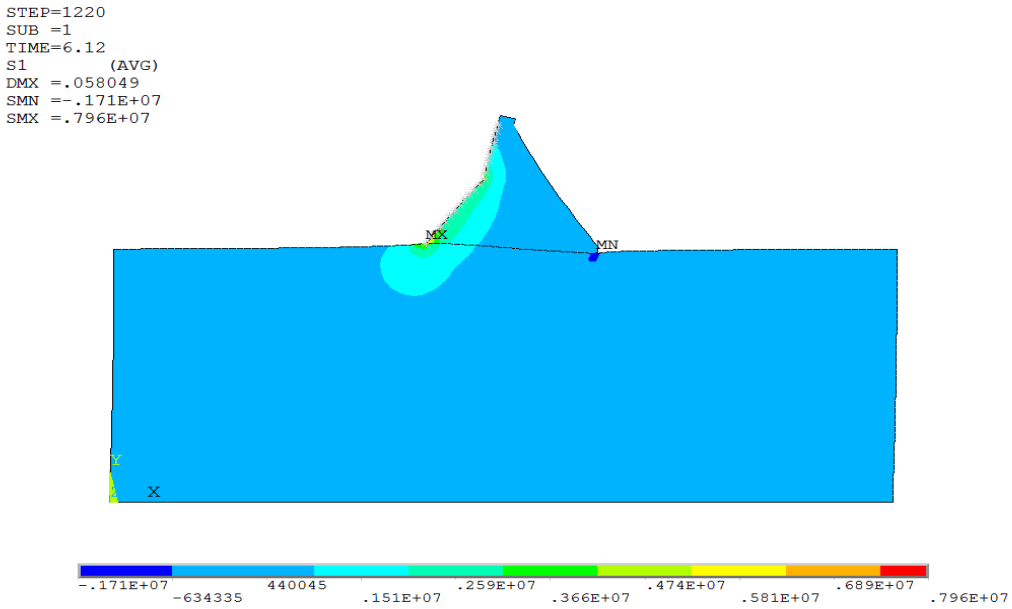

"Principal Stresses (N/m^2)"

Figure 4.37 Maximum Tensile Stress (+) Distributions at 6.12 sec. for Coyote Lake Earthquake – Westergaard Method

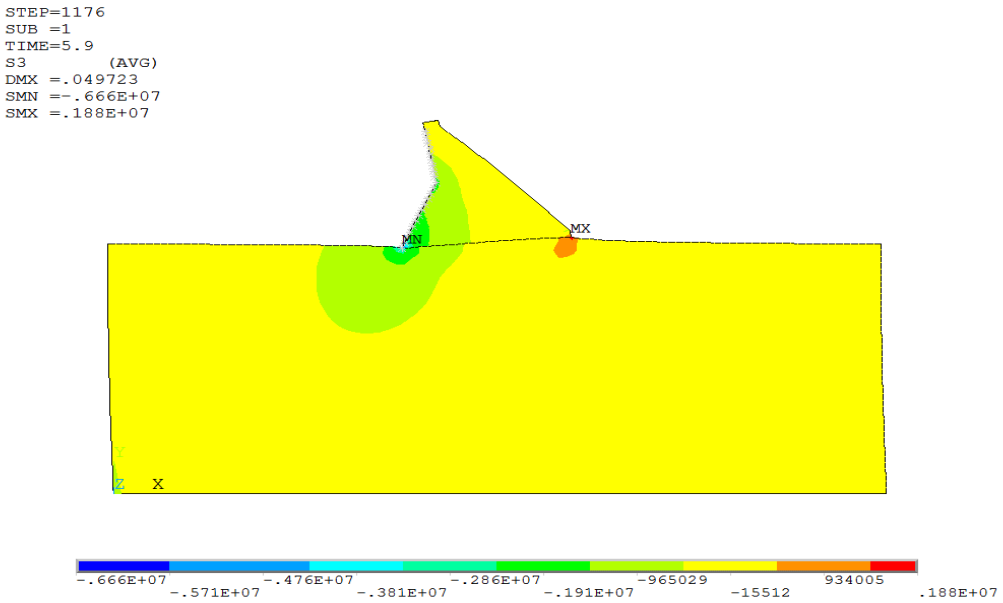

"Principal Stresses (N/m^2)"

Figure 4.38 Maximum Compressive Stress (-) Distributions at 5.9 sec. for Coyote Lake Earthquake – Westergaard Method

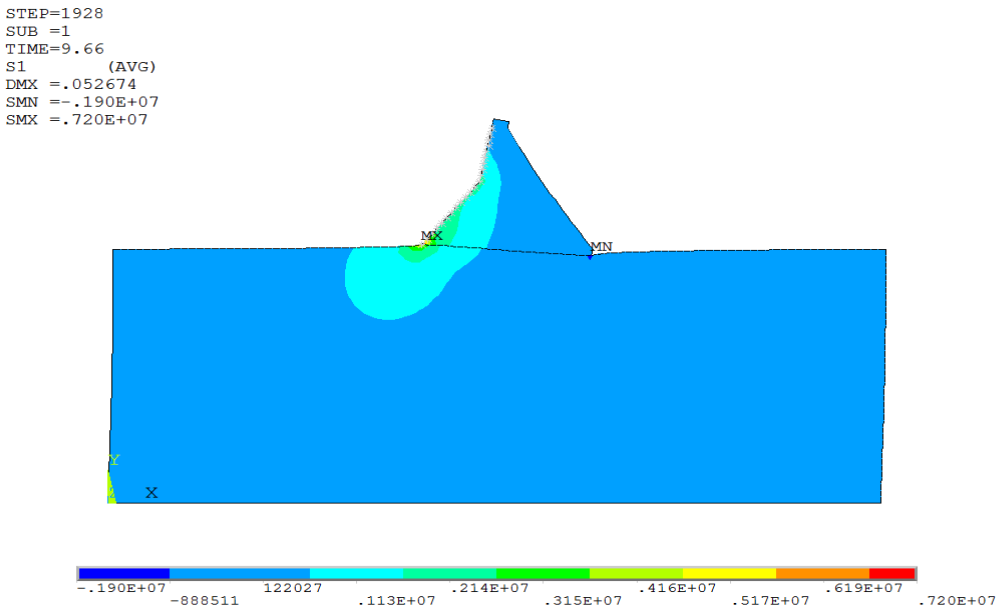

"Principal Stresses (N/m^2)"

Figure 4.39 Maximum Tensile Stress (+) Distributions at 9.66 sec. for Loma Prieta Earthquake – Westergaard Method

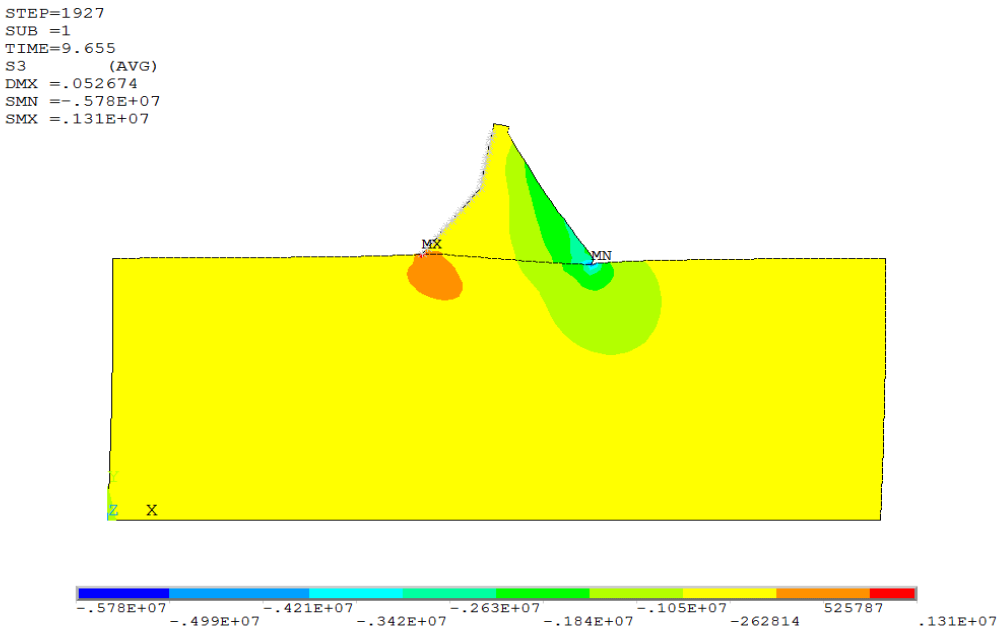

"Principal Stresses (N/m^2)"

Figure 4.40 Maximum Compressive Stress (-) Distributions at 9.655 sec. for Loma Prieta Earthquake – Westergaard Method

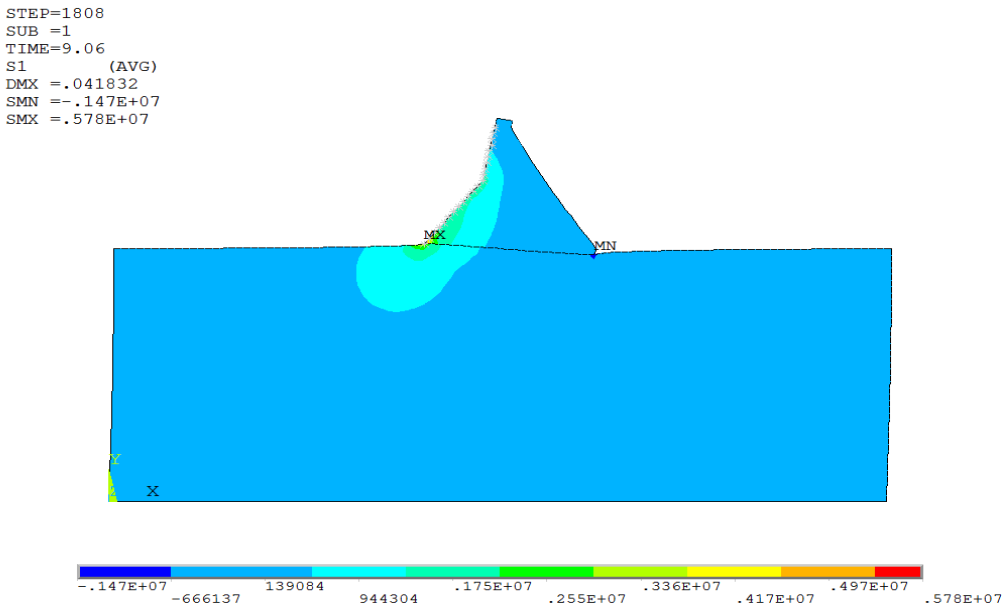

"Principal Stresses (N/m^2)"

Figure 4.41 Maximum Tensile Stress (+) Distributions at 9.06 sec. for Palm Springs Earthquake – Westergaard Method

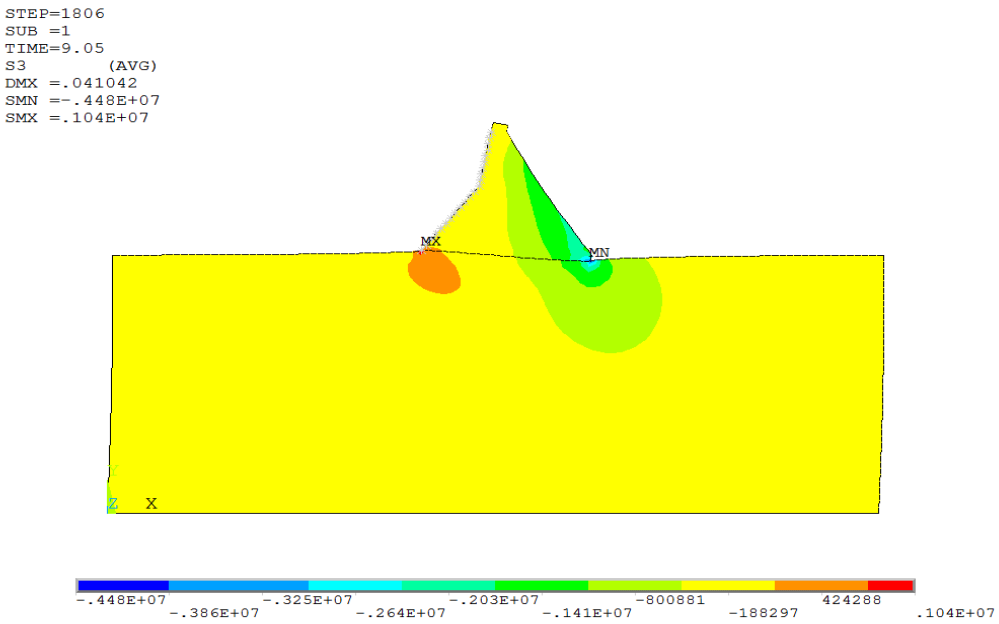

"Principal Stresses (N/m^2)"

Figure 4.42 Maximum Compressive Stress (-) Distributions at 9.05 sec. for Palm Springs Earthquake – Westergaard Method

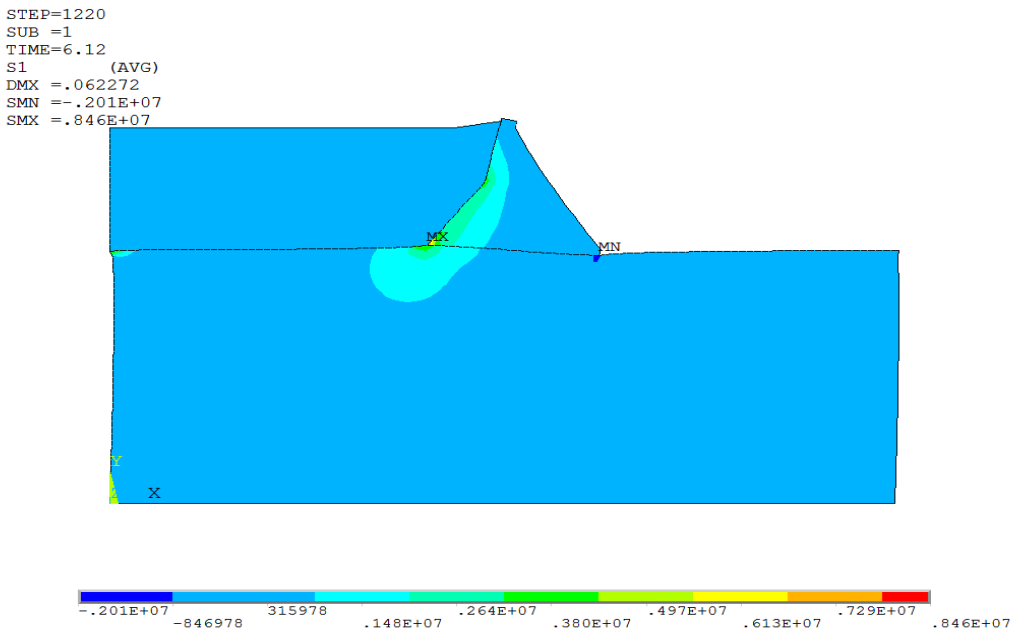

"Principal Stresses (N/m^2)"

Figure 4.43 Maximum Tensile Stress (+) Distributions at 6.12 sec. for Coyote Lake Earthquake – Euler Method

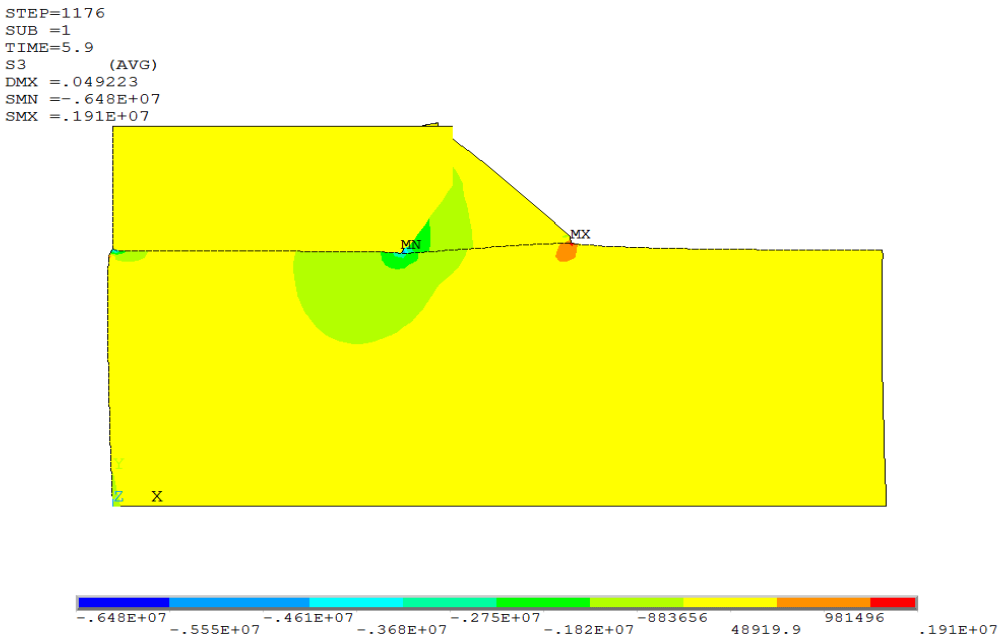

"Principal Stresses (N/m^2)"

Figure 4.44 Maximum Compressive Stress (-) Distributions at 5.9 sec. Coyote Lake Earthquake – Euler Method

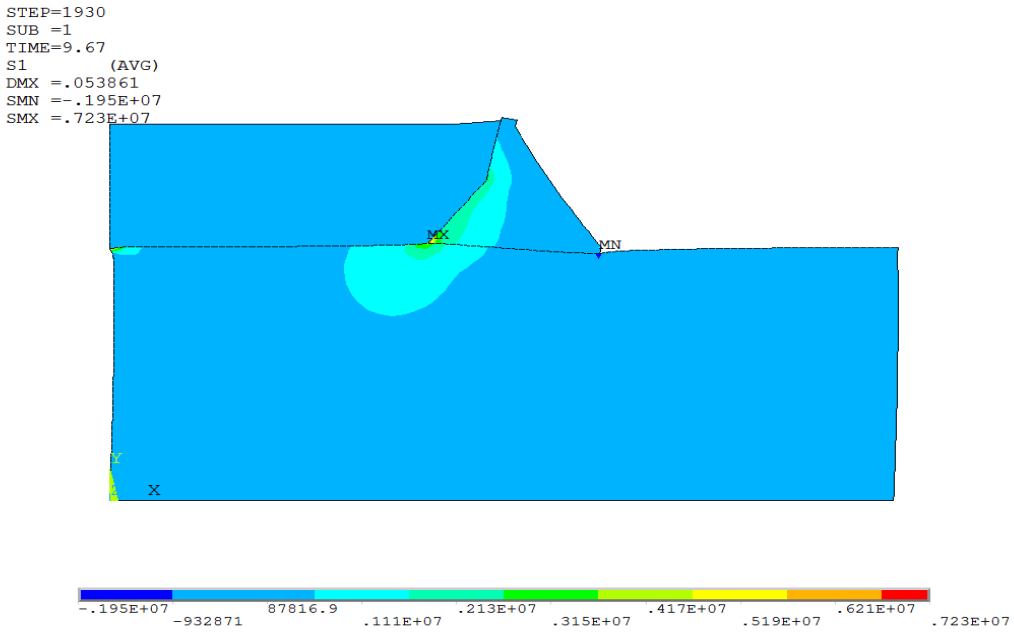

"Principal Stresses (N/m^2)"

Figure 4.45 Maximum Tensile Stress (+) Distributions at 9.67 sec. for Loma Prieta Earthquake – Euler Method

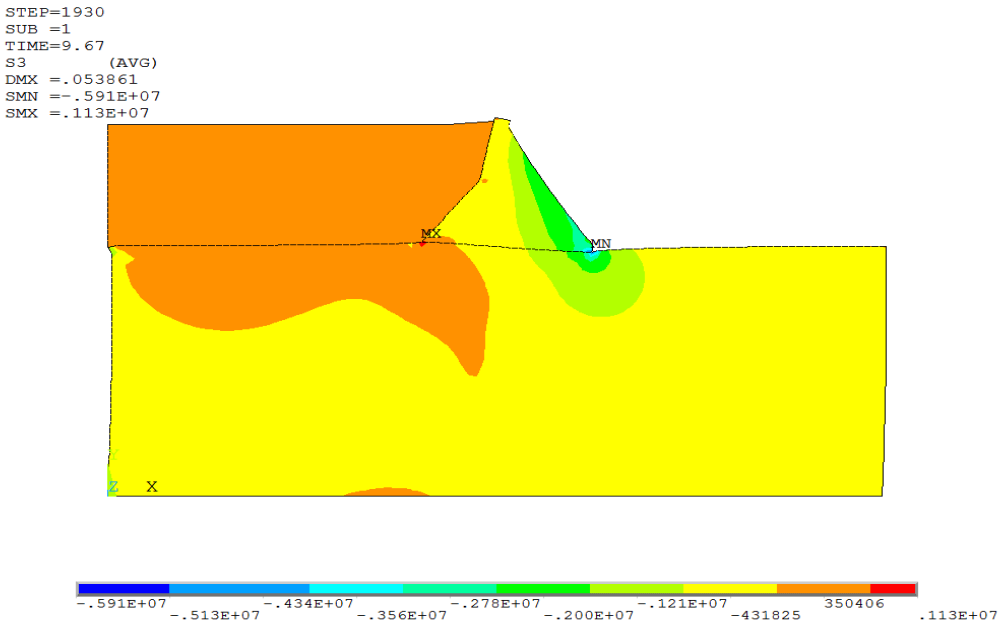

"Principal Stresses (N/m^2)"

Figure 4.46 Maximum Compressive Stress (-) Distributions at 9.67 sec. Loma Prieta Earthquake – Euler Method

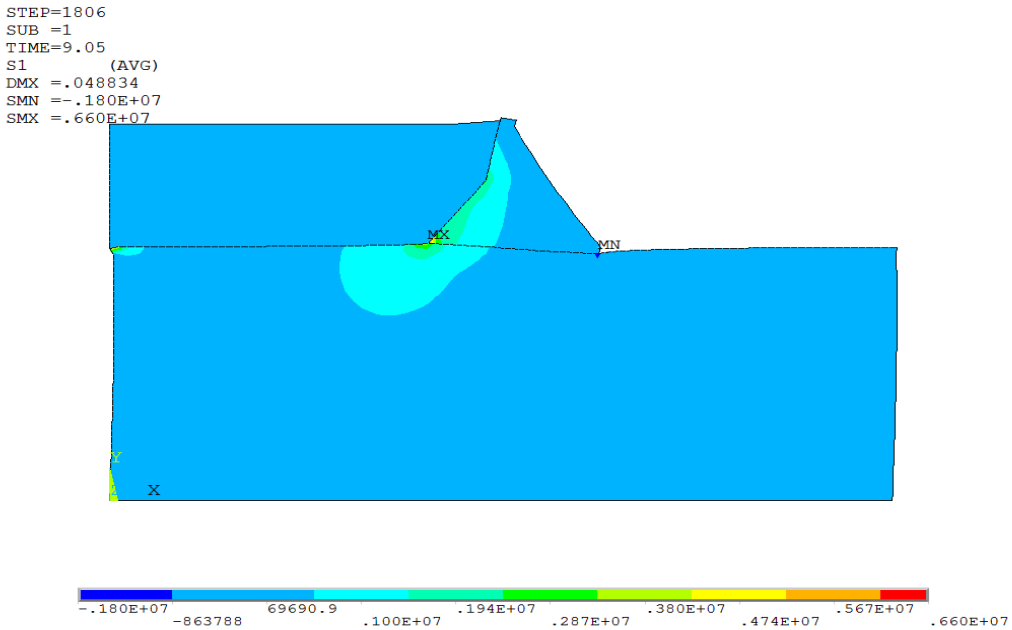

"Principal Stresses (N/m^2)"

Figure 4.47 Maximum Tensile Stress (+) Distributions at 9.05 sec. for Palm Springs Earthquake – Euler Method

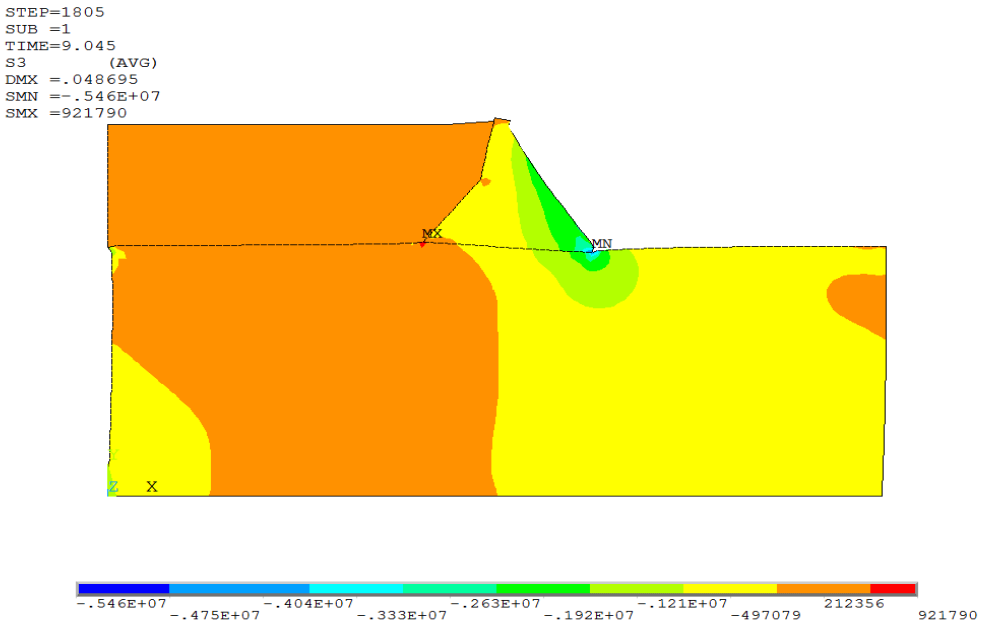

"Principal Stresses (N/m^2)"

Figure 4.48 Maximum Compressive Stress (-) Distributions at 9.045 sec. Palm Springs Earthquake – Euler Method

The attained maximum results related to 1st principal stress on the dam body from the linear analysis in the time-domain are demonstrated in Table 4.4. The maximum difference between the research and official results is approximately 5%. The difference can be resulted from the different selection of the boundary conditions relevant to the rock.

Table 4.4 Comparison Principal Stress Results with Official Results depending on Euler Method

Earthquakes	Research Results	Official Results
	Max. Tensile Stress (MPa)	Max. Tensile Stress (MPa)
Coyote Lake	8.46	8.35
Loma Prieta	7.23	7.19
Palm Springs	6.60	6.94

***Official Results are obtained from GF Proje ve Muhendislik [GF Project and Engineering, 2018].**

4.5 Nonlinear Dynamic Analysis of Narli Dam

The Drucker Prager approach is used for the dam-foundation-reservoir interaction in non-linear analysis. The results of linear and nonlinear analyses are compared based on the maximum displacements, principal stresses, and cracking on the critical points of the concrete gravity dam. Even if the compression values on the dam body never exceed the compressive strength of concrete in the linear transient analyses, they are again evaluated using the nonlinear time-history analyses to solve out the difference in the consequences. Furthermore, the changes in acceleration and displacement results of the dam crest associated with linear and nonlinear analyses will be displayed. More importantly, maximum principal stress values will be presented more precisely because nonlinear analyses enable more accurate results to estimate the level of damage of the structure than linear analyses. Moreover, if any plastic strain occurs after performing nonlinear time-history dynamic analysis, it will be discussed in this section.

The cohesion and the internal friction angle of the concrete for the Drucker Prager model are supposed as to be 1.5 MPa and 45°, respectively. Additionally, the cohesion and the internal friction angle of the foundation are assumed as to be 1.9 MPa and 27°, respectively (GF Proje ve Muhendislik, 2018 [GF Project and Engineering, 2018]). The dilatancy angle for the foundation and concrete are identical to the friction angle in the analysis. In this way, the model uses associated plasticity.

4.5.1 Nonlinear Time-History Results for Displacement and Acceleration

It can be concluded considering Tables 4.5 and 4.6 that linear dynamic analysis is a beneficial tool to estimate the displacement and acceleration of the crest of the dam since the

variation in two methods are sufficiently low when the massless foundation model is used for the Narli Dam.

Table 4.5 Comparison Nonlinear Displacement Results of the Crest of Dam with Linear Results depending on three different approaches

Earthquakes	Empty Reservoir Condition		Westergaard Approach		Euler Method	
	Max. Crest Displacement (cm)		Max. Crest Displacement (cm)		Max. Crest Displacement (cm)	
	Linear	Nonlinear	Linear	Nonlinear	Linear	Nonlinear
Coyote Lake	4.14	4.05	5.67	5.35	6.16	5.80
Loma Prieta	3.44	3.45	5.22	5.17	5.58	5.59
Palm Springs	3.57	3.58	5.11	5.09	5.42	5.53

Table 4.6 Comparison Nonlinear Acceleration Results of the Crest of Dam with Linear Results depending on three different approaches

Earthquakes	Empty Reservoir Condition		Westergaard Approach		Euler Method	
	Max. Crest Acceleration (g)		Max. Crest Acceleration (g)		Max. Crest Acceleration (g)	
	Linear	Nonlinear	Linear	Nonlinear	Linear	Nonlinear
Coyote Lake	1.19	1.15	1.15	1.17	1.19	1.16
Loma Prieta	0.98	0.97	1.07	1.04	1.23	1.18
Palm Springs	0.99	0.98	0.99	0.98	1.15	1.10

4.5.2 Nonlinear Time-History Results for Principal Stresses

In accordance with the nonlinear analyses, Westergaard and Euler approaches presented similar values related to the 1st principal stresses on the dam body. On the other hand, up to a 61%

reduction in the stresses happens when the reservoir is ignored in the finite element modeling. The maximum principal stresses on the heel of the dam in the upstream direction are attained as 2.71 MPa, 3.15 MPa, and 3.05 MPa for empty reservoir condition, Westergaard approach, and Euler method, respectively. In the contrast of linear time-history analyses, the tensile stresses do not exceed the tensile strength of concrete that are calculated as 3.99 MPa and 3.83 MPa depending on Raphael (1984) and Cannon (1995), respectively. Thus, failure of the dam caused by the tensile stresses on the dam heel under the same strong earthquakes is not expected in the light of nonlinear dynamic analyses.

By contrast with linear dynamic analysis, obtained 3rd principal stresses for the toe of the dam in the downstream direction considerably increase when the nonlinear analysis is considered. Maximum compressive stresses, which are demonstrated in Table 4.7, are attained as 5.74 MPa, 8.16 MPa, and 9.16 MPa for empty reservoir condition, Westergaard approach, and Euler method, respectively. Even if significant increasing in the minimum principal stress values occur by considering nonlinear time-history analyses, the compressive strength of concrete that is calculated as 15 MPa for the Narli Dam are sufficient to meet the criteria for the demand capacity ratio. Therefore, damages resulted from the stresses associated with compression under similar ground motions are not expected for the Narli Dam when examining the consequences of nonlinear transient dynamic analyses.

In comparing linear and nonlinear results, linear analyses provide accurate conclusions to estimate the effect of hydrodynamic forces on the displacements and accelerations of the dam. However, it leads to overestimated results for tensile stresses and underestimated results for the compressive stresses compared with the more refined analysis.

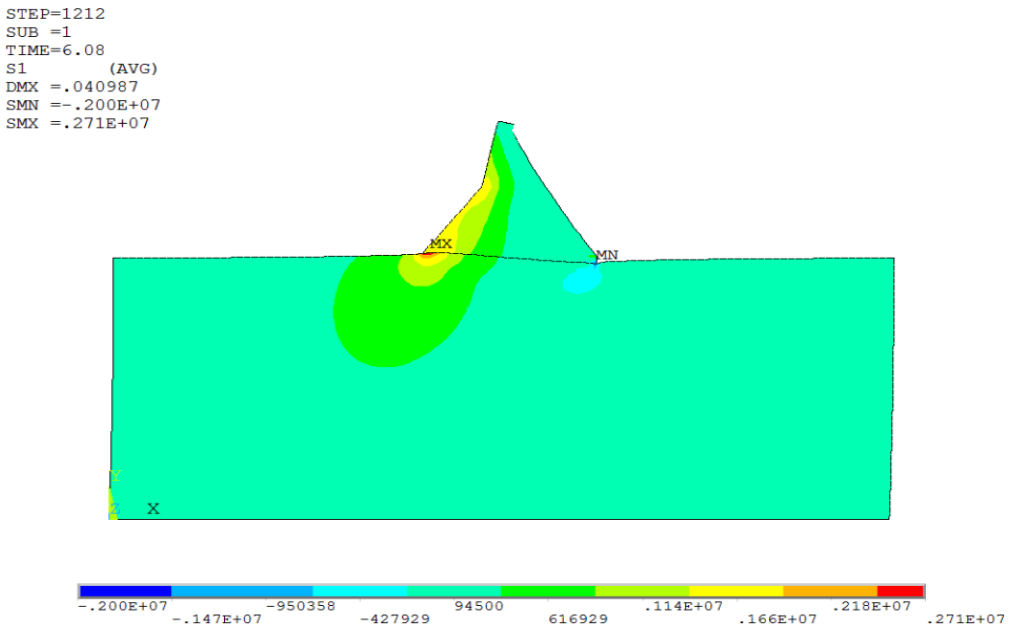

"Principal Stresses (N/m^2)"

Figure 4.49 Maximum Tensile Stress (+) Distributions at 6.08 sec. for Coyote Lake Earthquake – Empty Reservoir Condition

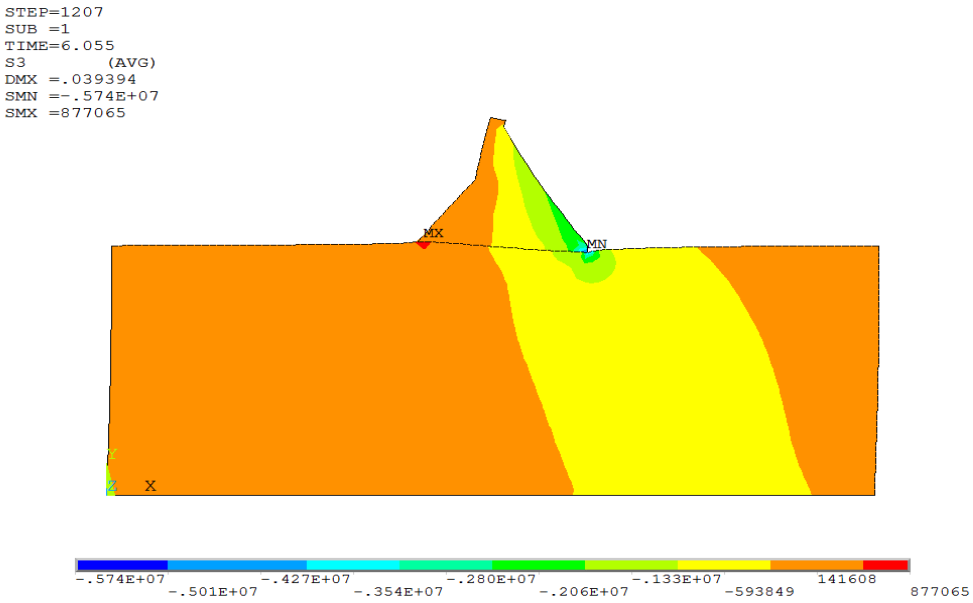

"Principal Stresses (N/m^2)"

Figure 4.50 Maximum Compressive Stress (-) Distributions at 6.055 sec. for Coyote Lake Earthquake – Empty Reservoir Condition

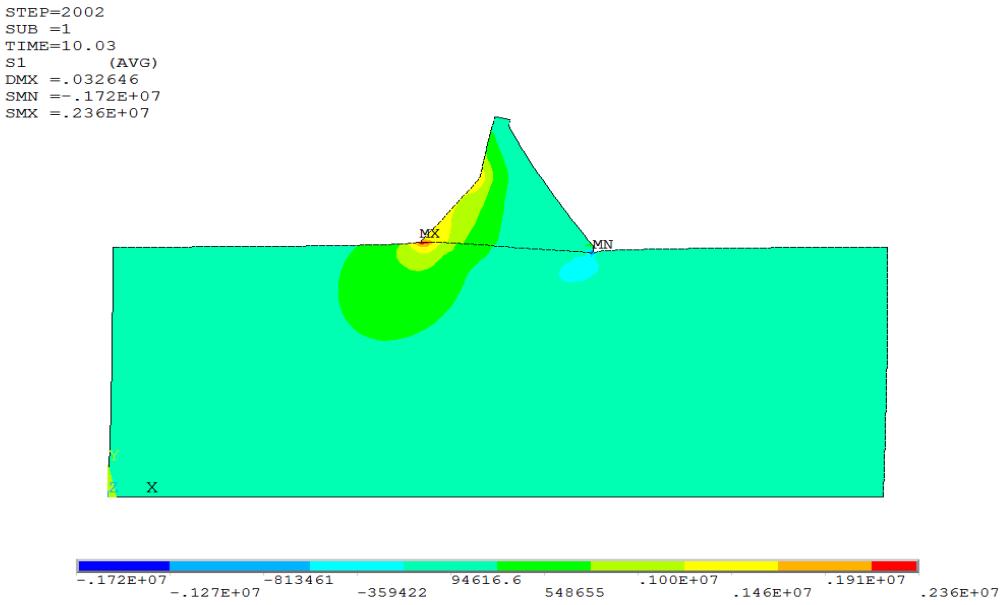

"Principal Stresses (N/m^2)"

Figure 4.51 Maximum Tensile Stress (+) Distributions at 10.03 sec. for Loma Prieta Earthquake – Empty Reservoir Condition

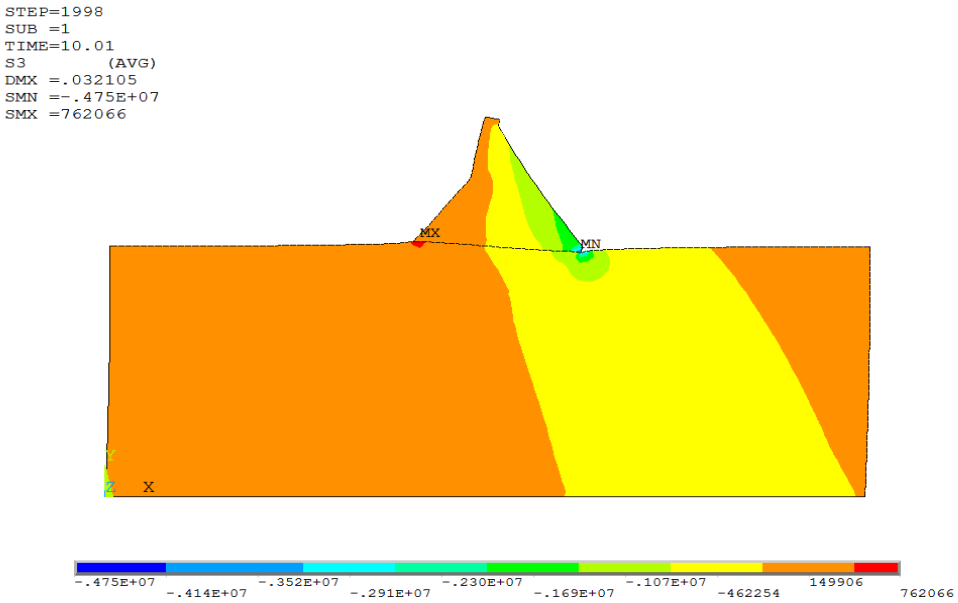

"Principal Stresses (N/m^2)"

Figure 4.52 Maximum Compressive Stress (-) Distributions at 10.01 sec. for Loma Prieta Earthquake – Empty Reservoir Condition

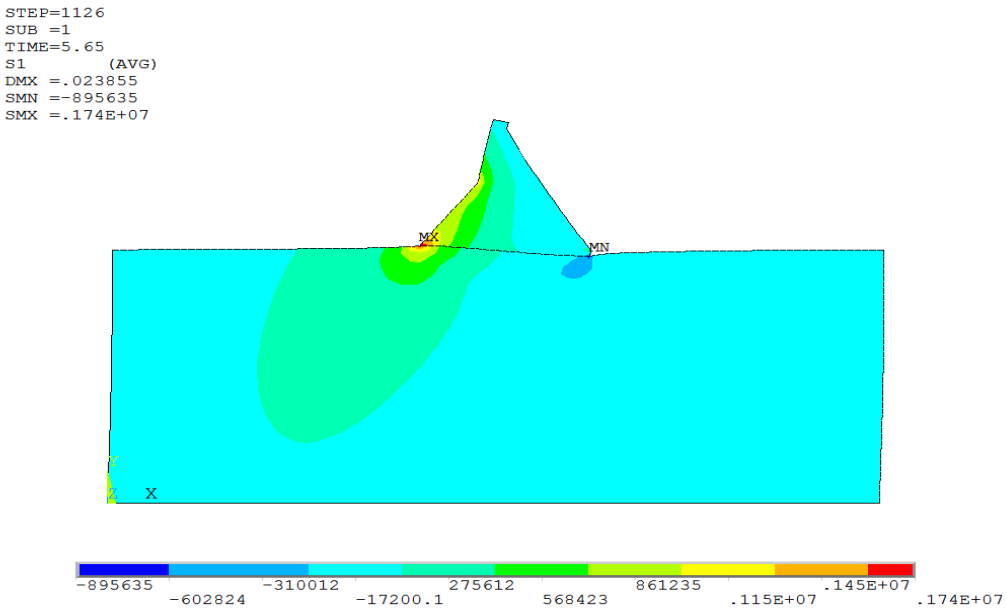

"Principal Stresses (N/m^2)"

Figure 4.53 Maximum Tensile Stress (+) Distributions at 5.65 sec. for Palm Springs Earthquake – Empty Reservoir Condition

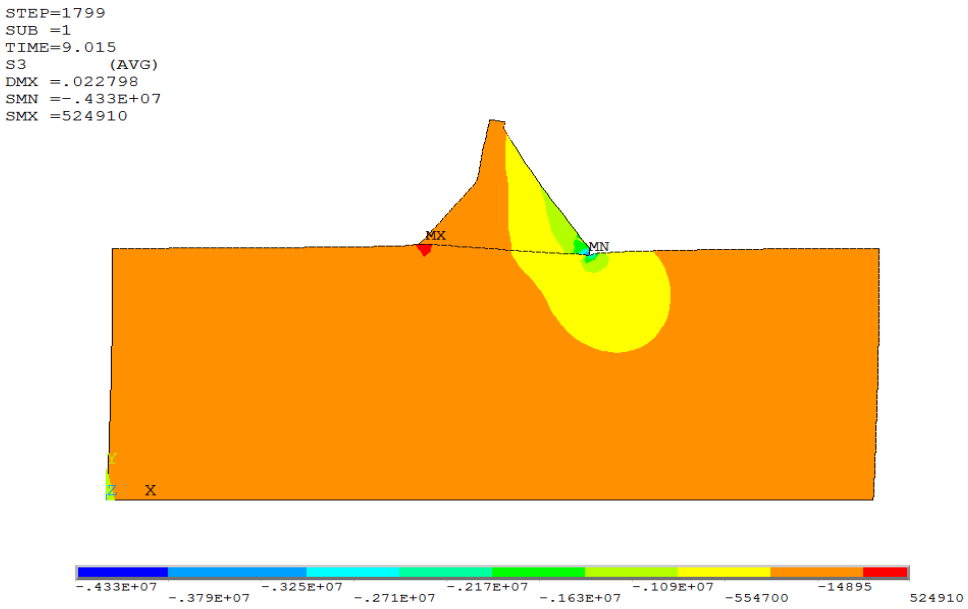

"Principal Stresses (N/m^2)"

Figure 4.54 Maximum Compressive Stress (-) Distributions at 9.015 sec. for Palm Springs Earthquake – Empty Reservoir Condition

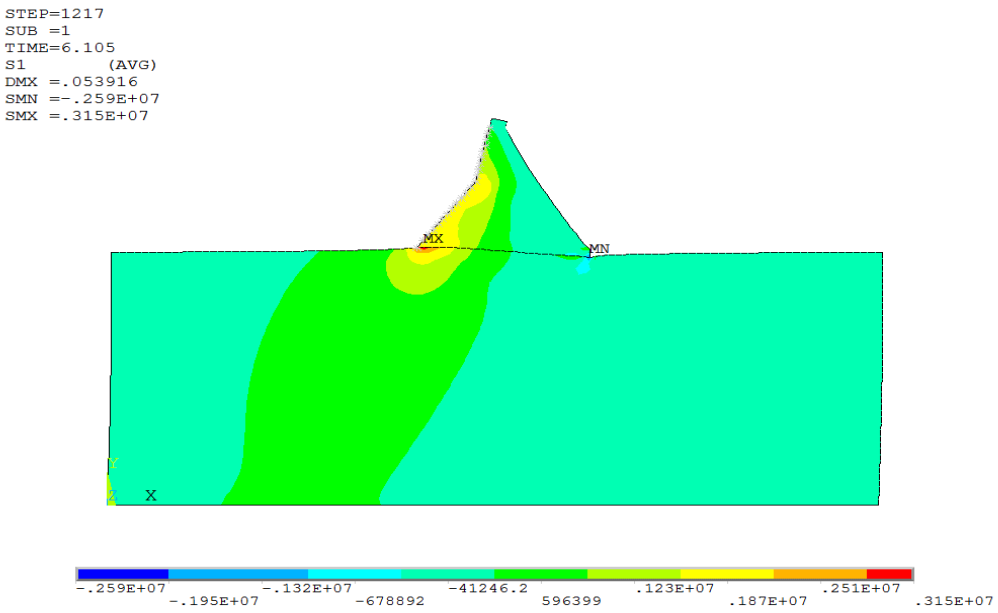

"Principal Stresses (N/m^2)"

Figure 4.55 Maximum Tensile Stress (+) Distributions at 6.105 sec. for Coyote Lake Earthquake – Westergaard Method

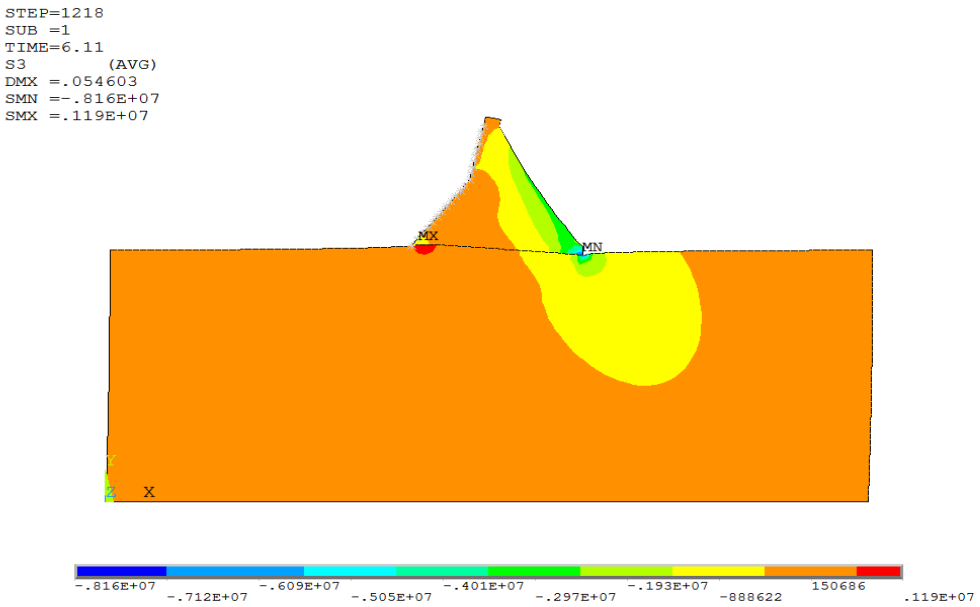

"Principal Stresses (N/m^2)"

Figure 4.56 Maximum Compressive Stress (-) Distributions at 6.11 sec. for Coyote Lake Earthquake – Westergaard Method

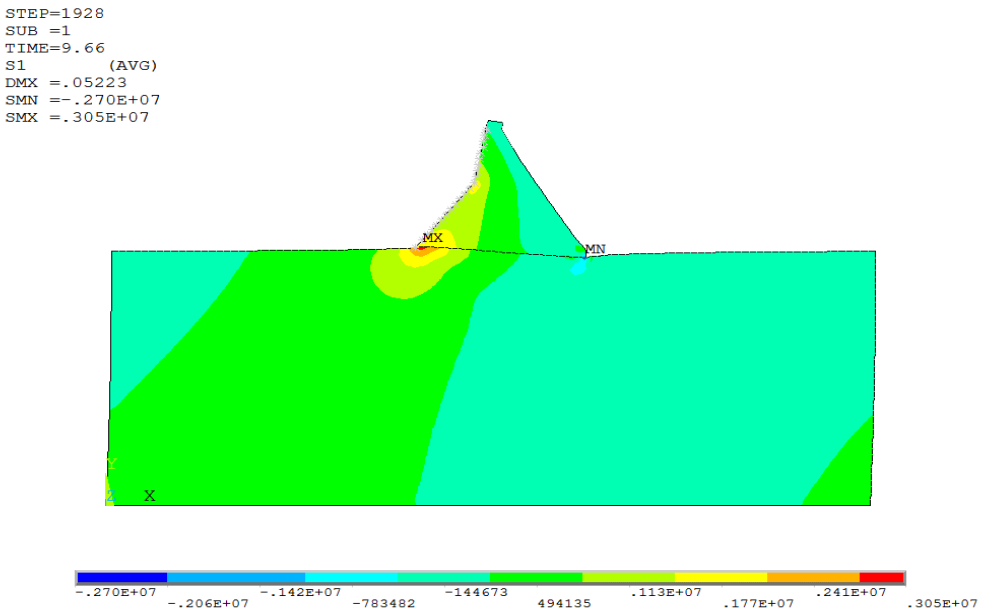

"Principal Stresses (N/m^2)"

Figure 4.57 Maximum Tensile Stress (+) Distributions at 9.66 sec. for Loma Prieta Earthquake – Westergaard Method

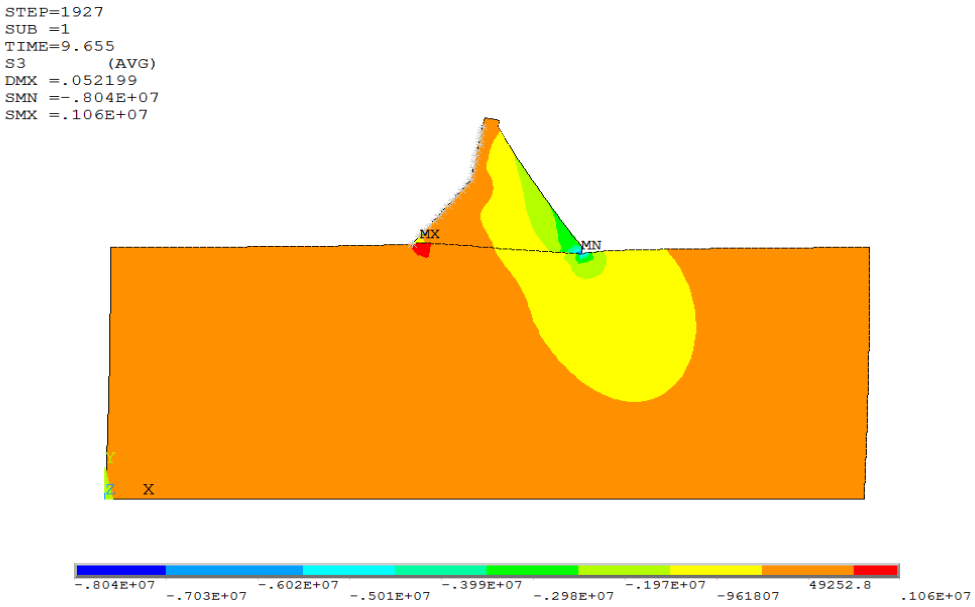

"Principal Stresses (N/m^2)"

Figure 4.58 Maximum Compressive Stress (-) Distributions at 9.655 sec. for Loma Prieta Earthquake – Westergaard Method

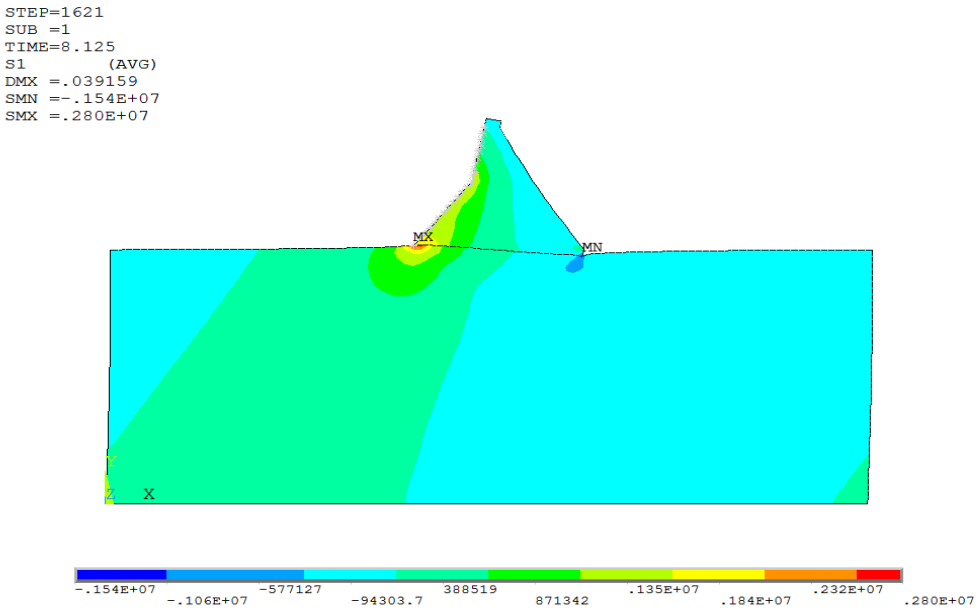

"Principal Stresses (N/m^2)"

Figure 4.59 Maximum Tensile Stress (+) Distributions at 8.125 sec. for Palm Springs Earthquake – Westergaard Method

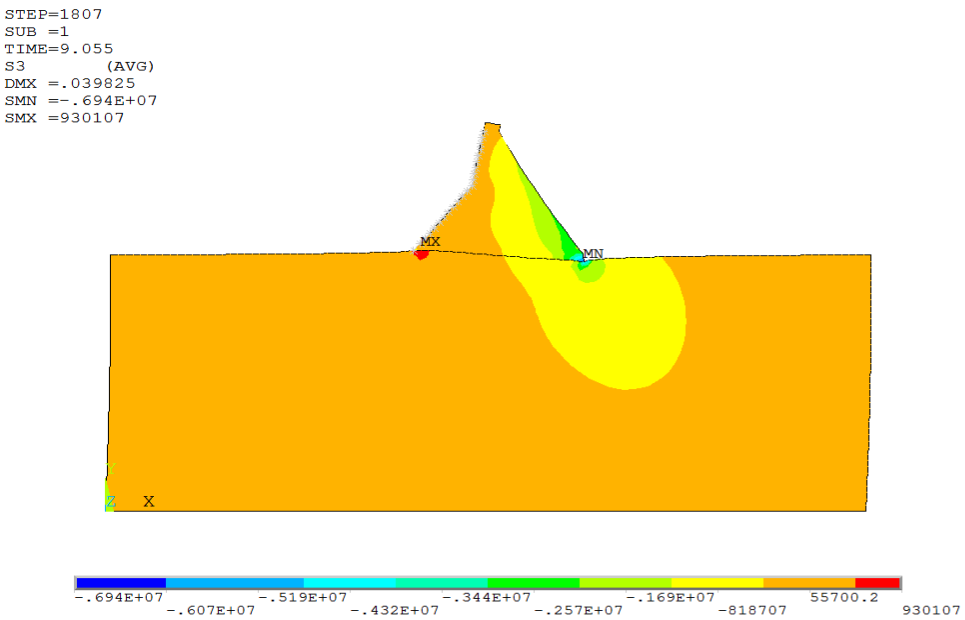

"Principal Stresses (N/m^2)"

Figure 4.60 Maximum Compressive Stress (-) Distributions at 9.055 sec. for Palm Springs Earthquake – Westergaard Method

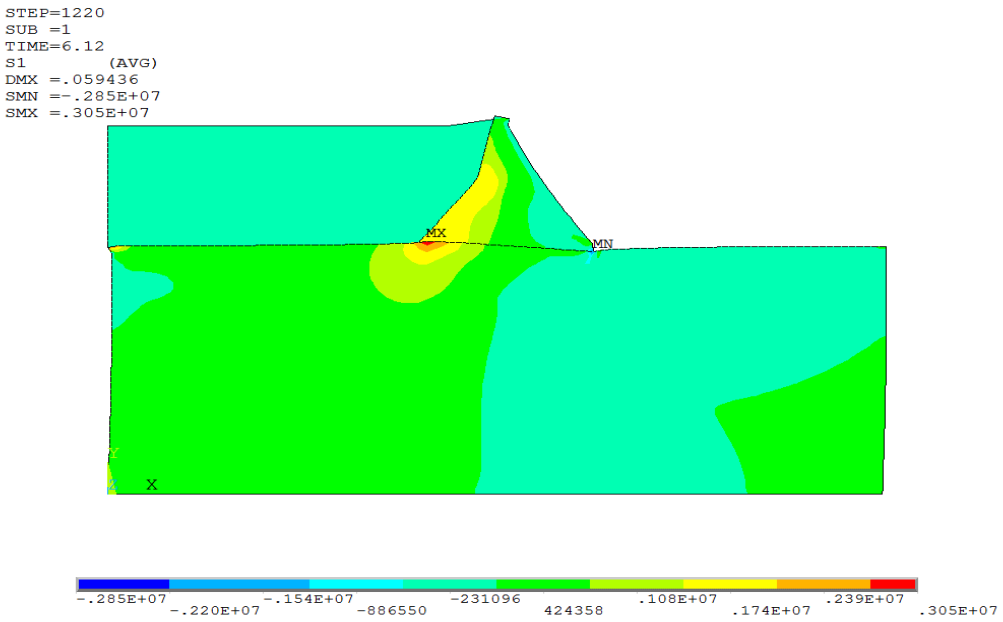

"Principal Stresses (N/m^2)"

Figure 4.61 Maximum Tensile Stress (+) Distributions at 6.12 sec. for Coyote Lake Earthquake – Euler Method

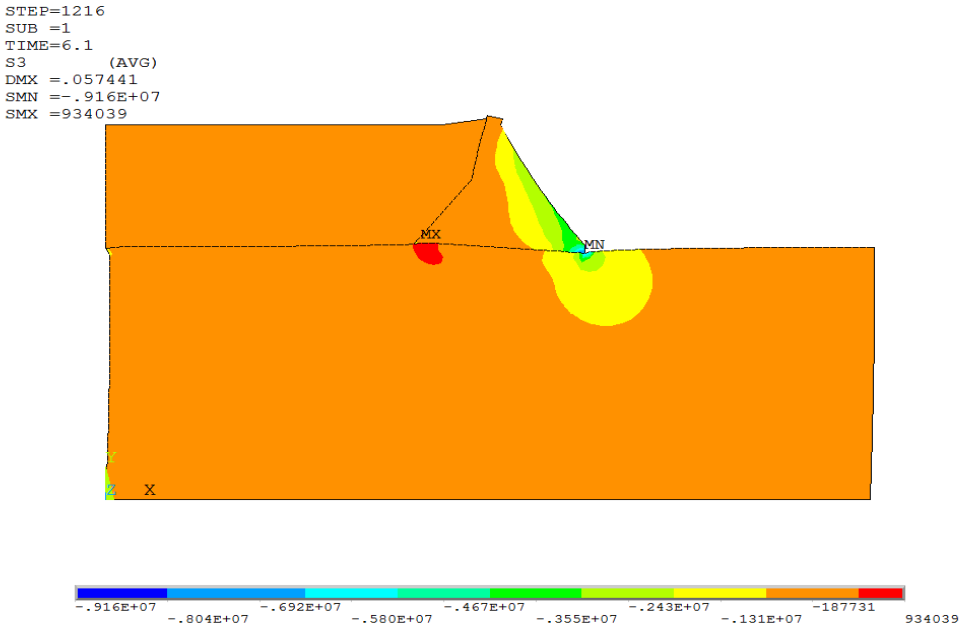

"Principal Stresses (N/m^2)"

Figure 4.62 Maximum Compressive Stress (-) Distributions at 6.10 sec. for Coyote Lake Earthquake – Euler Method

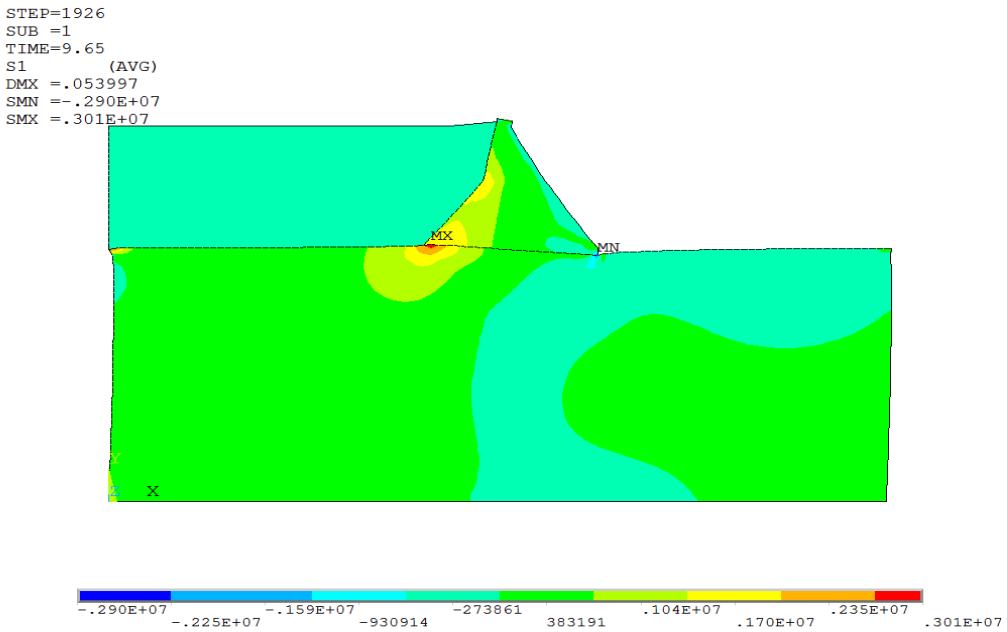

"Principal Stresses (N/m^2)"

Figure 4.63 Maximum Tensile Stress (+) Distributions at 9.65 sec. for Loma Prieta Earthquake – Euler Method

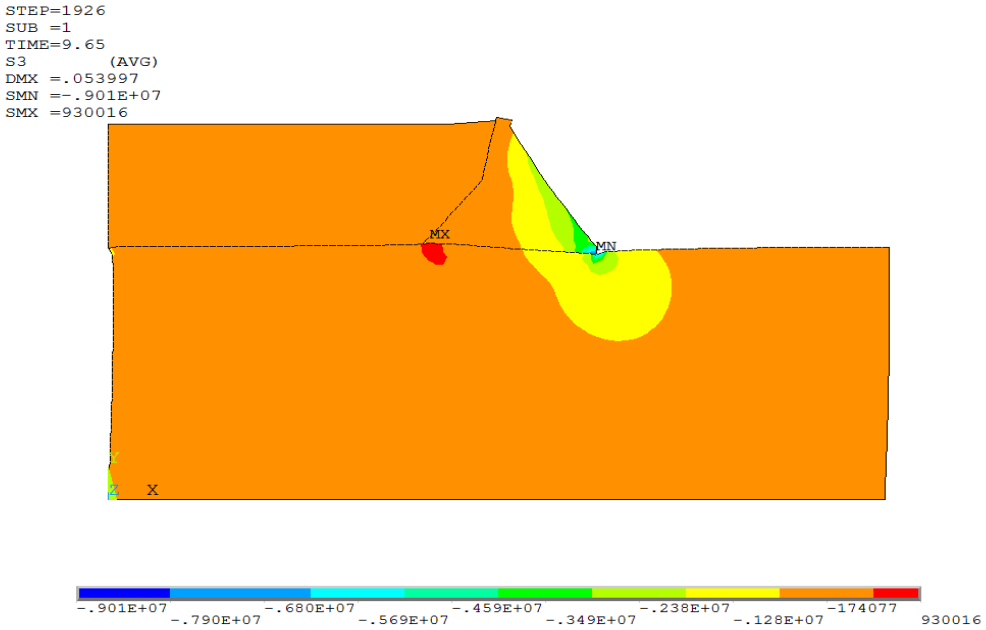

"Principal Stresses (N/m^2)"

Figure 4.64 Maximum Compressive Stress (-) Distributions at 9.65 sec. for Loma Prieta Earthquake – Euler Method

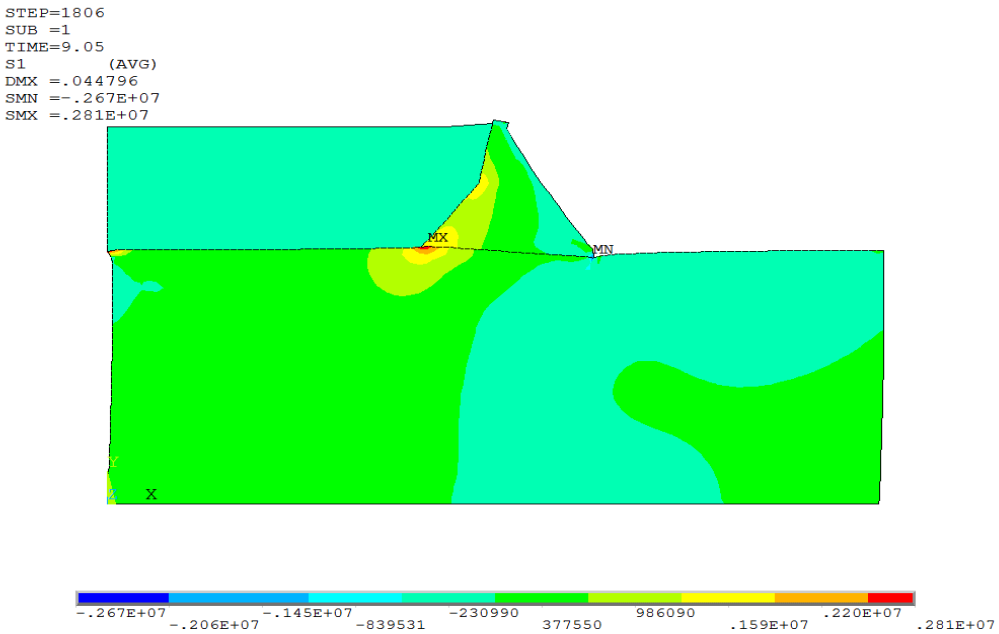

"Principal Stresses (N/m^2)"

Figure 4.65 Maximum Tensile Stress (+) Distributions at 9.05 sec. for Palm Springs Earthquake – Euler Method

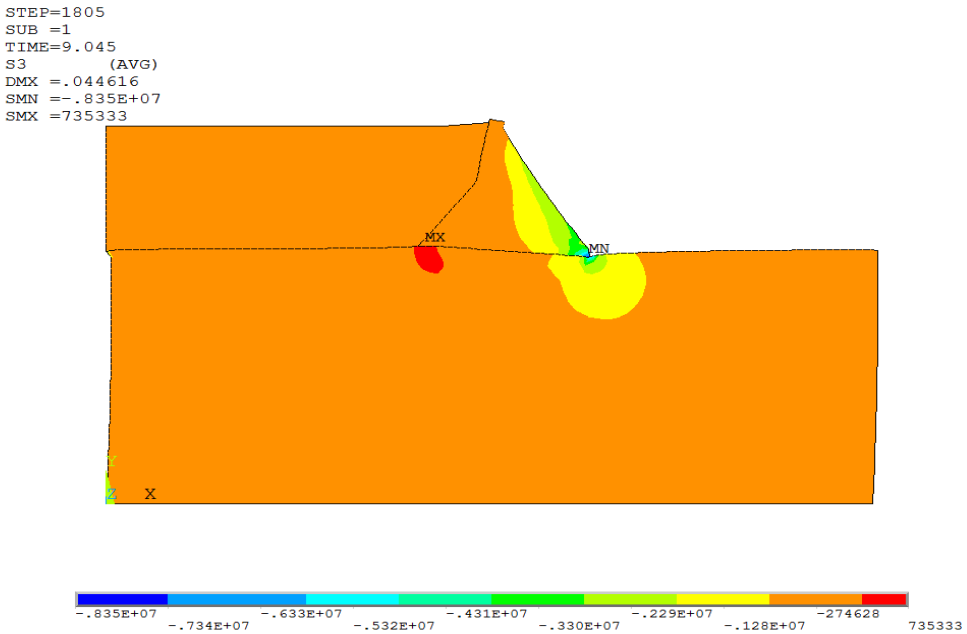

"Principal Stresses (N/m^2)"

Figure 4.66 Maximum Compressive Stress (-) Distributions at 9.045 sec. for Palm Springs Earthquake – Euler Method

Table 4.7 Obtained Maximum Tensile and Compressive Stresses from Nonlinear Dynamic Analyses

Method	Max. Tensile Stress (MPa)	Max. Compressive Stress (MPa)
Empty	2.71	5.74
Westergaard	3.15	8.16
Euler	3.05	9.16

In accordance with the nonlinear analysis, maximum principal plastic strains, which are shown in Table 4.8-4.10, happen on the dam-foundation interface. Maximum 1st principal strains are obtained as 0.0005, 0.0013, and 0,0014 depending on an empty reservoir, Westergaard, and Euler approaches, respectively. On the other hand, maximum 3rd principal strains on the dam-foundation interface are remarkably negligible. Based on USACE criteria, if a structure is in the almost elastic limit when subjected to MDE, the dynamic response of the structure can be acceptable. Even though the nonlinear response of the Narli Dam is in the inelastic limit, the maximum 1st principal strain values are negligible. Therefore, significant cracking on the dam-foundation interface is not expected in the light of the nonlinear results.

Table 4.8 Obtained Maximum Principal Plastic Strain Values from Nonlinear Dynamic Analyses based on Empty Reservoir Condition

Empty Reservoir Condition		
Earthquake	**Max. 1st Principal Plastic Strain (m/m)**	**Max. 3rd Principal Plastic Strain (m/m)**
Coyote Lake	0.0005	0.0000278
Loma Prieta	0.0004	0.0000229
Palm Springs	0.0005	0.0000251

Table 4.9 Obtained Maximum Principal Plastic Strain Values from Nonlinear Dynamic Analyses based on Westergaard Approach

Westergaard Approach		
Earthquake	**Max. 1st Principal Plastic Strain (m/m)**	**Max. 3rd Principal Plastic Strain (m/m)**
Coyote Lake	0.0013	0.0000433
Loma Prieta	0.0010	0.0000498
Palm Springs	0.0009	0.0000367

Table 4.10 Obtained Maximum Principal Plastic Strain Values from Nonlinear Dynamic Analyses based on Euler Approach

Euler Approach		
Earthquake	**Max. 1st Principal Plastic Strain (m/m)**	**Max. 3rd Principal Plastic Strain (m/m)**
Coyote Lake	0.0014	0.0000498
Loma Prieta	0.0012	0.0000507
Palm Springs	0.0013	0.0000430

CHAPTER 5

THE EFFECTS OF FOUNDATION FLEXIBILITY, POISSON'S RATIO, AND THE PRESENCE OF ALLUVIUM ON THE SEISMIC RESPONSE

5.1 Introduction

The deformation modulus is the same as Young's modulus (E_f or E_c) for the linear-elastic dynamic analyses. The deformation modulus of elasticity impacts the seismic response of the dam because it alters mode shapes, the values of modal frequency, and effective damping ratio (USACE EP 1110-2-12, 1995). Hence, the impact of deformation modulus on the seismic response of the dam will be figured out using the distinct elastic modulus of both foundation and structure. The influence of foundation flexibility (E_f/E_c) can be determined by considering different ratios associated with elastic modulus. While higher ratios of foundation flexibility represent a rigid foundation, lesser values are referred to as a very flexible foundation. In this chapter, the influence of the changes in the foundation flexibility ratio on the dynamic response of the structure considering structure-dam-reservoir interaction will be demonstrated.

The contribution of Poisson's ratio of both structure and rock to the seismic evaluation of the dam will be indicated with performing linear time-history analyses considering several possible Poisson's ratio values. Initially, the analysis will be performed with either different ratios for the foundation or distinct values for the structure. Then, the combination of them will be illustrated.

To reveal whether the presence of alluvium alters the dynamic response of the structure, various finite modeling that contains different alluvium thicknesses will be used. In this way, the alluvium will be evaluated whether it is a significant concern for the safety evaluation of the dams.

All linear time-history dynamic analyses for this chapter are performed based on the Coyote Lake earthquake, which is more intense compared with the other two ground motions. Since the principal stresses on the dam body caused by the Coyote Lake earthquake are more severe than the other two ground motions in former analyses, it was selected for the application in this section. Moreover, the differences in the results relevant to several parameters can be sufficiently illustrated by the linear analysis. Therefore, linear analyses are considered rather than using nonlinear analyses in this section.

5.2 The Foundation Flexibility Effect on the Seismic Response

The baseline foundation flexibility ratio is 0.37 for the Narli Dam. To understand the contribution of a more rigid foundation to the dynamic response, the deformation modulus of the foundation is increased while Young's modulus of concrete is used as a constant value. 0.30, 0.50, 1.0, and 3.0 ratios are selected for this purpose. A ratio of 3.0 would correspond to a shear wave velocity of 3460 m/s which can be used for intact crystalline rock. Additionally, the presence of water with the Euler method and empty reservoir condition are considered with the linear seismic analyses.

Table 5.1 clearly states that the deformation of modulus for the foundation alters the modal analysis results and more rigid foundations achieve higher natural frequency values. Also, the reduction in the value of Rayleigh coefficient β happens due to an increase in the natural frequency values when the rigidity of the system increases. More importantly, the additional parameter that

affects the seismic response of the dam is the effective damping ratio for the dam-foundation-reservoir interaction. As shown in Table 5.1, the damping of the system reduces for high rigidity foundations. The most significant factor is the additional damping ratio of the rock which decreases for more rigid foundations. When the foundation becomes more flexible, the effective damping ratio of the whole system increase and the natural frequencies decrease.

Table 5.1 Natural Frequency, Rayleigh Coefficients and Effective Damping Ratio Results for Different Foundation Flexibility Ratios based on Empty Reservoir Condition

Foundation Flexibility Ratio	W_1 (Hz)	W_2 (Hz)	α	β	ξ (%)
0.30	7.508	13.521	1.882	0.0185	19.5
0.37	8.360	15.020	1.894	0.0150	17.6
0.50	9.676	17.291	1.811	0.0110	14.6
1.00	13.628	22.984	1.711	0.0055	10.0
3.00	22.990	30.090	2.805	0.0030	8.0

Based on the obtained results from linear seismic analyses, which is shown in Table 5.2, it is obvious that the foundation flexibility ratios significantly change the dynamic response of the system. Both principal stresses on the dam body and displacement of the dam crest are getting smaller values when Young's modulus of the rock are high values. Thus, more rigid foundation materials offer better performance to avoid tensile cracking. On the other hand, the other important conclusion attained from results for the empty reservoir condition is that satisfactory reductions do not take place for the minimum principal stresses even if the more rigid foundation is selected as a construction site. The decrease in the significant parameters of the dynamic analysis results

may happen due to lower damping ratios and higher frequency values of the model relevant to less flexible foundations.

Table 5.2 Linear Dynamic Results for Different Foundation Flexibility Ratios based on Empty Reservoir Condition

Foundation Flexibility Ratios	Empty Reservoir Condition		
	Max. Crest Displacement (cm)	Max. Tensile Stress (MPa)	Max. Compressive Stress (MPa)
0.30	4.31	5.63	4.45
0.37	4.14	5.61	4.43
0.50	3.70	5.46	4.41
1.00	3.39	4.84	4.17
3.00	2.40	3.98	3.51

Depending on the linear seismic analysis results connected with Euler method, which are indicated in Table 5.3 and Table 5.4, it can be again claimed that the changes in the foundation flexibility alter modal analysis results, displacements, and the principal stresses on the dam body. However, considerable reductions in the stresses do not occur until the rigidity of the foundation reaches the ratio of 1.0 compared to empty reservoir modeling. Hence, it can be concluded with the Euler method that if the deformation modulus of the rock is at least akin to the elastic modulus of the structure, the foundation leads to less demand on the dam in terms of tensile and compressive stresses. This conclusion would be only valid for a dam that has similar characteristic features with the Narli Dam and is under similar ground accelerations.

Table 5.3 Natural Frequency, Rayleigh Coefficients and Effective Damping Ratio Results for Different Foundation Flexibility Ratios based on Euler Method

Foundation Flexibility Ratio	W_1 (Hz)	W_2 (Hz)	α	β	ξ (%)
0.37	8.610	14.510	1.952	0.0155	18.0
0.50	9.978	16.412	1.849	0.0113	14.9
1.00	13.892	20.822	1.667	0.0058	10.0
3.00	20.929	24.668	1.698	0.0033	7.5

Table 5.4 Linear Dynamic Results for Different Foundation Flexibility Ratios based on Euler Method

Foundation Flexibility Ratio	Euler Method		
	Max. Crest Displacement (cm)	Max. Tensile Stress (MPa)	Max. Compressive Stress (MPa)
0.37	6.16	8.46	6.48
0.50	6.00	8.45	6.36
1.00	5.00	7.17	5.65
3.00	3.36	5.65	3.75

5.3 The Poisson's Effect on the Seismic Response

The Poisson's ratio of the concrete and foundation for the Narli Dam is 0.20 and 0.30, respectively. However, the ratio can be a value between 0.20 and 0.33 for the concrete. Similarly, this ratio for the foundation is taken as a value between 0.20 and 0.35. To understand the Poisson's ratio effect on the dynamic response of the concrete gravity dam, several ratios for both concrete

and rock are selected in the linear dynamic analyses. The analyses are computed with empty reservoir condition and the Euler method.

Tables 5.5 and 5.6 show that the changes in the Poisson's ratio for either concrete or foundation slightly alter the modal response of the dam. Poisson's ratio does not have a significant effect, especially for the first modes of the models. In the second mode of the system, changes begin and lightly increase with the higher ratios. Moreover, the impact of the Poisson's ratio on the Rayleigh Coefficients and effective viscous damping ratio of the dam model is negligible.

Table 5.5 Natural Frequency, Rayleigh Coefficients and Effective Damping Ratio Results for Different Poisson's Ratios of Concrete based on Empty Reservoir Condition

Poisson's Ratio	W_1 (Hz)	W_2 (Hz)	α	β	ξ (%)
0.25	8.375	15.067	1.8950	0.0150	17.6
0.30	8.375	15.073	1.8951	0.0150	17.6
0.33	8.375	15.080	1.8954	0.0150	17.6

Table 5.6 Natural Frequency, Rayleigh Coefficients and Effective Damping Ratio Results for Different Poisson's Ratios of Foundation based on Empty Reservoir Condition

Poisson's Ratio	W_1 (Hz)	W_2 (Hz)	α	β	ξ (%)
0.20	8.696	14.000	1.8880	0.0155	17.6
0.25	8.533	14.451	1.8884	0.0153	17.6
0.35	8.231	15.510	1.8930	0.0148	17.6

According to Tables 5.7 and 5.8, we can come up with the idea that the Poisson's ratio of concrete and rock is not an influential parameter for both modal and dynamic responses of the concrete gravity dams when the hydrodynamic forces are negligible in the modeling. However, it

is important to note that while the principal stresses take higher values with the increase of the ratio for the concrete, they reduce with increasing Poisson's ratio for the foundation. Additionally, displacement on the crest of the dam decreases slightly with higher ratios in both ways.

Table 5.7 Linear Dynamic Results for Different Poisson's Ratios of Concrete based on Empty Reservoir Condition

Poisson's Ratio of Concrete	Empty Reservoir Condition		
	Max. Crest Displacement (cm)	Max. Crest Displacement (cm)	Max. Compressive Stress (MPa)
0.20	4.14	5.61	4.43
0.25	4.09	5.71	4.50
0.30	4.04	5.83	4.58
0.33	4.01	5.91	4.63

Table 5.8 Linear Dynamic Results for Different Poisson's Ratios of Foundation based on Empty Reservoir Condition

Poisson's Ratio of Foundation	Empty Reservoir Condition		
	Max. Crest Displacement (cm)	Max. Crest Displacement (cm)	Max. Compressive Stress (MPa)
0.20	4.20	5.79	4.70
0.25	4.17	5.71	4.57
0.30	4.10	5.61	4.43
0.35	4.06	5.47	4.26

Identical to empty reservoir modal analysis results, the first mode of the dam model is not affected by the changes of the Poisson's ratios. However, the second mode alters with changing in the ratios, especially for the ratios for the foundation. Even if the reservoir is considered in the model, neither Rayleigh Coefficients nor damping ratio vary.

Table 5.9 Natural Frequency, Rayleigh Coefficients and Effective Damping Ratio Results for Different Poisson's Ratios of Concrete based on Euler Method

Poisson's Ratio	W_1 (Hz)	W_2 (Hz)	α	β	ξ (%)
0.25	8.658	14.552	1.954	0.01551	18.0
0.30	8.658	14.571	1.955	0.01549	18.0
0.33	8.658	14.583	1.956	0.01548	18.0

Table 5.10 Natural Frequency, Rayleigh Coefficients and Effective Damping Ratio Results for Different Poisson's Ratios of Foundation based on Euler Method

Poisson's Ratio	W_1 (Hz)	W_2 (Hz)	α	β	ξ (%)
0.20	8.878	13.854	1.948	0.0158	18.0
0.25	8.765	14.238	1.953	0.0157	18.0
0.35	8.558	14.778	1.951	0.0154	18.0

In light of the results given in Tables 5.11 and 5.12, increasing of the ratio for the concrete and decreasing of the ratio for the foundation lead to slight reductions of 1st and 3rd principal stresses on the dam body. However, the Poisson ratio cannot be seen as the critical parameter for the seismic safety evaluation of the gravity dams based on the dynamic results of both empty reservoir condition and the Euler method.

Table 5.11 Linear Dynamic Results for Different Poisson's Ratios of Concrete based on Euler Method

Poisson's Ratio of Concrete	Euler Method		
	Max. Crest Displacement (cm)	Max. Tensile Stress (MPa)	Max. Compressive Stress (MPa)
0.20	6.16	8.46	6.48
0.25	6.12	8.60	6.55
0.30	6.06	8.78	6.64
0.33	6.02	8.90	6.70

Table 5.12 Linear Dynamic Results for Different Poisson's Ratios of Foundation based on Euler Method

Poisson's Ratio of Foundation	Euler Method		
	Max. Crest Displacement (cm)	Max. Tensile Stress (MPa)	Max. Compressive Stress (MPa)
0.20	6.26	8.73	6.68
0.25	6.21	8.60	6.59
0.30	6.16	8.46	6.48
0.35	6.08	8.24	6.35

5.4 The Presence of Alluvium Effect on the Seismic Response

The construction site of the dam had 7m-thick alluvium, but all alluvium was removed by the construction company. Thus, previous analyses do not consist of alluvium thickness in the finite element modeling. To reveal the influence of the lack of the alluvium on the seismic response, assorted alluvium thicknesses are considered such as 3m, 5m, and 7m. For this aim,

empty reservoir condition and Westergaard method are considered in the linear time-history dynamic analyses. The density, modulus of elasticity, and Poisson's ratio of the alluvium are supposed as 1835 kg/m^3, 0.12 GPa, and 0.30, respectively (Aydin and Er, 2017).

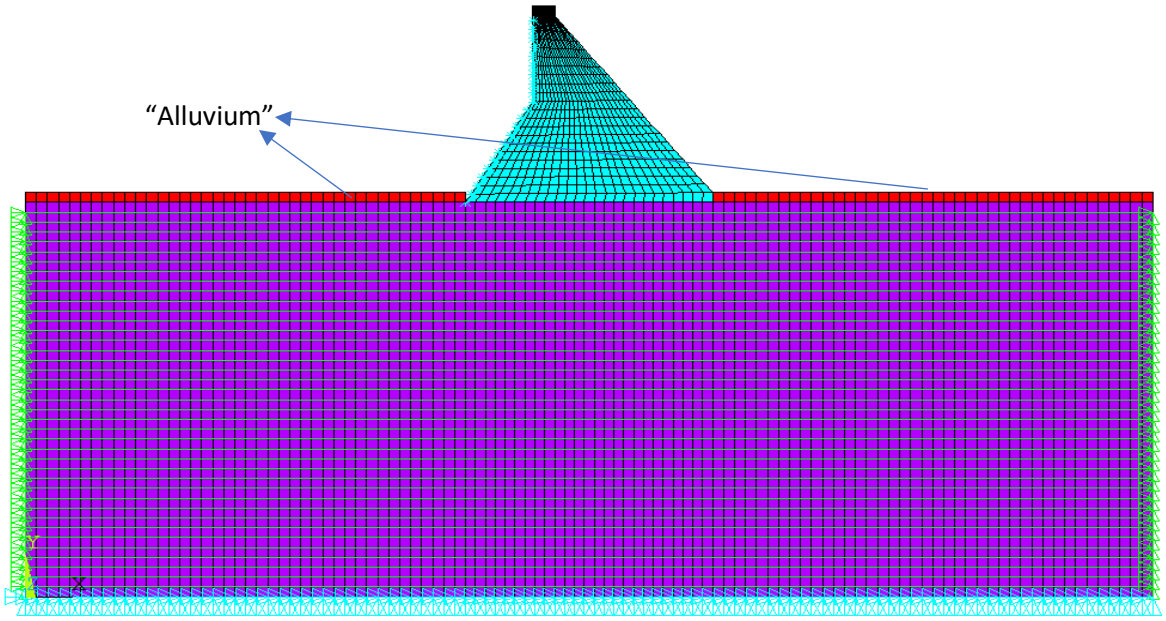

Figure 5.1 A Typical Included Alluvium Thickness (5 m) in the Finite Element Model

Tables 5.13 and 5.14 show results using an empty reservoir and the Westergaard approach with changing alluvium thickness. The decrease in the alluvium thickness brings about the growth of natural frequencies associated with both methods. On the other hand, there is no sufficient effect on the Rayleigh Coefficients and damping ratios of the system.

Table 5.13 Natural Frequency, Rayleigh Coefficients and Effective Damping Ratio Results for Various Alluvium Thicknesses based on Empty Reservoir Condition

Thickness of Alluvium (m)	W_1 (Hz)	W_2 (Hz)	α	β	ξ (%)
0	8.360	15.020	1.894	0.0150	17.6
3	8.319	15.000	1.884	0.0151	17.6
5	8.275	14.950	1.875	0.0152	17.6
7	8.231	14.900	1.866	0.0152	17.6

Table 5.14 Natural Frequency, Rayleigh Coefficients and Effective Damping Ratio Results for Various Alluvium Thicknesses based on Westergaard Method

Thickness of Alluvium (m)	W_1 (Hz)	W_2 (Hz)	α	β	ξ (%)
0	8.110	14.070	1.853	0.0162	18.0
3	8.074	13.990	1.843	0.0163	18.0
5	8.036	13.949	1.836	0.0164	18.0
7	8.000	13.900	1.828	0.0164	18.0

Based on the results shown in Tables 5.15 and 5.16, it can be concluded that the increase of alluvium thickness in the dam site impacts the seismic response considerably because it creates more vulnerable areas to tensile cracking. The difference between 0 m and 7 m of alluvium thicknesses in terms of maximum principal stress is about 10%. Hence, the removal of the alluvium in the site should be performed to reduce cracking caused by tension. However, the 3rd principal stresses did rise substantially even if thickness grew from 0 m to 7 m.

Table 5.15 Linear Dynamic Results for Various Alluvium Thicknesses based on Empty Reservoir Condition

Thickness of Alluvium (m)	Empty Reservoir Condition		
	Max. Crest Displacement (cm)	Max. Tensile Stress (MPa)	Max. Compressive Stress (MPa)
0	4.14	5.61	4.43
3	4.35	5.85	4.54
5	4.49	6.05	4.57
7	4.58	6.19	4.52

Table 5.16 Linear Dynamic Results for Various Alluvium Thickness based on Westergaard Method

Thickness of Alluvium (m)	Westergaard Method		
	Max. Crest Displacement (cm)	Max. Tensile Stress (MPa)	Max. Compressive Stress (MPa)
0	5.67	7.96	6.66
3	5.87	8.14	6.70
5	6.01	8.30	6.82
7	6.16	8.55	6.82

5.5 The Influence of the Combinations connected with Alluvium Thickness and Foundation Flexibility Ratio on the Seismic Response

Former analyses revealed that whilst the difference in the alluvium thicknesses and foundation flexibility ratios make a contribution to modal and dynamic responses of the dam, Poisson's ratios have no remarking outcomes on them. Hence, various combinations, which are shown in Table 5.17, are selected depending on distinct alluvium thicknesses and foundation

flexibility ratios. In this way, it emerges that whether the concrete gravity dams are prone to cracking stemmed from tension on the dam body when they are tackled with a strong ground motion. Empty reservoir condition and added mass method are considered for performing linear time-history analyses.

Table 5.17 Various Combinations for Linear Dynamic Analyses associated with Empty Reservoir Condition and the Westergaard Method

The Thickness of Alluvium (m)	**Foundation Flexibility Ratio**	
	0.50	**1.0**
3	Combination 1	Combination 2
5	Combination 3	Combination 4
7	Combination 5	Combination 6

Tables 5.18 and 5.19 point out that the effective viscous damping ratio of the system remains constant when alluvium thicknesses increase with the constant foundation flexibility ratio. However, the damping ratios cut down if the rigidity of the rock rises with the constant alluvium thickness. Moreover, the foundation flexibility ratio that significantly affects the natural frequency and Rayleigh Coefficients values in the modal analysis is the governing factor instead of alluvium thickness.

Table 5.18 Natural Frequency, Rayleigh Coefficients and Effective Damping Ratio Results for Various Combinations based on Empty Reservoir Condition

Combination	W_1 (Hz)	W_2 (Hz)	α	β	ξ (%)
The Narli Dam	8.360	15.020	1.894	0.0150	17.6
1	9.607	17.216	1.800	0.0110	14.6
2	13.534	22.902	1.701	0.0054	10.0
3	9.557	17.159	1.792	0.0109	14.6
4	13.464	22.833	1.694	0.0051	10.0
5	9.506	17.090	1.783	0.0109	14.6
6	13.383	22.733	1.685	0.0054	10.0

Table 5.19 Natural Frequency, Rayleigh Coefficients and Effective Damping Ratio Results for Various Combinations based on the Westergaard Method

Combination	W_1 (Hz)	W_2 (Hz)	α	β	ξ (%)
The Narli Dam	8.110	14.070	1.853	0.0162	18.0
1	9.318	15.802	1.747	0.0119	14.9
2	13.050	20.257	1.587	0.0060	10.0
3	9.274	15.758	1.740	0.0119	14.9
4	12.994	20.213	1.582	0.0060	10.0
5	9.230	15.702	1.732	0.0120	14.9
6	12.931	20.144	1.575	0.0060	10.0

It can be deduced from Tables 5.20 and 5.21 that the tensile stresses on the heel of the dam and displacement at the dam crest grow approximately 5% and 3.5%, respectively, if the rigidity of the rock is low based on both the empty reservoir condition and the Westergaard method. For foundations that have high rigidity, on the other hand, the effect of alluvium on the 1st principal stress and displacement disappears. It can be inferred from Tables 5.20 and 5.21, additionally, the least efficient combination is Combination 5, which consists of low rigidity and high alluvium thickness; while the most efficient combination for the seismic analysis is Combination 2, which is composed of high rigidity and low alluvium thickness. When the foundation flexibility ratio increases from 0.5 to 1.0, and the alluvium thickness drops from 7 m to 3 m, the displacement, 1st principal stress, and 3rd principal stress decline up to 25%, 30%, and 20%, respectively. When the reservoir is neglected in finite element modeling, those proportions decrease up to 16%, 20%, and 10%, respectively.

Table 5.20 Linear Dynamic Results for Various Combinations based on Empty Reservoir Condition

Combination	Empty Reservoir Condition		
	Displacement (cm)	**Tensile Stress (MPa)**	**Compressive Stress (MPa)**
The Narli Dam	4.14	5.61	4.43
1	3.98	5.68	4.53
2	3.54	5.01	4.29
3	4.09	5.90	4.57
4	3.64	5.25	4.32
5	4.12	5.95	4.46
6	3.60	5.10	4.15

Table 5.21 Linear Dynamic Results for Various Combinations based on the Westergaard Method

Combination	Westergaard Method		
	Displacement (cm)	Tensile Stress (MPa)	Compressive Stress (MPa)
The Narli Dam	5.67	7.96	6.66
1	5.98	8.75	5.86
2	5.03	7.02	5.14
3	6.14	8.94	5.91
4	5.12	7.25	5.20
5	6.23	9.21	6.11
6	5.16	7.39	5.28

CHAPTER 6

CONCLUSIONS

6.1 Summary

The main objective of the research is to determine dynamic responses of the Narli Dam under several ground motions that are representative of the seismic hazard in the area and to evaluate the dynamic results considering USACE criteria. Moreover, the research considers the empty reservoir condition, the Westergaard method, and the Euler method to reveal the hydrodynamic pressure effects on the seismic response of the dam. Furthermore, the project aims to reveal the possible parameters that can impact the seismic response such as foundation flexibility ratio, Poisson's ratio of concrete and foundation, and the presence of alluvium in the dam site.

The results of these analyses show that linear time-history analyses predict tensile stresses on the dam body that are considerably higher than the nonlinear dynamic analyses. On the other hand, the linear transient dynamic analyses showed lower values in terms of compressive stresses on the dam body in comparison to nonlinear analyses. The results obtained from both linear and nonlinear time-history analyses of the Narli Dam showed that the 3rd principal stresses never exceed the compressive strength of the concrete. Moreover, the tensile strength of the concrete is insufficient based on estimated tensile stress results associated with linear dynamic analyses which would suggest the possibility of cracking. However, the outcomes of nonlinear analyses demonstrate that the tensile stresses never exceed the flexural strength of the structure. Hence,

significant tensile cracking that causes the failure of the dam is not to be expected on either the heel or toe of the dam based on the nonlinear results. Moreover, the maximum principal strains are significantly ignorable on the dam-foundation interface. All dynamic results display that the heel of the dam is susceptible to more tensile stresses than the toe of the dam, whereas the toe of the dam is prone to more compressive stresses than the heel of the dam.

The results reveal that the presence of the reservoir in finite element modeling substantially influences the seismic response. When the water is assumed as incompressible and included only as added mass (Westergaard method), the tensile and compressive stresses grow up to 60% and 70% on the dam body, respectively. If the reservoir is considered as compressible (Euler method), the 1st principal and 3rd principal stresses increase by approximately 70% relative to the empty condition. The results of the nonlinear dynamic analyses agree with the linear results, as both show about 60% reduction takes place in the stresses when the reservoir is removed from the finite element model. Additionally, the presence of the fluid leads to growth in the effective damping ratio of the system.

It can be concluded from dynamic analysis results that the linear time-history analysis is a beneficial tool to estimate the maximum displacement and acceleration on the crest of this dam since the results of linear transient analyses are nearly similar to the consequences of the nonlinear analyses. This statement is only valid for a dam which has similar features of the Narli Dam and is exposed to similar earthquakes.

Results attained from various foundation flexibility ratios show that the deformation modulus of the foundation directly impacts the dynamic characteristics of the dam-foundation-reservoir interaction such as mode shapes, natural frequencies, and effective damping ratios. Once the elastic modulus of the foundation increases with the constant deformation modulus of the

structure, the natural frequencies considerably increase. But, the effective viscous damping ratio decreases as the foundation flexibility ratio rises. The alterations in the modal response of the dam significantly change the seismic response. The high flexible foundations increased the tensile and compressive stresses compared to more stiff foundations by up to 40% and 26% relying on the empty reservoir condition, respectively. When the reservoir is considered in the linear dynamic analyses, these percentages increase up to 50% and 70%, respectively.

It can be deduced from the research that neither Poisson's ratio of concrete nor Poisson's ratio of the foundation has a remarkable impact on the modal characteristics of the dam. Similarly, the Poisson's ratios do not dominate the seismic response of the dam. However, it is important to note that while increasing in the Poisson's ratio of concrete raises the principal stresses up to 5%, increasing the Poisson's ratio of the rock declines the principal stresses up to 10%.

It can be inferred from the linear results that the presence of the alluvium in the dam site is not an influential factor to alter the modal response of the dam. Similarly, the alluvium does not sufficiently govern the seismic response in terms of compressive stresses. On the other hand, the maximum principal stresses can grow up to 10% when the thickness is increased from 0 to 7 meters.

The combination of foundation flexibility and alluvium thickness has a considerable effect on the dynamic response of the gravity dam. Therefore, sites with more rigid foundations and less alluvium thickness might lead to less demand on the dam body.

6.2 Future Scope and Recommendations

The research can be extended with the following topics:

1. Performing dynamic analyses considering the foundation with mass.

The viscous boundary condition, which is also referred to as the Lysmer and Kuhlemeyer boundary condition, allows the researchers to include the foundation mass in the seismic analysis of the dam. In this way, the exact influence of the foundation could be reflected to the analysis. The viscous boundary condition provides the absorption of ground accelerations at the boundaries and should be applied on the whole surface of the rock.

2. Using the Lagrange method to create the water effects on the dam body.

Even though some water approaches were considered in the research, the study can be extended with the Lagrange method, which is created by the Fluid 79 element in the model. Moreover, the Lagrange method uses different boundary conditions compared to the Euler method. In this way, the impact of boundary condition relevant to the reservoir on the seismic response of dams can be solved out using both Euler and Lagrange methods.

3. Performing the dynamic analysis using three dimensional model and revealing the effect of the location of contraction joints on the dynamic response.

If tensile cracking does not happen on the non-overflow sections of the concrete gravity dams during time-history analyses, the overflow sections are not a concern in terms of dynamic analyses. Therefore, two-dimensional modeling sufficiently presents the seismic response of the concrete gravity dam. However, three-dimensional modeling is required to perform the dynamic analysis of arch dams since the curve can not be illustrated with the two-dimensional model. Moreover, the location of contraction joints on the dam body can be a significant parameter on the dynamic response of the dams. Hence, the impact of contraction joints can be revealed by using the three-dimensional model of the dams.

REFERENCES

Akkose, M., & Simsek, E. (2010). *Nonlinear Seismic Response of Concrete Gravity Dams to Near Fault Ground Motions Including Dam-Water-Sediment-Foundation Interaction*. Appl. Math. Model, Vol. 34, 3685-3700.

Altunisik, A.C., & Sesli, H. (2015). *Dynamic Response of Concrete Gravity Dams using Different Water Modelling Approaches: Westergaard, Lagrange and Euler*. Computers and Concrete, 16(3), 429-448.

Aydin, S. & Er, Y. (2017). *Evaluation of Earthquake Performance of Andiraz Dam by Considering Compressible Reservoir and Dam-Foundation Interaction.* 2017 UDSMR Conference, October 11-13.

Bayraktar, A., Altunisik, A.C., Sevim, B., Kartal, M.E., Turker, T., & Bilici, Y. (2009). *Comparison of Near and Far Fault Ground Motion Effect on the Nonlinear Response of Dam-Reservoir-Foundation Systems*. Nonlinear Dynamics, Vol. 58, 655-673.

Bayraktar, A., Turker, T., Akkose, M., & Ates, S. (2010). *The Effect of Reservoir Length on Seismic Performance of Gravity Dams to Near and Far Fault Ground Motions*. Nat. Hazards, Vol. 52, 257-275.

Brahtz, H. A., & Heilbron, C. H. (1933). *Water Pressures on Dams during Earthquakes*. Trans. ASCE, Vol. 98.

Cannon, R. W. (1995). *Seismic Design Provisions for Roller Compacted Concrete Dams; Appendix E, Tensile Strength of Roller Compacted Concrete*, EP 1110-2-12, USACE.

Chakrabarti, P., & Chopra, A. K. (1973). *A Computer Program for Earthquake Analysis of Gravity Dams Including Reservoir Interaction*. EERC 73-7, Earthquake Engineering Research Center.

Chopra, A. K. (1970). *Earthquake Response Analysis of Concrete Gravity Dams*. Proc. ASCE, EM4.

Chopra, A. K. (January 01, 1967). *Hydrodynamic Pressures on Dams during Earthquakes*. Journal of the Engineering Mechanics Division, *93*, 205-223

Chopra, A. K., & Lokke A. (2015). *Response Spectrum Analysis of Concrete Gravity Dams including Dam-Water-Foundation Interaction*. Journal of Structural Engineering, Vol. 141, Issue 8.

Clough, R. W., & Penzien, J. (1993). *Dynamics of Structures*, second edition, McGraw-Hill.

Cook, R. D., Malkus, D. S., & Plesha, M. E. (1989). *Concept and Applications of Finite Element Analysis*. John Wiley and Sons.

Fathi, A., & Lotfi, V. (2008). *Effects of Reservoir Length on Dynamic Analysis of Concrete Gravity Dams*. Proceedings of the 14th World Conference on Earthquake Engineering.

FEMA. (2005). *Federal Guidelines for Dam Safety, Earthquake Analysis and Design of Dams*. FEMA-65

Fenves, G. L., & Chopra, A. K. (1987). *Simplified Earthquake Analysis of Concrete Gravity Dams*. Journal of Structural Engineering (United States), Vol. *113*(8), 1688-1708.

Fenves, G., & Chopra, A. K. (1985). *Effects of Reservoir Bottom Absorption and Dam-Water-Foundation Interaction on Frequency Response Functions for Concrete Gravity Dams*. Earthquake Engineering and Structural Dynamics, Vol. 13, 13-31.

G.F. Proje Muhendislik (2018). *Narli Baraji Analiz Raporu [The Analysis Report of the Narli Dam]*. DSI. Ankara, Turkey.

Hall, J. F., & Chopra, A. K. (1982). *Hydrodynamic Effects in the Dynamic Response of Concrete Gravity Dams*. Earthquake Engineering and Structural Dynamics, Vol. 10, 333-345.

Hughes, T. J. R. (1987). *The Finite Element Method Linear Static and Dynamic Finite Element Analysis*. Prentice-Hall.

Kohnke, P. C., & ANSYS, Inc. (1999). *ANSYS (Manual): Theory Reference Release 5.6*. Canonsburg, PA: ANSYS Inc.

Leger, P., & Leclerc, M. (1996). *Evaluation of Earthquake Ground Motions to Predict Cracking Response of Gravity Dams*. Engineering Structures, Vol. 18, No. 3, 227-239.

Newmark, N. M. (1959). *Method of Computation for Structural Dynamics*. ASCE Journal of Engineering Mechanics Division, Vol. 85, 67-94.

Raphael, J. M. (1984). *Tensile Strength of Concrete*. ACI Journal, 158-165.

Sevim, B., Altunisik, A.C., Bayraktar, A., Akkose, M., & Calayir, Y. (2011). *Water Length and Height Effects on the Earthquake Behavior of Arch Dam-Reservoir-Foundation Systems*. KSCE. J. Civil. Eng., Vol. 15, 295-303.

Subramani, T., & Ponnuvel, D. (2012). *Seismic and Stability Analysis of Gravity Dams using Staad PRO*. International Journal of Engineering Research and Development, Volume 1, Issue 5, 44-54.

Thandaveswara, B. S. (2009). *Hydraulics.* Retrieved from https://nptel.ac.in/courses/105106114/.

United States Department of the Interior Bureau of Reclamation (USBR). (1977). *Design Criteria for Concrete Arch and Gravity Dams*. A Water Resources Technical Publication, No. 19.

U.S. Army Corps of Engineers (USACE). (1995). *Gravity Dam Design*, EM 1110-2-2200.

U.S. Army Corps of Engineers (USACE). (1995*). Seismic Design Provisions for Roller Compacted Concrete Dams*, EP 1110-2-12.

U.S. Army Corps of Engineers (USACE). (2000). *Concrete*, EM-1110-2-2006.

U.S. Army Corps of Engineers (USACE). (2003). *Time-History Dynamic Analysis of Concrete Hydraulic Structures*, EM 1110-2-6051.

U.S. Army Corps of Engineers (USACE). (2007). *Earthquake Design and Evaluation of Concrete Hydraulic Structures*, EM 1110-2-6053.

USSD. (2017). *Seismic Analysis of Concrete Dams*. 2017 USSD Annual Conference, April 6-7.

Westergaard, H. M. (1933). *Water Pressure on Dams during* Earthquakes. Transactions ASCE, Vol. 98, 418-433.

Zeidan, B. A. (2014). *Design and Analysis of Concrete Gravity Dams*. Tanta University.

Zienkiewicz, O. C., & Taylor, R. L. (1991). *The Finite Element Method*; volume 2, 4th edition, 407-419. McGraw-Hill, London.

Zienkiewicz, O. C., & Taylor, R. L. (2000). *The Finite Element Method*; 5th edition. Butterworth-Heinemann.

APPENDIX A:

Table A.1 Added Mass Calculation regarding to the Westergaard Method

The Distance from the max. Operating Water Level (m)	The added mass on the Dam Body (kg)
4.60	57778
9.20	105644
13.80	136804
18.40	162003
23.00	183756
27.60	203184
32.20	220906
36.80	237306
41.40	252642
46.00	267098
50.25	258977
54.25	270173
58.75	280924
63.00	291278

67.25	301277
71.50	310953
75.75	320338
80.00	329455
84.25	338327
88.50	346972
92.75	355406
97.00	363645

APPENDIX B:

Nonlinear Time-History Graphs related to Displacement and Acceleration

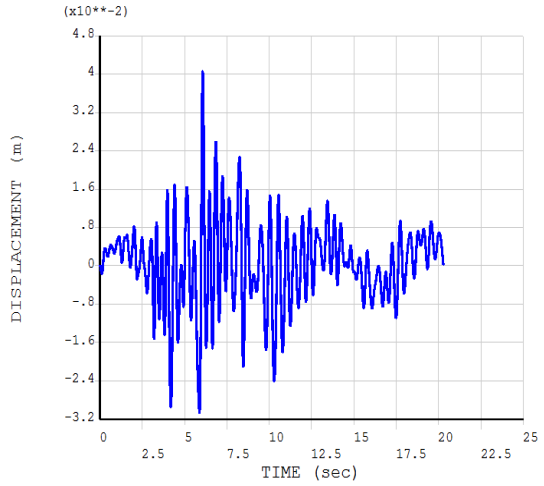

Figure B.1 Displacement (m) vs Time History (sec) for Coyote Lake Earthquake – Empty Reservoir Condition

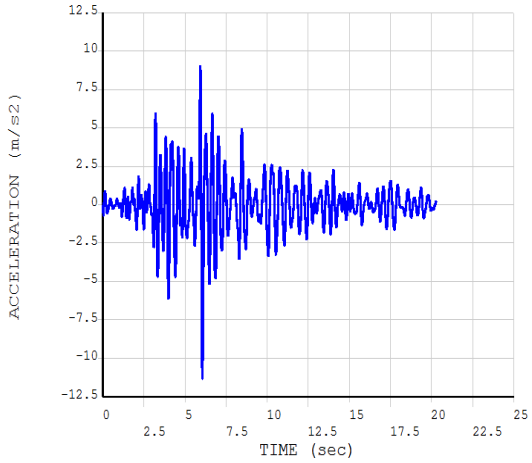

Figure B.2 Acceleration (m/s^2) vs Time History (sec) for Coyote Lake Earthquake – Empty Reservoir Condition

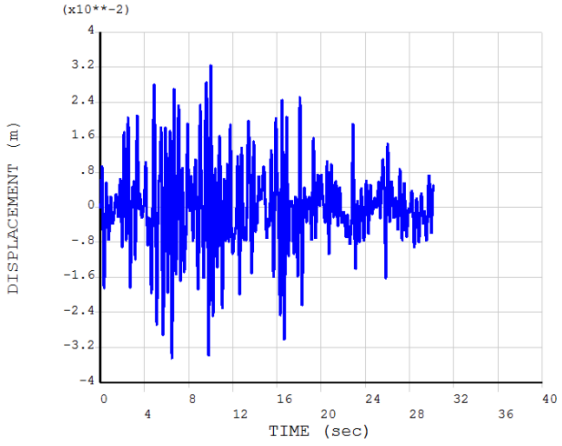

Figure B.3 Displacement (m) vs Time History (sec) for Loma Prieta Earthquake – Empty Reservoir Condition

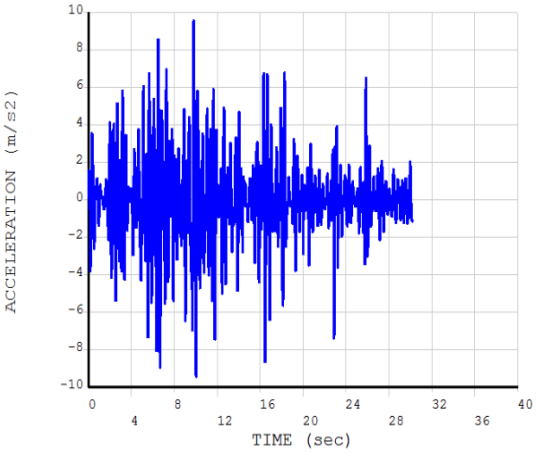

Figure B.4 Acceleration (m/s^2) vs Time History (sec) for Loma Prieta Earthquake – Empty Reservoir Condition

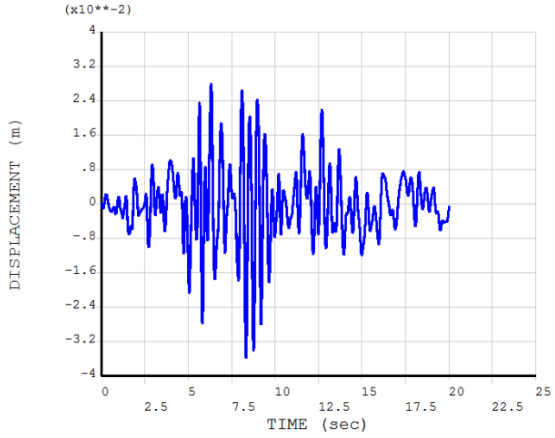

Figure B.5 Displacement (m) vs Time History (sec) for Palm Springs Earthquake – Empty Reservoir Condition

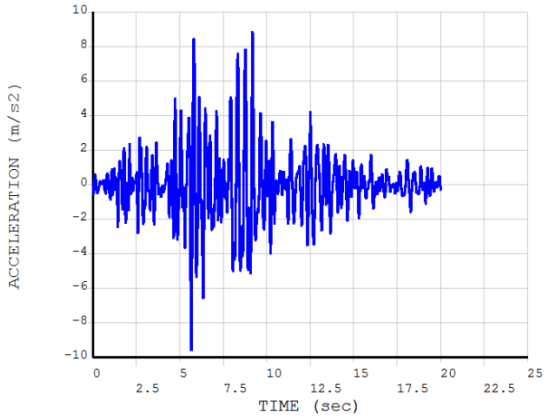

Figure B.6 Acceleration (m/s^2) vs Time History (sec) for Palm Springs Earthquake – Empty Reservoir Condition

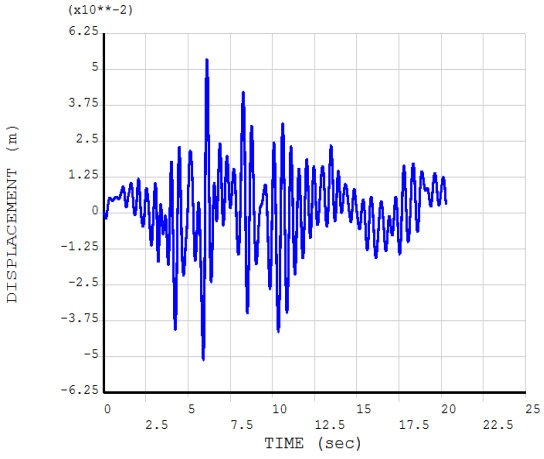

Figure B.7 Displacement (m) vs Time History (sec) for Coyote Lake Earthquake – Westergaard Method

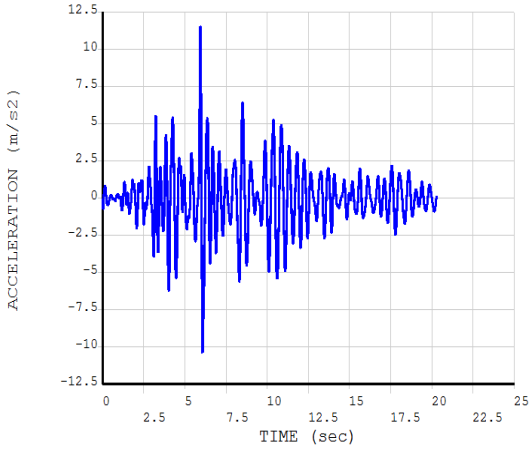

Figure B.8 Acceleration (m/s^2) vs Time History (sec) for Coyote Lake Earthquake – Westergaard Method

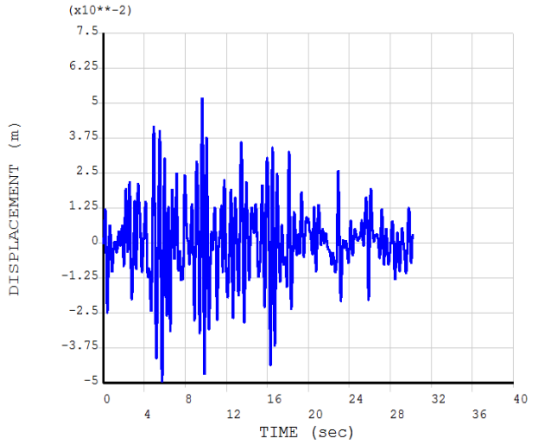

Figure B.9 Displacement (m) vs Time History (sec) for Loma Prieta Earthquake – Westergaard Method

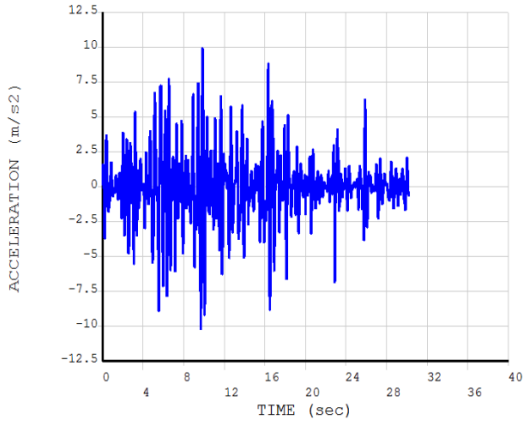

Figure B.10 Acceleration (m/s^2) vs Time History (sec) for Loma Prieta Earthquake – Westergaard Method

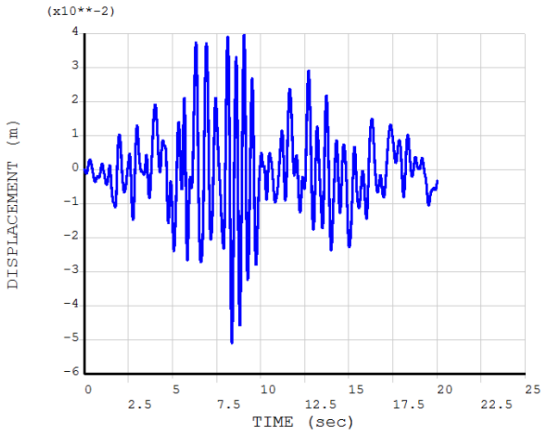

Figure B.11 Displacement (m) vs Time History (sec) for Palm Springs Earthquake – Westergaard Method

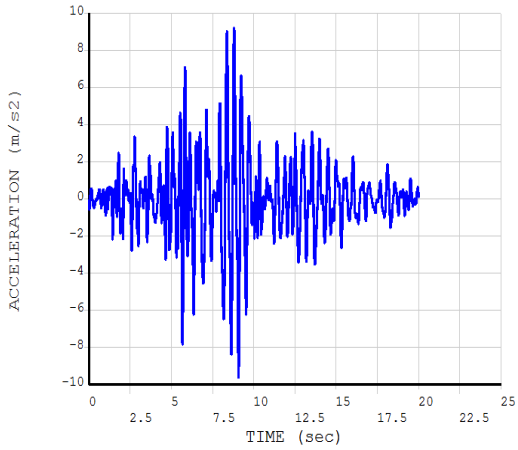

Figure B.12 Acceleration (m/s^2) vs Time History (sec) for Palm Springs Earthquake – Westergaard Method

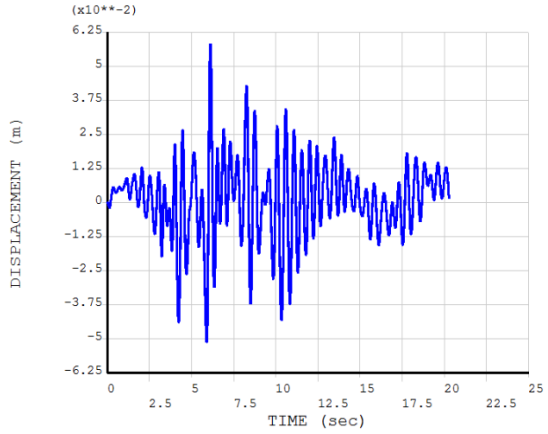

Figure B.13 Displacement (m) vs Time History (sec) for Coyote Lake Earthquake – Euler Method

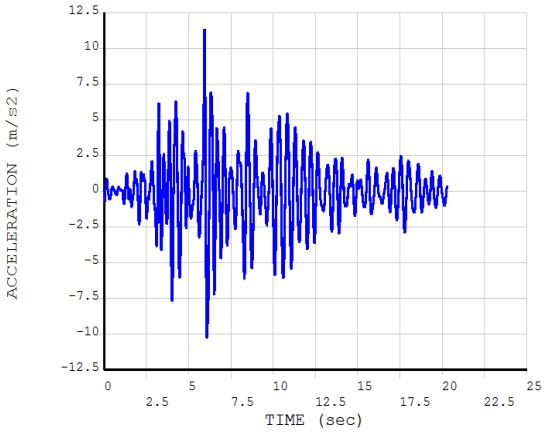

Figure B.14 Acceleration (m/s^2) vs Time History (sec) for Coyote Lake Earthquake – Euler Method

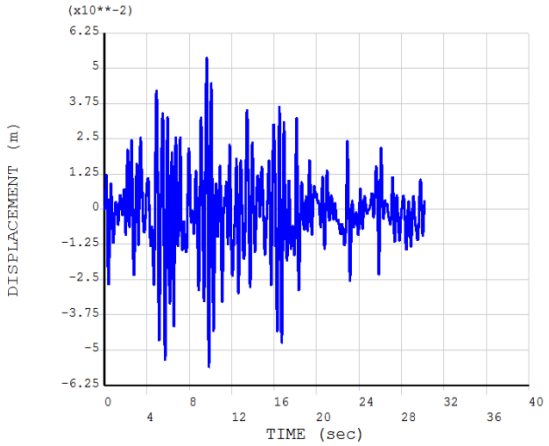

Figure B.15 Displacement (m) vs Time History (sec) for Loma Prieta Earthquake – Euler Method

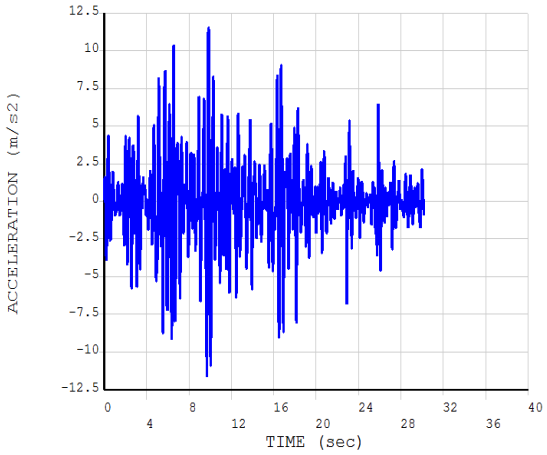

Figure B.16 Acceleration (m/s^2) vs Time History (sec) for Loma Prieta Earthquake – Euler Method

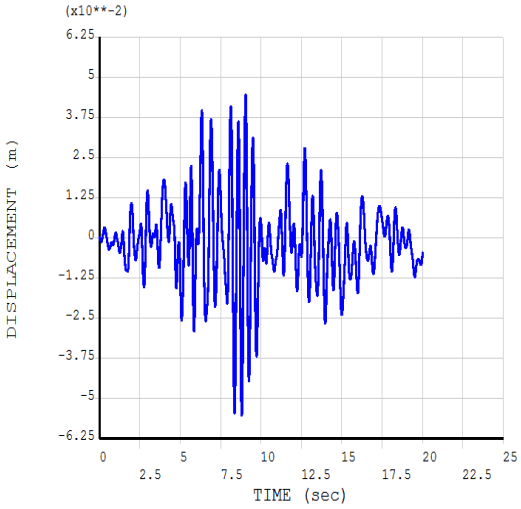

Figure B.17 Displacement (m) vs Time History (sec) for Palm Springs Earthquake – Euler Method

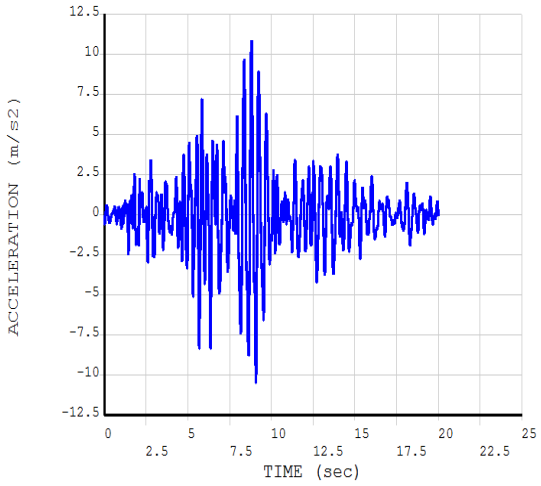

Figure B.18 Acceleration (m/s^2) vs Time History (sec) for Palm Springs Earthquake – Euler Method

APPENDIX C:

The Detailed Principal Stress Results based on Various Combinations

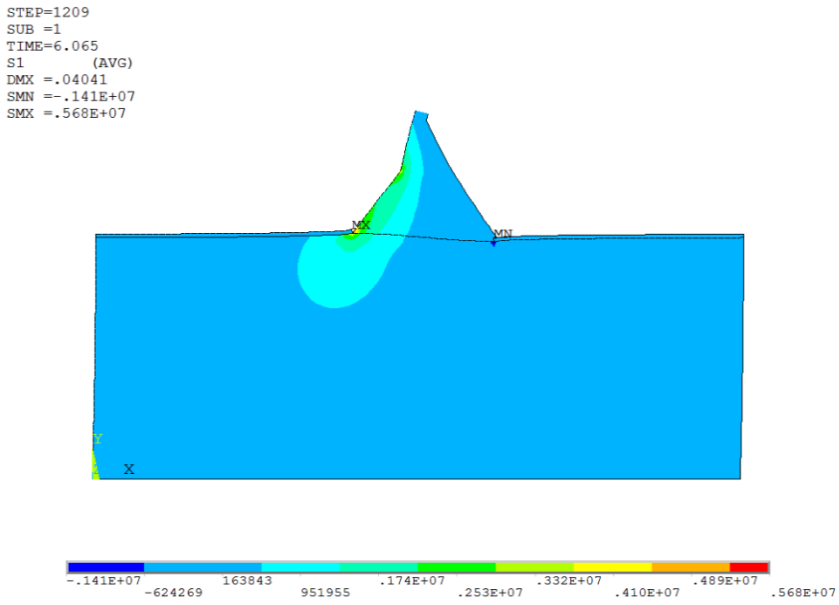

"Principal Stresses (N/m^2)"

Figure C.1 Maximum Tensile Stress (+) Distributions of Combination 1 at 6.065 sec. – Empty Reservoir Condition

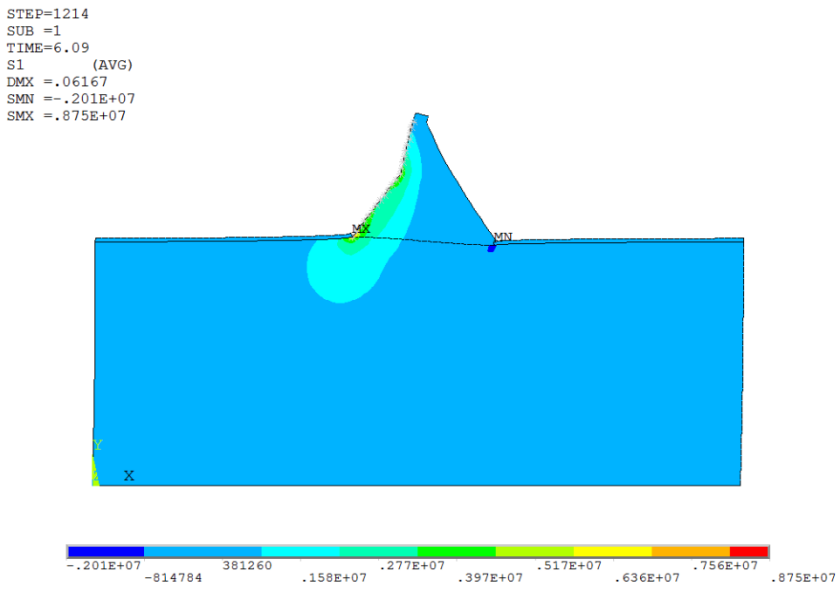

"Principal Stresses (N/m^2)"

Figure C.2 Maximum Tensile Stress (+) Distributions of Combination 1 at 6.09 sec. – Westergaard Method

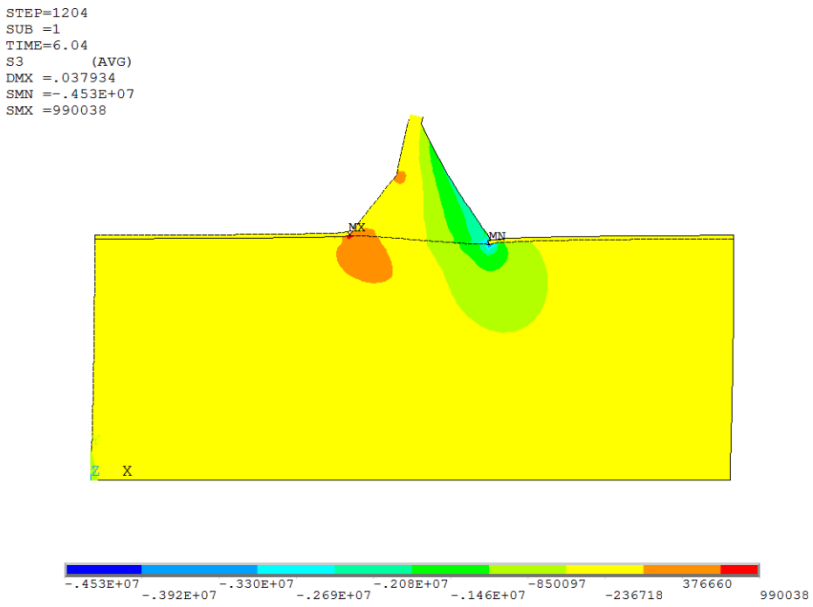

"Principal Stresses (N/m^2)"

Figure C.3 Maximum Compressive Stress (-) Distributions of Combination 1 at 6.04 sec. – Empty Reservoir Condition

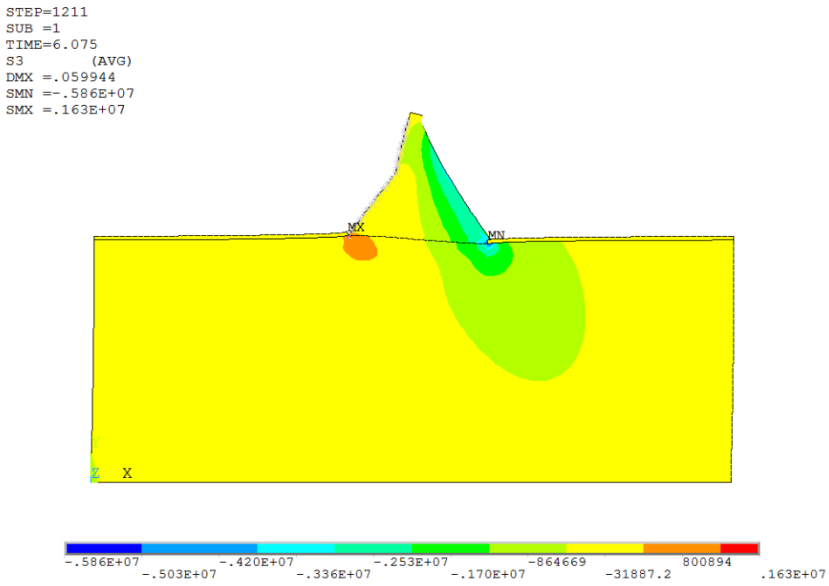

"Principal Stresses (N/m^2)"

Figure C.4 Maximum Compressive Stress (-) Distributions of Combination 1 at 6.075 sec. – Westergaard Method

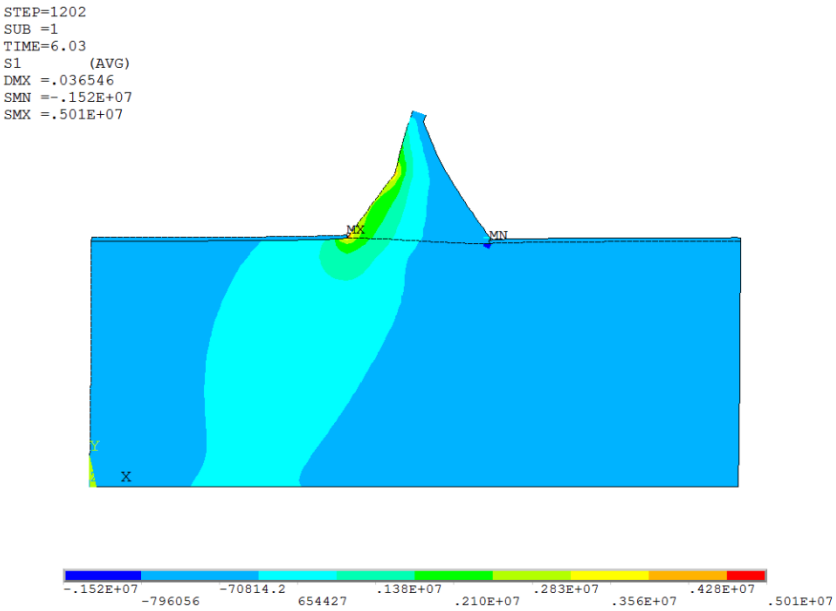

"Principal Stresses (N/m^2)"

Figure C.5 Maximum Tensile Stress (+) Distributions of Combination 2 at 6.03 sec. – Empty Reservoir Condition

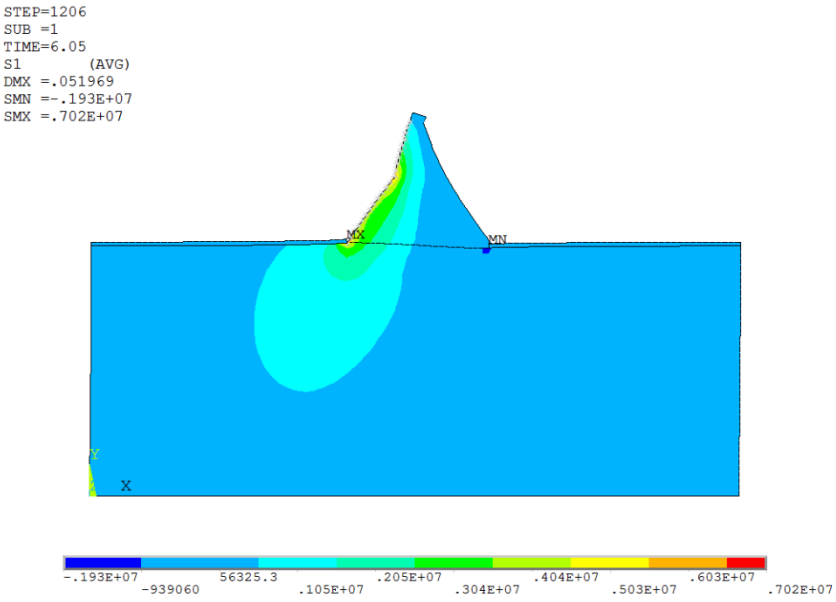

"Principal Stresses (N/m^2)"

Figure C.6 Maximum Tensile Stress (+) Distributions of Combination 2 at 6.05 sec. – Westergaard Method

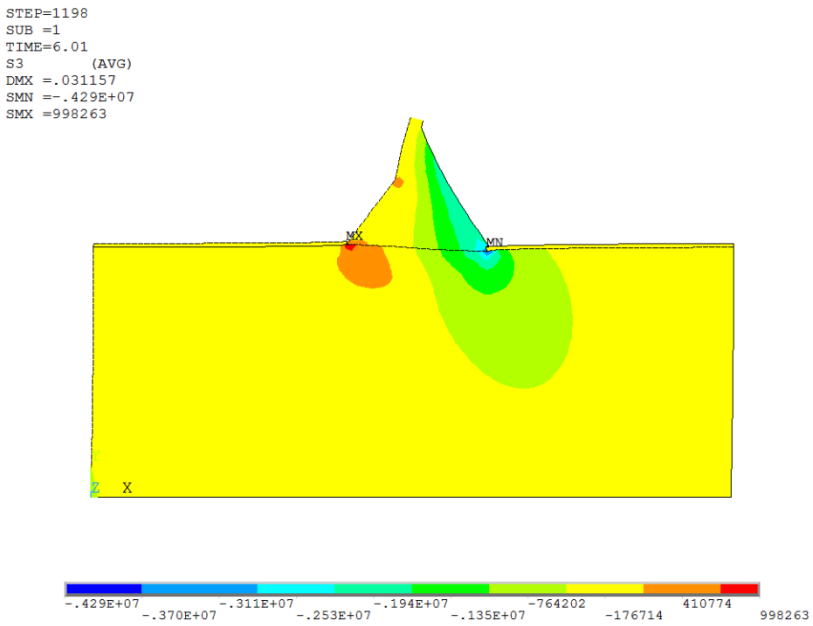

"Principal Stresses (N/m^2)"

Figure C.7 Maximum Compressive Stress (-) Distributions of Combination 2 at 6.01 sec. – Empty Reservoir Condition

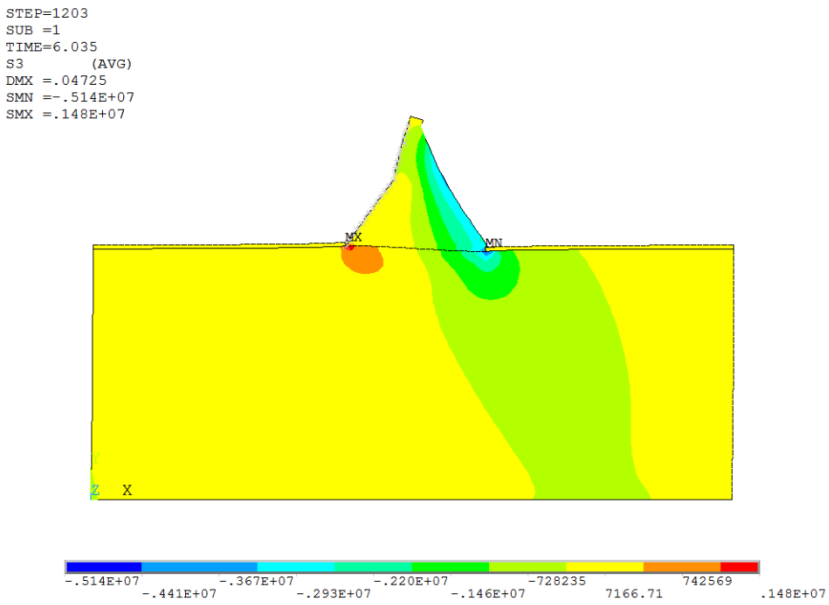

"Principal Stresses (N/m^2)"

Figure C.8 Maximum Compressive Stress (-) Distributions of Combination 2 at 6.035 sec. – Westergaard Method

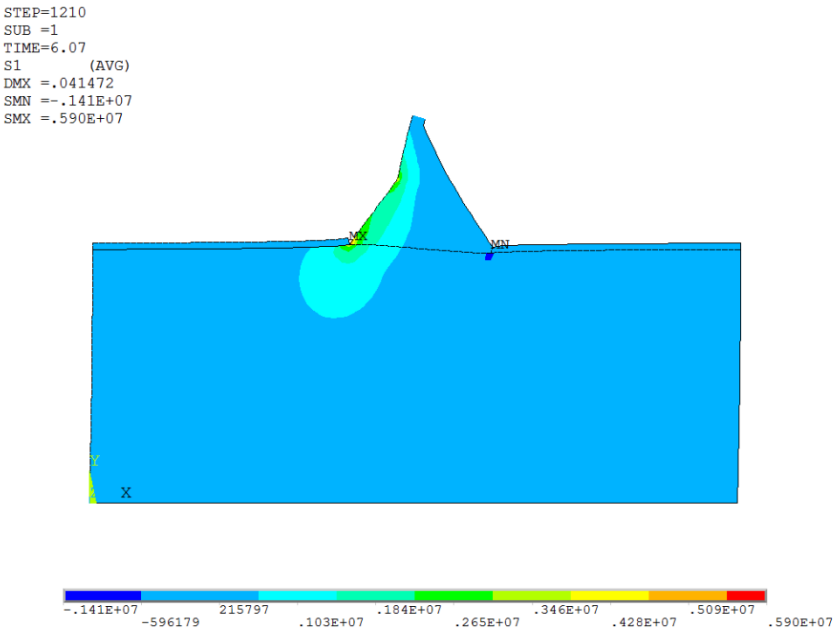

"Principal Stresses (N/m^2)"

Figure C.9 Maximum Tensile Stress (+) Distributions of Combination 3 at 6.07 sec. – Empty Reservoir Condition

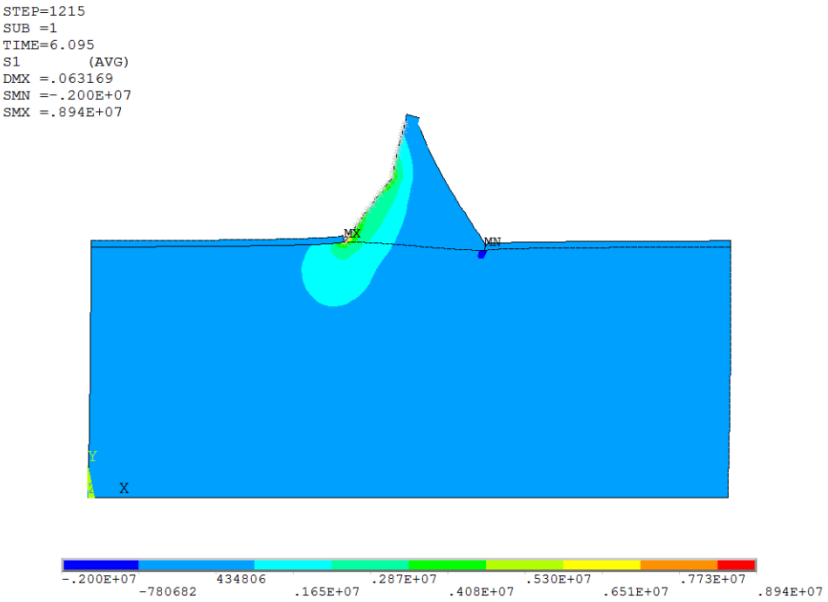

"Principal Stresses (N/m^2)"

Figure C.10 Maximum Tensile Stress (+) Distributions of Combination 3 at 6.095 sec. – Westergaard Method

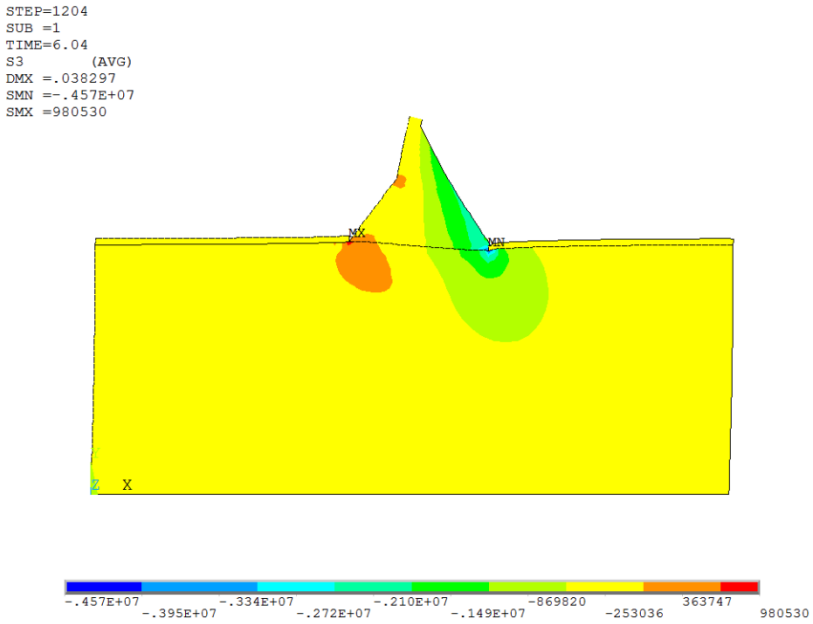

"Principal Stresses (N/m^2)"

Figure C.11 Maximum Compressive Stress (-) Distributions of Combination 3 at 6.04 sec. – Empty Reservoir Condition

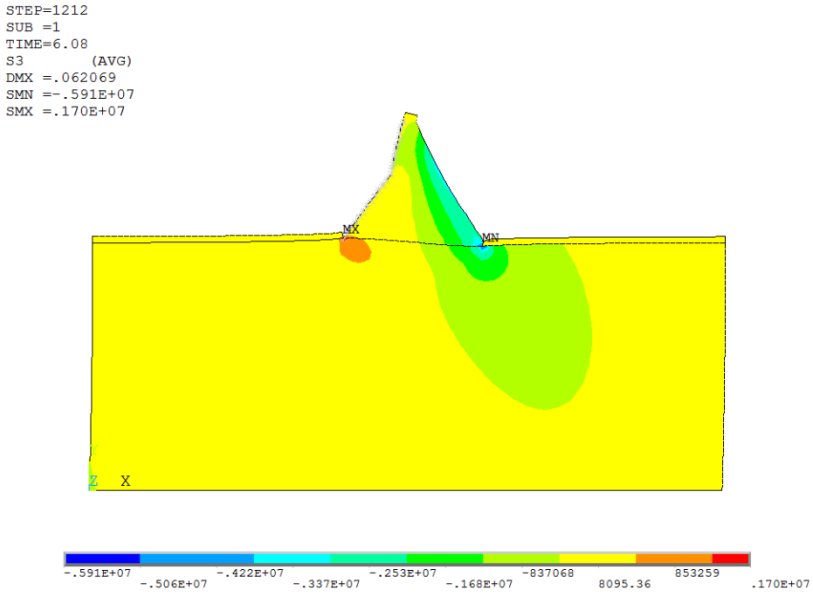

"Principal Stresses (N/m^2)"

Figure C.12 Maximum Compressive Stress (-) Distributions of Combination 3 at 6.08 sec. – Westergaard Method

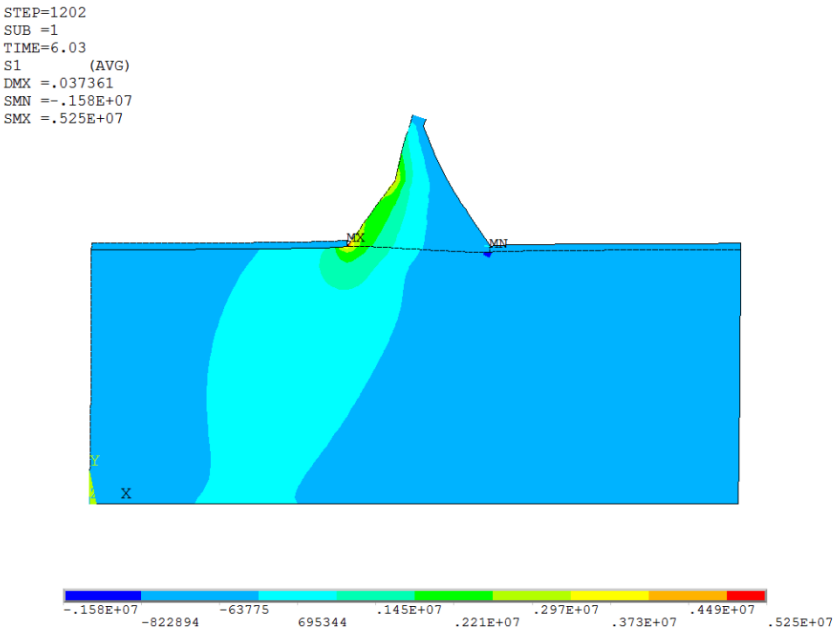

"Principal Stresses (N/m^2)"

Figure C.13 Maximum Tensile Stress (+) Distributions of Combination 4 at 6.03 sec. – Empty Reservoir Condition

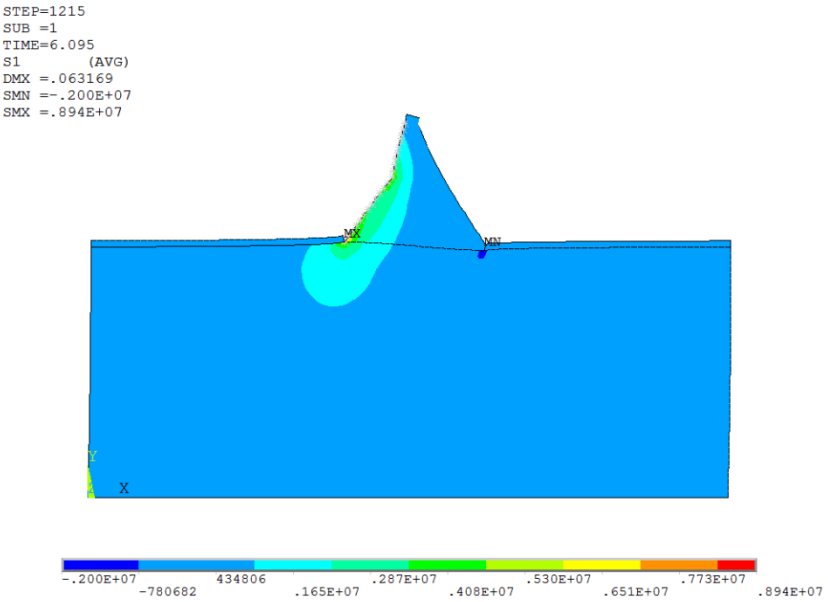

"Principal Stresses (N/m^2)"

Figure C.14 Maximum Tensile Stress (+) Distributions of Combination 4 at 6.095 sec. – Westergaard Method

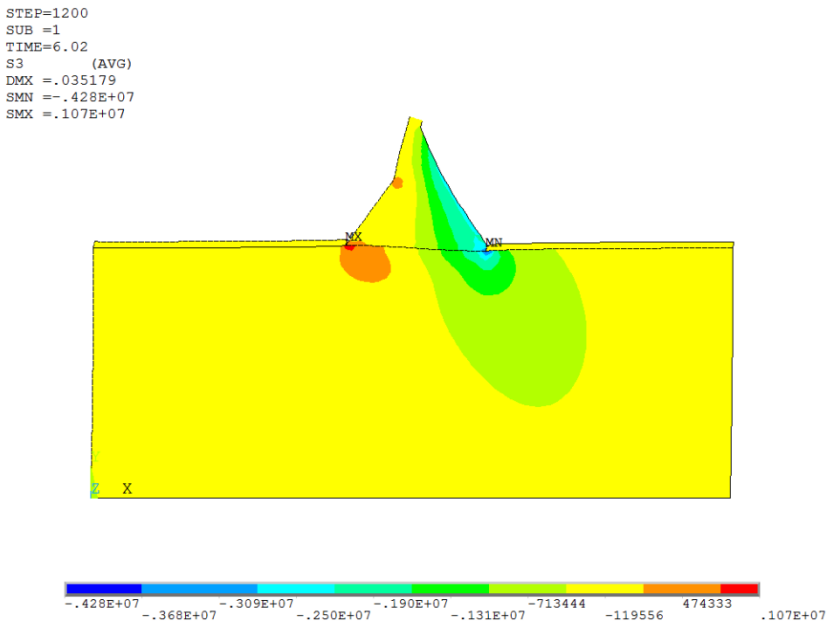

"Principal Stresses (N/m^2)"

Figure C.15 Maximum Compressive Stress (-) Distributions of Combination 4 at 6.02 sec. – Empty Reservoir Condition

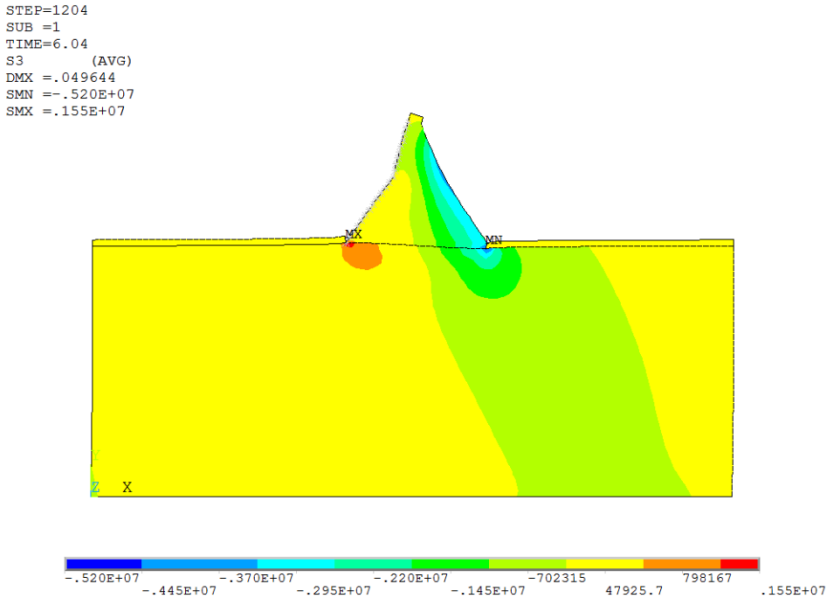

"Principal Stresses (N/m^2)"

Figure C.16 Maximum Compressive Stress (-) Distributions of Combination 4 at 6.04 sec. – Westergaard Method

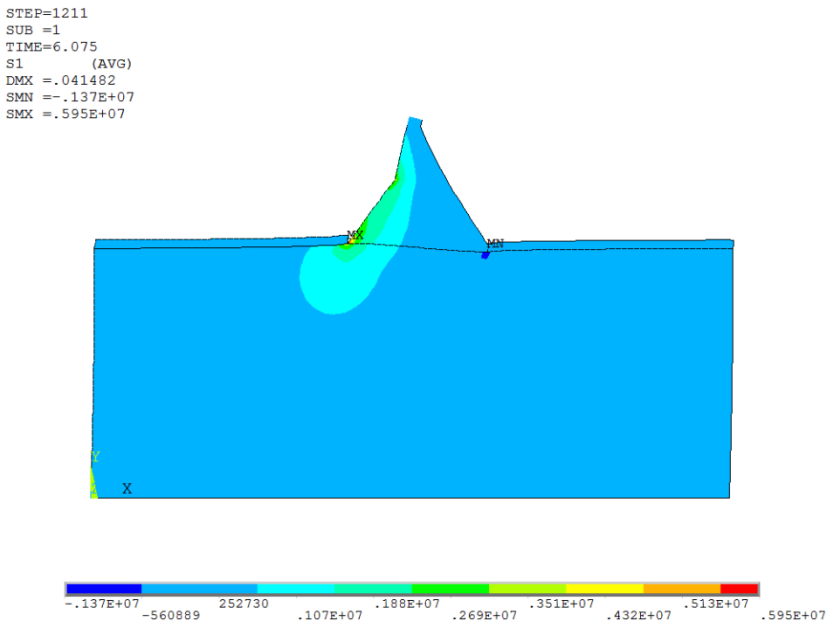

"Principal Stresses (N/m^2)"

Figure C.17 Maximum Tensile Stress (+) Distributions of Combination 5 at 6.075 sec. – Empty Reservoir Condition

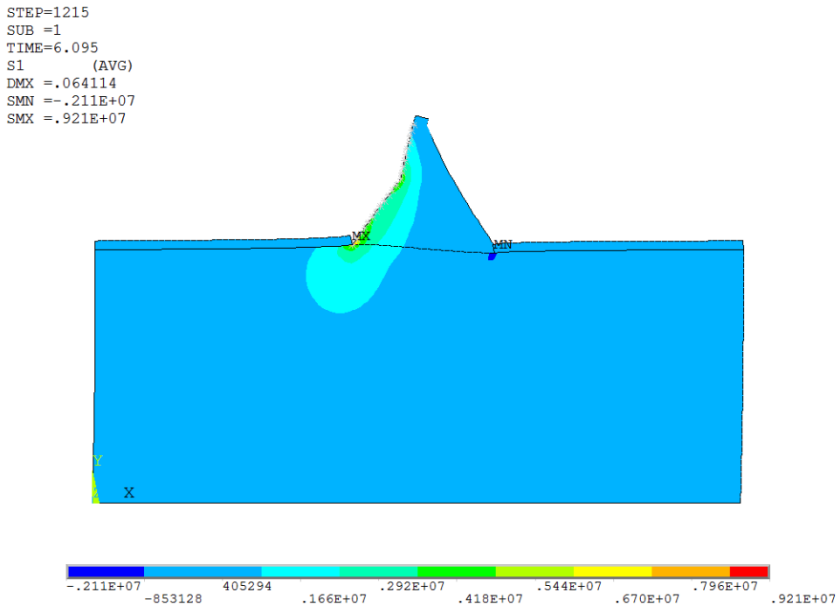

"Principal Stresses (N/m^2)"

Figure C.18 Maximum Tensile Stress (+) Distributions of Combination 5 at 6.095 sec. – Westergaard Method

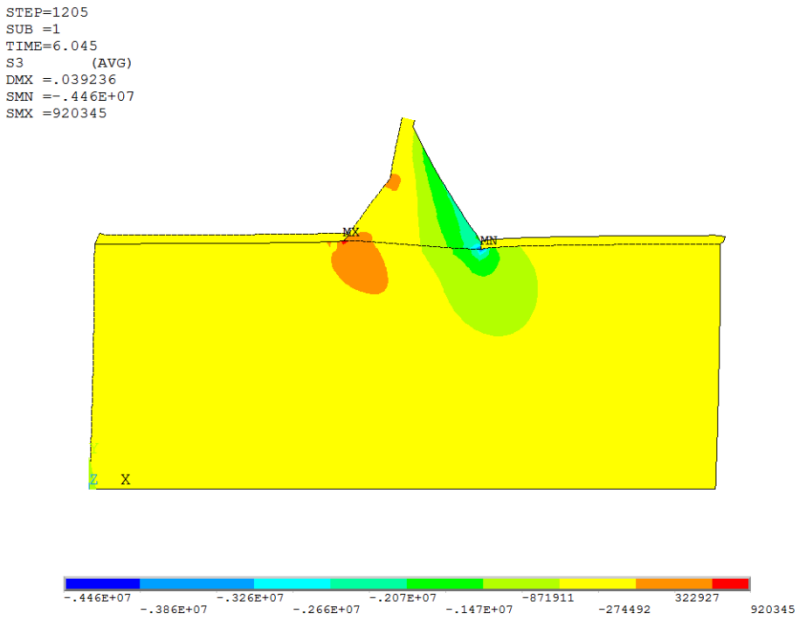

"Principal Stresses (N/m^2)"

Figure C.19 Maximum Compressive Stress (-) Distributions of Combination 5 at 6.045 sec. – Empty Reservoir Condition

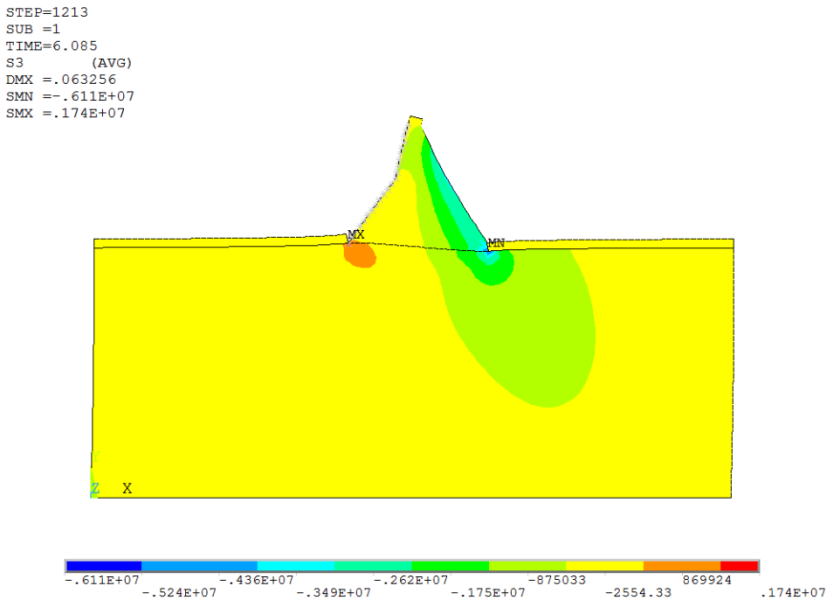

"Principal Stresses (N/m^2)"

Figure C.20 Maximum Compressive Stress (-) Distributions of Combination 5 at 6.085 sec. – Westergaard Method

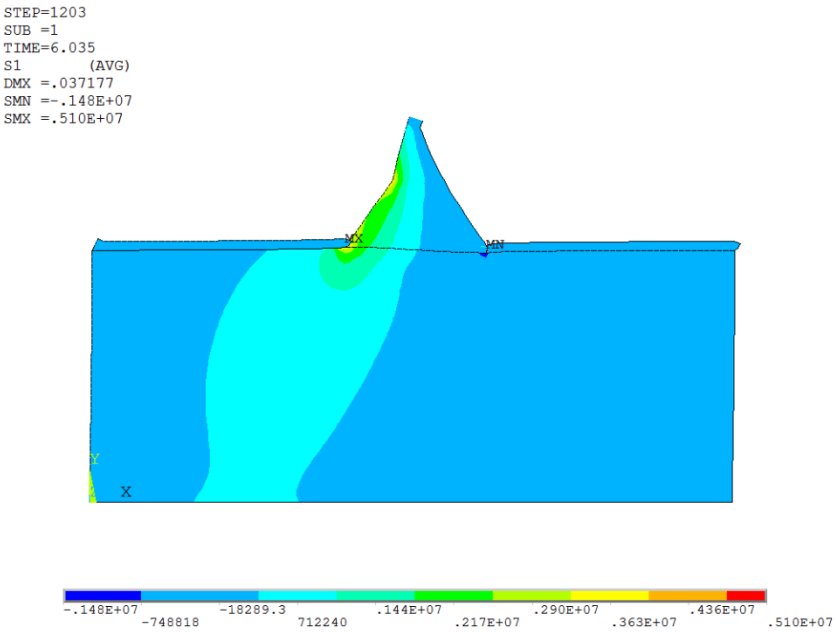

"Principal Stresses (N/m^2)"

Figure C.21 Maximum Tensile Stress (+) Distributions of Combination 6 at 6.035 sec. – Empty Reservoir Condition

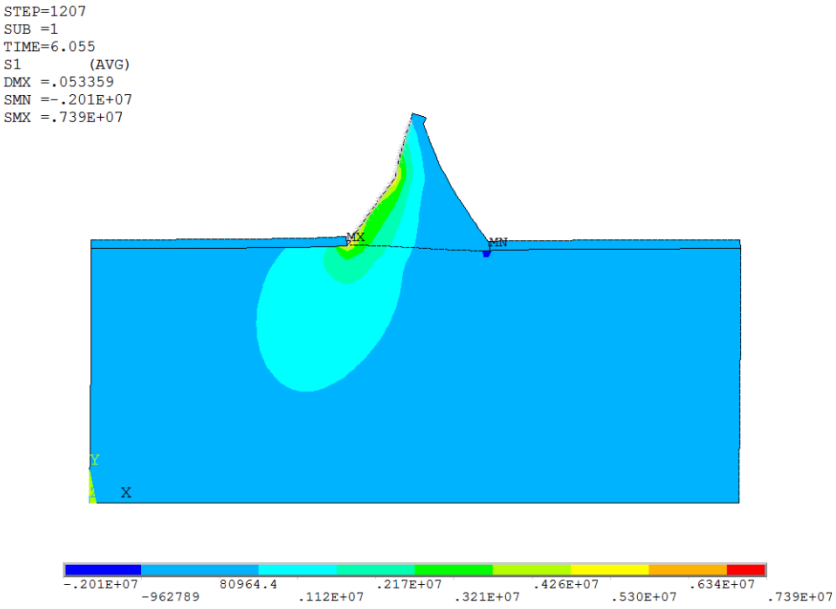

"Principal Stresses (N/m^2)"

Figure C.22 Maximum Tensile Stress (+) Distributions of Combination 6 at 6.055 sec. – Westergaard Method

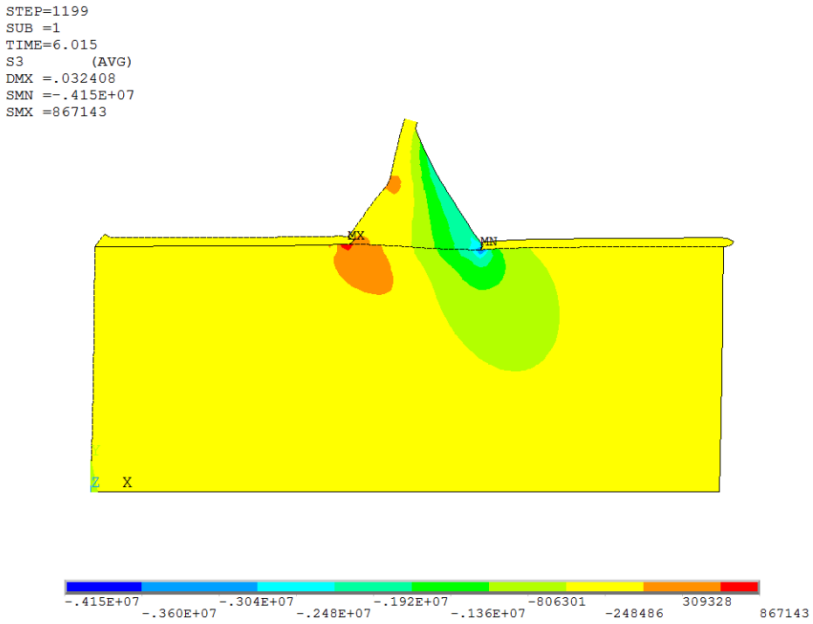

"Principal Stresses (N/m^2)"

Figure C.23 Maximum Compressive Stress (-) Distributions of Combination 6 at 6.015 sec. – Empty Reservoir Condition

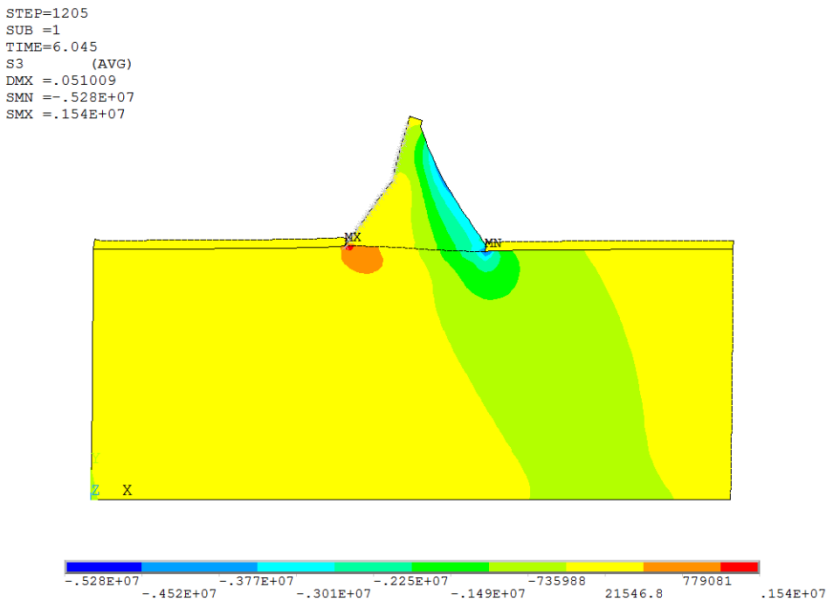

"Principal Stresses (N/m^2)"

Figure C.24 Maximum Compressive Stress (-) Distributions of Combination 6 at 6.045 sec. – Westergaard Method